10. Nonlinear Devices

Nonlinear optical devices, such as harmonic generators and parametric oscillators, provide a means of extending the frequency range of available laser sources. In 1961, Franken and coworkers detected ultraviolet light at twice the frequency of a ruby laser when the beam was propagated through a quartz crystal [10.1]. This experiment marked the beginning of an intense investigation into the realm of the nonlinear optical properties of matter.

Frequency conversion is a useful technique for extending the utility of high-power lasers. It utilizes the nonlinear optical response of an optical medium in intense radiation fields to generate new frequencies. It includes both elastic (optical-energy-conserving) processes, such as harmonic generation, and inelastic processes (which deposit some energy in the medium), such as stimulated Raman or Brillouin scattering.

There are several commonly used elastic processes. Frequency doubling generates a single harmonic from a high-power source. The closely related processes of sum- and difference-frequency generation also produce a single new wavelength but require two input wavelengths. These processes have been used to generate high-power radiation in all spectral regions, from the ultraviolet to the far-infrared. Optical parametric oscillators and amplifiers generate two waves of lower frequency from a pump source. They are capable of generating a range of wavelengths from a single frequency source, in some cases spanning the entire visible and near-infrared regions.

As far as inelastic processes are concerned, the Raman process can be utilized in solid-state lasers for the generation of additional spectral output lines. The strongest interaction is for the output shifted toward a longer wavelength (first Stokes shift), but at sufficiently high-pump intensities additional lines at longer, as well as shorter, wavelengths with respect to the pump wavelength will appear (Stokes and anti-Stokes lines).

Although it produces a small wavelength shift, stimulated Brillouin scattering is mainly of interest for the realization of phase-conjugating mirrors. The application of phase conjugation, or wave front reversal, via stimulated Brillouin scattering, offers the possibility of minimizing thermally induced optical distortions which occur in solid-state laser amplifiers.

10.1 Nonlinear Optical Effects

Nonlinear optical effects are analyzed by considering the response of the dielectric material at the atomic level to the electric fields of an intense light beam. The propagation

of a wave through a material produces changes in the spatial and temporal distribution of electrical charges as the electrons and atoms react to the electromagnetic field of the wave. The main effect of the forces exerted by the field on the charged particles is a displacement of the valence electrons from their normal orbits. This perturbation creates electric dipoles whose macroscopic manifestation is the polarization. For small field strengths this polarization is proportional to the electric field. In the nonlinear case, the reradiation comes from dipoles whose amplitudes do not faithfully reproduce the sinusoidal electric field that generates them. As a result, the distorted reradiated wave contains additional frequencies from that of the original wave.

On a microscopic scale, the nonlinear optical effect is rather small even at relatively high-intensity levels, as the following example illustrates. We will compare the applied electric field strength of a high-intensity beam to the atomic electric field which binds the electrons to the nucleus. The magnitude of the atomic field strength is approximately equal to $E_{\text{at}} = e/4\pi\varepsilon_0 r^2$, where e is the charge of an electron, ε_0 is the permittivity of free space, and r is the radius of the electron orbit. With $r = 10^{-8}$ cm, one obtains $E_{\text{at}} = 10^9$ V/cm. A laser beam with a power density of $I = 100\text{MW/cm}^2$ generates an electric field strength in the material of about $E = 10^5$ V/cm according to $I = n_0 E^2 (\mu_0/\varepsilon_0)^{-1/2}$, where n_0 is the refractive index and $(\mu_0/\varepsilon_0)^{1/2}$ is the impedance of free space. To observe such a small effect, which is on the order of 10^{-4}, it is important that the waves add coherently on a macroscopic scale. This requires that the phase velocities of the generated waves and the incident wave are matched.

In a given material, the magnitude of the induced polarization per unit volume $\mathbf{P}$ will depend on the magnitude of the applied electric field $\mathbf{E}$. We can therefore expand $\mathbf{P}$ in a series of powers of $\mathbf{E}$ and write

$$\mathbf{P} = \varepsilon_0 \boldsymbol{\chi}^{(1)} \mathbf{E} + \varepsilon_0 \boldsymbol{\chi}^{(2)} \mathbf{E}\mathbf{E} + \varepsilon_0 \boldsymbol{\chi}^{(3)} \mathbf{E}\mathbf{E}\mathbf{E} + \cdots, \tag{10.1}$$

where ε_0 is the permittivity of free space and $\boldsymbol{\chi}^{(1)}$ is the linear susceptibility representing the linear response of the material. The two lowest order nonlinear responses are accounted for by the second- and third-order nonlinear susceptibilities $\boldsymbol{\chi}^{(2)}$ and $\boldsymbol{\chi}^{(3)}$. The expression of the polarization in anisotropy materials is rather complicated, for the induced polarization depends not only on the magnitude of the electric vector but also on the magnitude and direction of all vectors that characterize the electromagnetic field. Normally $\boldsymbol{\chi}^{(1)} \gg \boldsymbol{\chi}^{(2)} \gg \boldsymbol{\chi}^{(3)}$ and therefore the nonlinear effects will be negligible unless the electric field strength is very high.

The linear term in (10.1) represents three separate equations, one for each value of the ith Cartesian coordinate of $\mathbf{P}$, that is,

$$\mathbf{P}_i = \varepsilon_0 \boldsymbol{\chi}_{ij} \mathbf{E}_j \quad (i, j = 1, 2, 3). \tag{10.2}$$

The linear polarization tensor, which is rank 2, has an array of nine coefficients. The linear susceptibility, related to the refractive index through $\boldsymbol{\chi} = n_0^2 - 1$ and to the dielectric constant $\varepsilon = \varepsilon_0(1 + \boldsymbol{\chi})$, is responsible for the linear optical properties of the medium such as refraction, dispersion, absorption, and birefringence. In the linear regime optical properties are independent of light intensity and the wavelength of radiation does not change.

The nonlinear optical susceptibilities of second and third order which describe three- and four-wave mixing processes, respectively, give rise to a large variety of optical phenomena since each electric field can have a different frequency, propagation vector, polarization, and relative phase. Therefore **P** can contain many different product terms of the various interacting fields. In the following overview only interactions that are utilized in the nonlinear devices described in the remainder of this chapter are described.

The subject of nonlinear optics has been treated in several books [10.2–6] and tutorial review articles [10.7].

10.1.1 Second-Order Nonlinearities

The second-order susceptibility $\boldsymbol{\chi}^{(2)}$ is responsible for second harmonic generation, sum and difference frequency generation, and optical parametric amplification. Sections 10.2 and 10.3 describe devices based on these nonlinear phenomena. The abovementioned second-order nonlinear effects are produced by two waves, which interact to produce a third wave. Conservation of momentum and photon energy is always required in these processes. The optical fields of the three waves are coupled to one another through the second-order susceptibility. The coupling provides the mechanism for the exchange of energy among the interacting fields. The second-order nonlinear susceptibility in a Cartesian coordinate system can be written as

$$\mathbf{P}_j = \varepsilon_0 \boldsymbol{\chi}^{(2)}_{ijk} \mathbf{E}_j \mathbf{E}_k, \quad i, j, k = 1, 2, 3. \tag{10.3}$$

The tensor $\boldsymbol{\chi}^{(2)}_{ijk}$ in general has 27 independent coefficients. By taking into account symmetry conditions, the second-order susceptibility can be expressed by a two-dimensional 3×6 tensor, commonly known as the d-tensor. The nonlinear coefficients ranging from d_{11} to d_{36} will be frequently used throughout this chapter.

Most nonlinear crystals are described by only a few d-coefficients. For example, the nonlinear crystal KDP has only three nonvanishing terms (d_{14}, d_{25}, d_{36}). Furthermore, for those crystals of main interest there is usually one predominant coefficient associated with a beam propagation direction which yields maximum harmonic power. In centrosymmetric crystals the $\boldsymbol{\chi}^{(2)}$ tensor is actually zero; therefore second-order nonlinear processes are only possible in crystals that lack inversion symmetry. Using the d-coefficients, the nonlinear polarization is given by

$$\mathbf{P} = \varepsilon_0 d \mathbf{E}\mathbf{E}, \tag{10.4}$$

where d has the dimension of meter per volt.

Sum and Difference Frequency Generation

Two waves of comparable intensity and frequency ω_1 and ω_2 are initially present, and a wave at the third frequency ω_3 is created through the nonlinear interaction

$$\mathbf{P}(\omega_3) = \varepsilon_0 \boldsymbol{\chi}^{(2)} \mathbf{E}(\omega_1) \mathbf{E}(\omega_2), \tag{10.5}$$

where $\omega_3 = \omega_1 + \omega_2$. Similarly, a wave at the difference frequency $\omega_3 - \omega_2 = \omega_1$ may be generated ($\omega_3 > \omega_2 > \omega_1$). Sum frequency generation is described in Sect. 10.2.5. A very common technique to produce the third harmonic of a neodymium laser is, first, the generation of the second harmonic and then sum frequency generation by mixing the second harmonic (ω_2) with the unconverted portion of the fundamental beam (ω_1).

Second Harmonic Generation

This is a special case of frequency mixing with the initial waves having a common frequency, i.e., $\omega = \omega_1 = \omega_2$ and $\omega_3 = 2\omega$ in (10.5). The generation of a second harmonic can be readily shown if we describe the applied field by $E = E_0 \sin(\omega t)$. The induced polarization, according to (10.1), takes the form

$$\mathbf{P} = \varepsilon_0[\boldsymbol{\chi}^{(1)}\mathbf{E}\sin(\omega t) + \boldsymbol{\chi}^{(2)}\mathbf{E}^2\sin^2(\omega t) + \cdots], \tag{10.6a}$$

which can be written as

$$\mathbf{P} = \varepsilon_0[\boldsymbol{\chi}^{(1)}\mathbf{E}\sin(\omega t) + 1/2\boldsymbol{\chi}^{(2)}\mathbf{E}^2(1 - \cos 2\omega t) + \cdots]. \tag{10.6b}$$

In the last expression, the presence of the second term shows that a wave having twice the frequency of the fundamental can be formed in a nonlinear medium. Second harmonic generation is described in Sect. 10.2.

Parametric Amplification

Parametric amplification refers to the growth of two waves in the presence of a strong input wave, which will be referred to as the pump. Energy and momentum are conserved if $\omega_3 = \omega_2 + \omega_1$, where ω_3 is the frequency of the input pump beam and ω_2 and ω_1 are the frequencies of the resulting signal and idler beams. Parametric oscillators are described in Sect. 10.3.

10.1.2 Third-Order Nonlinearities

Third-order optical nonlinearities involve the nonlinear susceptibility tensor $\boldsymbol{\chi}^{(3)}$ in (10.1). This term governs third harmonic generation, optical Kerr effect, Raman effect, and Brillouin scattering. In general, $\boldsymbol{\chi}^{(3)}$ will couple together four frequency components, that is, three fields interact to produce a fourth field,

$$\mathbf{P}(\omega_4) = \varepsilon_0\boldsymbol{\chi}^{(3)}\mathbf{E}(\omega_3)\mathbf{E}(\omega_2)\mathbf{E}(\omega_1), \tag{10.7}$$

where $\omega_4 = \omega_3 + \omega_2 + \omega_1$. In the above equation $\boldsymbol{\chi}^{(3)}$ is a four-rank tensor with 81 elements, because an array of 3×27 coefficients couple a single component of the polarization $\mathbf{P}$ to three independent components of three electric field vectors.

The third-order optical nonlinearity is thus a four-photon process. There can be up to three different input laser frequencies, but several of the frequencies can also be the same. In a lossless medium the susceptibility coefficients of $\boldsymbol{\chi}^{(3)}$ are real. In

this case, the primary nonlinear optical effects are the generation of new frequency components and the intensity-dependent change in the refractive index (Kerr effect). In third-order interactions involving absorption, the imaginary part of $\chi^{(3)}$ describes Raman and Brillouin scattering.

Third Harmonic Generation

The third harmonic generated by an intense beam at frequency ω can be described by (10.7) with $\omega = \omega_1 = \omega_2 = \omega_3$ and $\omega_4 = 3\omega$. The expression of a sinusoidal electric field raised to the third power will include a term $\sin^3(\omega t) = 3/4 \sin(\omega t) - 1/4 \sin(3\omega t)$, which illustrates the creation of a third harmonic. The possibility of third harmonic generation exists in principle, although it suffers from practical drawbacks. Typical values of $\chi^{(3)}$ are orders of magnitude smaller than $\chi^{(2)}$ coefficients found in nonlinear crystals. Therefore the preferred method of third harmonic generation is the utilization of two second-order effects. (Second harmonic generation, followed by sum frequency mixing to generate the third harmonic, is explained in Sect. 10.2.5.)

Optical Kerr Effect

The third-order nonlinearity can lead to an intensity-dependent refractive index known as the optical Kerr effect. With $\omega_2 = -\omega_1$, (10.7) transforms to

$$\mathbf{P}(\omega) = [\chi^{(3)}\mathbf{E}_{\text{av}}^2]\mathbf{E}(\omega), \tag{10.8}$$

where $\mathbf{E}_{\text{av}}$ is the average electric field strength. The tensor $\chi^{(3)}$ describes the effect of an intense light beam upon the propagation path of the beam. The self-induced effect manifests itself as an intensity-dependent contribution to the index of refraction

$$n_2 = n_0 + (12\pi/n_0)\chi^{(3)}\mathbf{E}_{\text{av}}^2. \tag{10.9}$$

The effect of an intensity-dependent refractive index is exploited in Kerr lens mode locking (KLM), which is described in Sect. 9.2.3. In high-intensity beams the nonlinear refractive index can be the source of optical damage because it can lead to self-focusing and small-scale ripple growth. Both phenomena are discussed in Sect. 4.6.

Stimulated Raman Scattering

This nonlinear process involves the interaction of a laser beam with the molecular vibrations in gases or liquids. In the presence of a strong external electric field, the charge distribution of a diatomic molecule is polarized. The molecule acquires a dipole that can interact with the driving field. The external field exerts a force on the molecule proportional to E^2. This implies that there must be two input photons driving the interaction. Therefore two electric fields in (10.7) have the same frequency and represent the pump beam ω_{p} which drives the interaction to provide amplification at $\omega_{\text{p}} - \omega_0$, where ω_0 is the frequency of the molecular vibration wave. In accordance

with (10.7) three waves produce a fourth wave via the third-order polarization, and energy at the pump frequency can be transferred to the signal frequency $\omega_p - \omega_0$. In addition, nonlinear mixing processes create additional frequency components at $\omega_p - j\omega_0$ and $\omega_p + j\omega_0$, where $j = 1, 2, 3 \ldots$. Raman lasers employed to shift the wavelength of solid-state lasers are described in Sect. 10.4.

Stimulated Brillouin Scattering

In this process an optical beam interacts with an acoustic wave in the medium. The acoustic wave is associated with the propagation of pressure in the medium, leading to periodic density fluctuations. Electrostriction provides the coupling mechanism between the acoustic wave and electromagnetic wave, that is, a local compression of the medium in response to the strength of the electromagnetic field. An incident laser beam can scatter with the periodic index variations associated with a propagating acoustic wave. The interaction is stimulated because the acoustic and scattered waves can grow as the pump beam is depleted. The acousto-optic interaction with the laser pump beam depends on the intensity of the pump, just as in stimulated Raman scattering; therefore, the polarizability is a function of E^2. The four-wave mixing process is characterized by two electromagnetic fields with the same frequency ω_p interacting with an acoustic wave of frequency ω_a to produce a fourth wave at $\omega_p - \omega_a$. The frequency of the acoustic wave is determined by the conservation of energy and momentum. The stimulated wave is usually radiated backward toward the incoming pump beam. The acoustical frequency for a backward wave is $\omega_a = 2\omega_p(n_0 v_a/c)$, where v_a is the speed of sound in the medium. Since v_a is very small compared to the speed of light in the medium c/n_0, the frequency shift is very small.

Acoustic waves occur at frequencies orders of magnitude smaller than molecular vibrations. Brillouin scattering is therefore frequency-shifted from the incident radiation by a much smaller amount as compared to Raman scattering. From an engineering point of view, interest in Brillouin scattering is not related to the frequency shift which occurs in the interaction, but in the phase-conjugate reflection of the pump beam. Brillouin scattering is the mechanism for phase conjugation discussed in Sect. 10.5.

10.2 Harmonic Generation

In this section we will review the basic theory and discuss system parameters and material properties that affect harmonic generation.

Harmonic generation is achieved by sum frequency mixing in birefringent crystals which possess a second-order nonlinear optical susceptibility. In the sum frequency mixing process, two input waves, at frequencies ω_1 and ω_2, interact in a nonlinear medium to produce a third wave at $\omega_3 = \omega_1 + \omega_2$ via the second-order nonlinear polarization. This process is described mathematically by three coupled differential equations that are obtained from Maxwell's equations. To simplify our analytical treatment we assume absorption losses in the nonlinear crystal to be negligible.

The combination of Maxwell's equations for a lossless, nonlinear dielectric medium leads to the following wave equation [10 8]:

$$\nabla^2 E + \mu_0 \varepsilon \frac{\partial^2 E}{\partial t^2} = -\mu_0 \frac{\partial^2 P_{\mathrm{NL}}}{\partial t^2} \tag{10.10}$$

The nonlinear source term on the right side of (10.10) is the nonlinear polarization P_{NL}. The polarization P consists of a linear and a nonlinear term

$$P = \varepsilon_0 \chi_{\mathrm{L}} E + P_{\mathrm{NL}}, \tag{10.11}$$

where

$$P_{\mathrm{NL}} = 2 d_{ijk} E_j E_k. \tag{10.12}$$

For $P_{\mathrm{NL}} = 0$, Eq. (10.10) is a homogeneous equation describing propagation of a wave in a linear medium.

We limit our discussion to three monochromatic plane waves of frequencies ω_1, ω_2, and ω_3 propagating in the z-direction. The electric field of each wave is expressed as the product of a complex amplitude and exponent summed with the complex conjugate of that product. The addition of the complex conjugate keeps the electric field real. The corresponding fields of the traveling plane waves are

$$E_i(z,t) = \frac{1}{2}[E_{1i}(z) \exp i(\omega_1 t - k_1 z) + \text{c.c.}], \tag{10.13a}$$

$$E_k(z,t) = \frac{1}{2}[E_{2k}(z) \exp i(\omega_2 t - k_2 z) + \text{c.c.}], \tag{10.13b}$$

$$E_j(z,t) = \frac{1}{2}[E_{3j}(z) \exp i(\omega_3 t - k_3 z) + \text{c.c.}], \tag{10.13c}$$

where i, j, k are Cartesian coordinates that are either x or y, k_1, k_2, k_3 are the propagation constants of the three waves, and c.c. denotes the complex conjugate.

For these traveling waves we obtain from the wave equation three coupled, first-order nonlinear differential equations

$$\frac{dE_1}{dz} = -i\omega_1 \sqrt{\mu_0/\varepsilon_1}\, d_{ijk} E_3 E_2^* \exp(-i\,\Delta k z), \tag{10.14a}$$

$$\frac{dE_2}{dz} = -i\omega_2 \sqrt{\mu_0/\varepsilon_2}\, d_{kij} E_1^* E_3 \exp(-i\,\Delta k z), \tag{10.14b}$$

$$\frac{dE_3}{dz} = -i\omega_3 \sqrt{\mu_0/\varepsilon_3}\, d_{jik} E_1 E_2 \exp(i\,\Delta k z). \tag{10.14c}$$

The difference of the propagation constants, i.e., the phase mismatch is expressed by

$$\Delta k = k_3 - k_1 - k_2. \tag{10.15}$$

Equations (10.14), which are solved by integration over the length $z = L$ of the nonlinear medium, provide the basis for our discussion of second and third harmonic generation. We note from (10.14) that the waves at frequencies ω_1 and ω_2 are decaying as they propagate through the crystal, whereas the wave at ω_3 is increasing in amplitude.

10.2.1 Basic Theory of Second Harmonic Generation

Second harmonic generation is the degenerate case of three-wave interaction where two of the waves have equal frequencies $\omega_1 = \omega_2 = \omega$ and $\omega_3 = 2\omega$. Therefore E_1 and E_2 in (10.14) are the electric fields of the same fundamental beam. Since $E_1 = E_2 = E_\omega$ and $E_3 = E_{2\omega}$, Equations (10.14a) and (10.14b) are identical and (10.14) reduces to two coupled differential equations

$$\frac{dE_\omega}{dz} = i\omega\sqrt{\mu_0/\varepsilon_\omega}\, d_{ijk} E_{2\omega} E_\omega^* \exp(-i\Delta k z), \tag{10.16a}$$

$$\frac{dE_{2\omega}}{dz} = -i2\omega(1/2)\sqrt{\mu_0/\varepsilon_{2\omega}}\, d_{jik} E_\omega^2 \exp(i\Delta k z). \tag{10.16b}$$

The factor of (1/2) has to be included in (10.16b) to account for the degeneracy $\omega_2 = \omega_1$. For efficient energy transfer it is necessary that the interacting waves remain in phase. With $k_3 = k_{2\omega}$, $k_1 = k_2 = k_\omega$ and $\Delta k = 0$ in (10.15) we obtain from (10.15)

$$k_{2\omega} = k_\omega + k_\omega \tag{10.17}$$

Since $k_\omega = 2\pi n_\omega/\lambda_0$ and $k_{2\omega} = 4\pi n_{2\omega}/\lambda_0$ from the above condition (10.17) follows $n_\omega = n_{2\omega}$. Therefore the phase mismatch expressed by (10.15) can be written in the case of frequency doubling as follows

$$\Delta k = \frac{4\pi}{\lambda_0}(n_\omega - n_{2\omega}), \tag{10.18}$$

where λ_0 is the wavelength at the fundamental wave in vacuum.

Before discussing the exact solution of (10.16) we will consider two special cases which are usually treated in textbooks [10.9], namely (a) frequency conversion at low efficiency and (b) conversion under perfect phase matching conditions.

Second Harmonic Conversion at Low Efficiency

In this case we can make the assumption that the fundamental beam is not depleted, and therefore $dE_\omega/dz = 0$ in (10.16a) and only Eq. (10.16b) has to be considered. By observing the tensor properties of d_{jik}, integration of (10.16b) yields

$$I_{2\omega} = C^2 L^2 I_\omega^2 \frac{\sin^2(\Delta k L/2)}{(\Delta k L/2)^2}, \tag{10.19a}$$

where

$$C^2 = \frac{8\pi^2 d_{\text{eff}}^2}{\varepsilon_0 c \lambda_0^2 n_0^3}, \tag{10.19b}$$

L is the length of the nonlinear crystal, n_0 is the refractive index at the fundamental wavelength λ_0, and d_{eff} is the effective nonlinear coefficient of the tensor d_{ijk} for a particular nonlinear crystal

$$d_{ijk} = \varepsilon_0 d_{\text{eff}}. \tag{10.20}$$

The unit of d_{eff} in (10.19b) is m/V. Some authors include ε_0 in the nonlinear coefficient in this case the unit of d_{ijk} is As/V^2 and d_{ijk} [As/V^2] $= 8.855 \times 10^{-12} d_{\text{eff}}$ [m/V]. Introducing the appropriate constants into (10.19b) we obtain

$$C = 5.46 \frac{d_{\text{eff}}}{\lambda_0 n_0^{3/2}}, \tag{10.21}$$

where the unit of d_{eff} is pm/V, λ_0 is measured in μm, and the unit of C is GW$^{-1/2}$. In deriving (10.19a) we used the conversion of electric field strength E to intensity I

$$I = n_0 E^2 / 2 Z_0, \tag{10.22}$$

where Z_0 is the plane wave impedance in vacuum $Z_0 = (\mu_0/\varepsilon_0)^{1/2} = 120\pi$[V/A].

The conversion efficiency for frequency doubling follows from (10.19a)

$$\eta = C^2 L^2 I_\omega \operatorname{sinc}^2(\Delta k L/2). \tag{10.23}$$

The second harmonic power generation is strongly dependent on the phase mismatch expressed by the sinc^2 function, as is illustrated in Fig. 10.1. In this case, a variation of Δk was obtained by changing the crystal temperature. The harmonic power is at maximum when $\Delta k = 0$, that is, at the exact phase matching temperature. For a fixed Δk, second harmonic power as a function of distance l along the crystal grows or

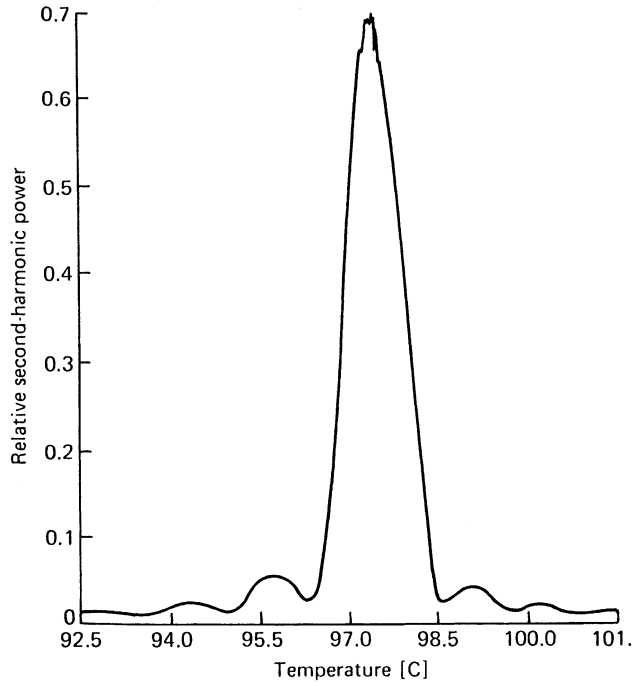

Fig. 10.1. Second-harmonic generation as a function of temperature in a $Ba_2NaNb_5O_{15}$ crystal employed to frequency-double a Nd:YAG laser.

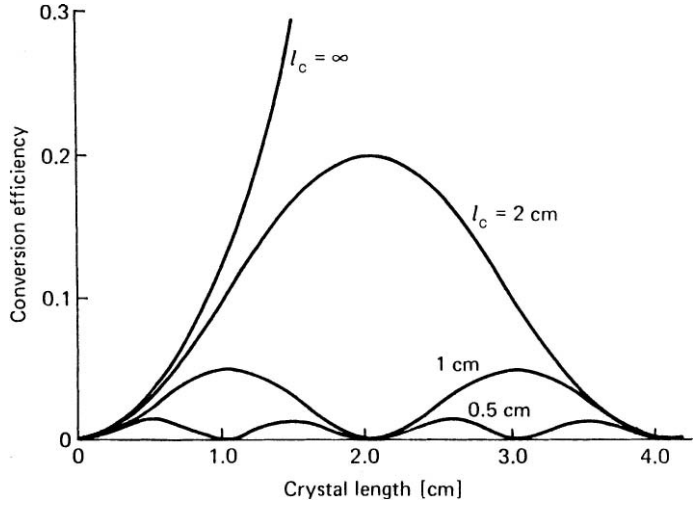

Fig. 10.2. Second-harmonic power conversion efficiency as a function of distance l from the entrance surface of a CDA crystal. Parameter is the coherence length l_c ($C = 1.1\,\mathrm{GW}^{-1/2}$; $\lambda = 1.06\ \mu\mathrm{m}$; $I = 100\ \mathrm{MW/cm}^2$).

decays with a period of $\Delta k l/2 = \pi$. Half of this distance has been termed coherence length l_c. It is the distance from the entrance face of the crystal to the point at which the second harmonic power will be at its maximum value. This parameter is not to be confused with the coherence length l_c the laser beam, which was defined in Chap. 5. For normal incidence the coherence length is given by

$$l_c = \pi/\Delta k. \tag{10.24}$$

If one expresses the phase mismatch Δk in terms of coherence length in (10.23) one obtains

$$\eta = C^2 L^2 I_\omega \,\mathrm{sinc}^2(\pi L/2l_c) \tag{10.25}$$

The oscillatory behavior of (10.25) is shown in Fig. 10.2 for several values of l_c. In the ideal case of perfect phase matching conditions, i.e., $\Delta k = 0$ or $l_c = \infty$, the second harmonic conversion efficiency is proportional to the square of the crystal length. This is of course only true for small signals or low conversion efficiencies.

If the crystal is not perfectly phase-matched the highest second harmonic power we can expect to generate will be the signal obtained after the beam propagates one coherence length, independent of the length of the crystal.

The decrease in harmonic power, for example, between l_c and $2l_c$, is explained by a reversal of the power flow. Power at the second harmonic is coupled back into the input beam. Thus we find that in a lossless medium the power oscillates back and forth between the harmonic and the fundamental wave.

In almost all practical cases the coherence length is limited by the divergence and the line width of the laser beam and by angular and thermal deviations of the crystal from the phase matching angle and temperature.

Following the work of Eimerl [10.10], the subsequent calculations of nonlinear conversion can be substantially simplified if one combines the various parameters of (10.23). The terms in front of the sinc function can be combined in the so-called drive η_0

$$\eta_0 = C^2 L^2 I_\omega. \tag{10.26}$$

The terms in the argument of the sinc function are combined in the dephasing δ

$$\delta = \Delta k L/2. \tag{10.27}$$

With the definition of the drive and dephasing factors we can restate (10.23) as follows

$$\eta = \eta_0 \operatorname{sinc}^2 \delta. \tag{10.28}$$

Frequency Doubling Assuming Perfect Phase Matching Conditions

When the fundamental and second harmonic waves propagate through the nonlinear crystal with exactly equal phase velocities, the propagation vector mismatch is zero. With the assumption of $\Delta k = 0$, Eqs. (10.16a, b) are greatly simplified and can be integrated to yield

$$\eta = \tanh^2 \sqrt{\eta_0}. \tag{10.29}$$

This equation predicts that the conversion efficiency asymptotically approaches one as the drive becomes very large (see uppermost curve in Fig. 10.3). For small η_0 one obtains $\eta = \eta_0$, which also follows from (10.28) for $\Delta k = 0$. Equation (10.29) takes the depletion of the fundamental beam into account, but dephasing as it occurs in real systems is ignored.

Harmonic Generation with Pump Depletion and Dephasing

Most modern laser systems generate high peak powers with good beam quality and incorporate nonlinear crystals of high optical quality which leads to conversion efficiencies typically between 50 and 80%. In this case depletion of the fundamental beam as well as phase mismatch has to be considered to adequately describe the experimental results. Armstrong et al. [10.8] have solved the coupled nonlinear differential equations (10.16) for arbitrary Δk and intensities. We will use the solution in a format which is particular useful for numerical calculations [10.10]

$$\eta = \eta_m sn^2[\sqrt{\eta_0/\eta_m}, \eta_m^2], \tag{10.30a}$$

where

$$\eta_m = 1 + (\delta^2/2\eta_0) - \sqrt{[1 + (\delta^2/2\eta_0)]^2 - 1}. \tag{10.30b}$$

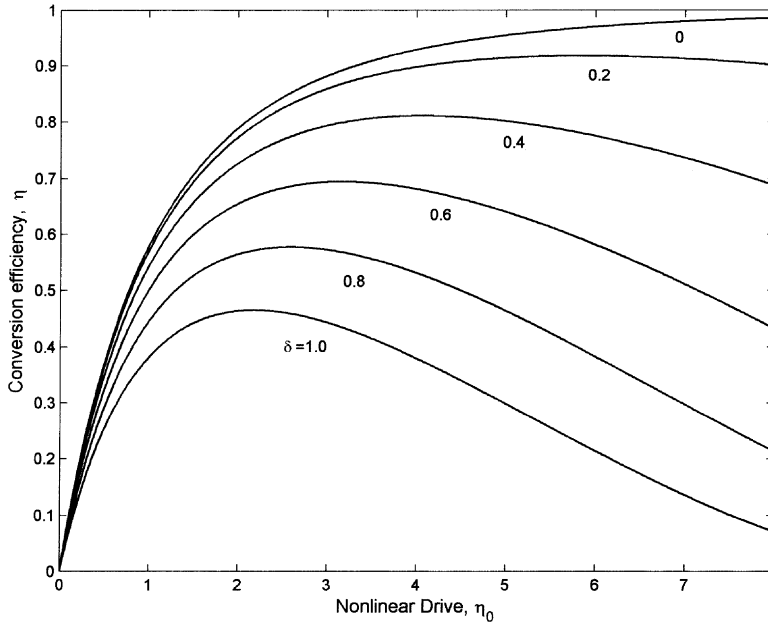

Fig. 10.3. Plane wave conversion efficiency as a function of the nonlinear drive. Parameter is the dephasing δ

The expression for the conversion efficiency contains the Jacobi elliptic function $\mathrm{sn}(u, m)$. This is a periodic function with argument u and a period determined by the modulus m. For $m = 0$, the elliptic function reduces to the sine function $\mathrm{sn}(u, 0) = \sin u$, and for $m = 1$ the period is infinite $\mathrm{sn}(u, 1) = \tanh u$. Since the highest value $\mathrm{sn}^2(u, m)$ can reach is 1, the term η_m in front of the Jacobi function determines the maximum efficiency that can be achieved at the optimum nonlinear drive.

Math packages such as MATLAB or MATHEMATICA include the $\mathrm{sn}(u, m)$ function and therefore the expression can easily be evaluated for specific system parameters. The conversion efficiency in (10.30) is a function of only two parameters: the phase mismatch between the two beams expressed by the dephasing factor δ, and the nonlinear drive η_0 which is proportional to the input beam intensity. Figure 10.3 shows a plot of second harmonic conversion efficiency as a function of the nonlinear drive with the dephasing factor as parameter. When perfect phase matching is achieved ($\delta = 0$), the transfer of energy from the input wave to the second harmonic is maximized and the curve is identical to the one obtained from (10.29). When the drive η_0 is small relative to unity, the slope of the curves is the same as given by the no-depletion expression (10.28).

When both fundamental wave depletion and dephasing are considered, second harmonic efficiency rises with increasing drive until an optimum value is reached. Back-conversion is the reason for the reduction of the conversion efficiency after a peak value has been reached. When the phases are not perfectly matched, power is cycled between the fundamental and harmonic waves. The efficiency peaks and then oscillates between the peak and zero in a nonsinusoidal fashion. Mathematically

this is expressed in (10.30) by a rapid rise of efficiency for small values of η_0 (i.e., low intensities or short crystal length), until the terms containing δ dominate and the efficiency decreases.

We note also from Fig. 10.3 that second harmonic generation becomes increasingly more sensitive to dephasing δ as the drive η_0 increases. This explains why focusing a beam beyond the optimum spot rise does not lead to a further increase in efficiency. Focusing the beam into the nonlinear crystal increases intensity as well as beam divergence and therefore dephasing. At one point the adverse effect of dephasing on the efficiency dominate over any benefits gained from a further increase in intensity.

In comparing the results of (10.30) with the approximations of (10.28) and (10.29) we note that the exact solution predicts that for a fixed crystal length and phase mismatch there is an optimum pump energy at which the conversion efficiency is maximized. The approximations predict no such optimum. Furthermore the conversion efficiencies calculated from (10.30) are considerably below the values obtained from the approximations. For example, if we consider harmonic generation with a drive of $\eta_0 = 1$ and dephasing $\delta = 1$, we obtain from (10.30) a conversion efficiency of $\eta = 0.38$. The approximation (10.28) which ignores depletion of the fundamental beam yields $\eta = 0.71$, and the approximation that does not take phase mismatch into account (10.29) gives a value for the efficiency of $\eta = 0.62$.

Figure 10.4 shows the same result as Fig. 10.3 but on an expanded scale for the region of greatest interest for most laser systems.

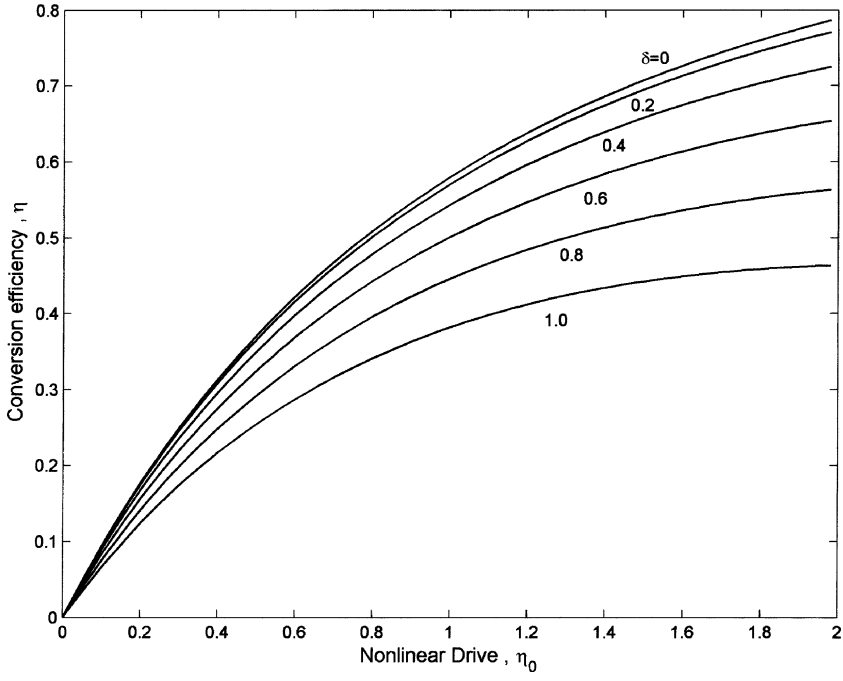

Fig. 10.4. Conversion efficiency vs. nonlinear drive on an expanded scale with dephasing as parameter

Before we can relate the results of (10.30) to real situations we have to express dephasing in terms of systems parameters.

Second harmonic conversion depends on parameters that are related to the laser source, such as power density, beam divergence, and spectral line width, and parameters associated with the harmonic generator, such as the value of the nonlinear coefficient, crystal length, and angular, thermal, and spectral sensitivity to deviations from the exact phase matching angle.

The most critical *laser parameters* are power density and beam divergence. In general, one finds that Nd-doped crystals have sufficiently narrow line widths for efficient harmonic generation. In these lasers attention is focused mainly on obtaining a diffraction limited beam, i.e., TEM_{00} mode operation. Nd:Glass lasers and tunable lasers require in addition a reduction of the spectral line width.

The most important intrinsic *crystal parameters* are the nonlinear coefficient and the angular sensitivity to the phase match condition. In the technique of index matching, the dependence of the refractive index of the extraordinary ray on the propagation direction in birefringent crystals is exploited to match the phase velocity of the fundamental and second harmonic waves.

In principle, by adjusting the crystal orientation we can achieve $\Delta k = 0$ for plane waves. However, real beams have a curved wavefront that can be thought of as a bundle of rays with different slope angles and intensities. Consequently, it is impossible to achieve perfect phase matching for all rays simultaneously.

In the phenomenological model described here the fundamental beam is characterized by an average intensity and an average beam angle. Half of this beam angle multiplied by the crystal's sensitivity to angular deviations from the phase match condition defines the phase mismatch

$$\Delta k = (\beta_\theta / n_0)(\theta/2), \tag{10.31}$$

where θ is the FWHM beam divergence of the fundamental beam measured *outside* the crystal, (β_θ / n_0) is the angular sensitivity, and n_0 is the refractive index. The parameter β_0 is the angular sensitivity of the wave-vector mismatch caused by a deviation of the beam from the phase-matched direction *inside* the crystal. For the special case of a noncritically phase-matched crystal, the dependence of Δk on $\theta/2$ becomes a second-order effect, as will be discussed in the next section. The beam divergence of a diffraction-limited or a multimode beam as a function of diameter, wavelength, and beam quality factor M can be calculated from the equations provided in Chap. 5.

Numerical calculations based on (10.30) can be carried out if we know the relevant parameters that describe the nonlinear medium and the input laser beam. The nonlinear crystal is characterized by the nonlinear parameter C, the angular sensitivity (β_θ / n_0), and length L, and the fundamental beam is described by the intensity I_ω and divergence θ. These five parameters are needed to calculate the drive η_0 and dephasing δ.

Although (10.30) is considerably more accurate compared to the approximations (10.28) and (10.29), second harmonic generation efficiency is still somewhat overstated because the input and output electromagnetic fields have been assumed to be plane waves, i.e., the input beam is flat in time and spatial extent. Real beams are nonuniform in both space and time, and the spatial and temporal wings convert with different efficiencies than do the peaks.

Instead of characterizing the fundamental beam by an average intensity and beam angle, a more accurate calculation can be based on a detailed numerical model that includes the effects of diffraction and beam nonuniformity. This requires calculation of the harmonic conversion according to (10.30) for rays having different intensities and slope angles and integration over the cross section of the beam.

For example, one can divide the beam into strips oriented along the angular sensitive direction of the crystal. Each strip has a different intensity and deviates by a different angle from the exact phase match condition. Conversion efficiency is calculated for each strip with subsequent integration over the angular extent of the beam.

A number of important conclusions can be drawn from Fig. 10.3.

(a) Tighter focusing of the fundamental beam into the nonlinear crystal will increase beam intensity and beam divergence; consequently, both the nonlinear drive and dephasing will increase. For a given crystal length and laser input power there is an optimum spot size that maximizes the conversion efficiency. Beyond this point tighter focusing will not result in a higher efficiency because any further increase in intensity is counteracted by the adverse effect of a larger dephasing factor δ.

(b) At a fixed input intensity and beam divergence there is an optimum length of the nonlinear material. As the length is increased both the drive and dephasing will increase. The drive varies quadratically with crystal length whereas the dephasing varies linearly. The optimum crystal length is a tradeoff between drive and dephasing. Conversion efficiency as a function of crystal length in KTP for different input beams is illustrated in Fig. 10.5. Efficiency increases rapidly

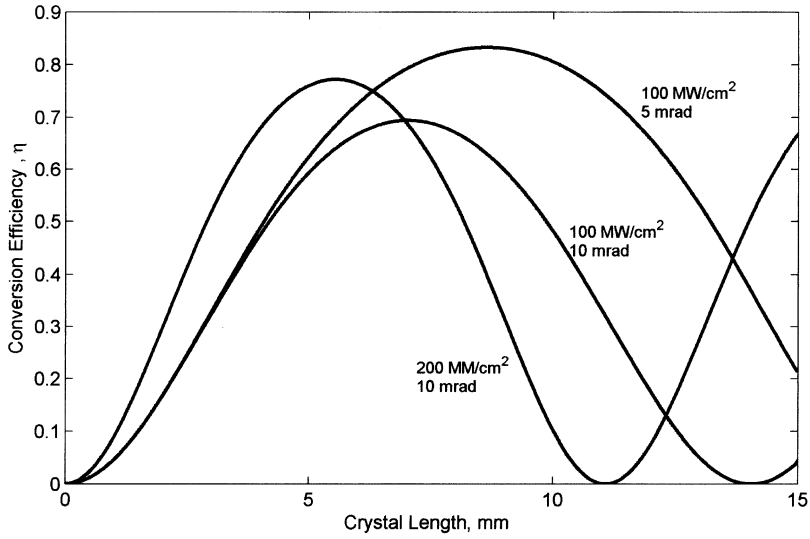

Fig. 10.5. Conversion efficiency in KTP as a function of crystal length for different values of beam intensities and beam angles

for very short lengths because both the drive and dephasing are small. After an optimum length is reached, dephasing, which is proportioned to length, starts to dominate over a further increase in drive, and the conversion decreases.

(c) A telescope inserted in front of the nonlinear crystal has the same effect as a length change since the drive (i.e., intensity) will change quadratically with the telescope magnification, and dephasing (i.e., beam divergence) will change linearly.

We will consider second harmonic generation of a 1.06-μm beam with an 8-mm-long KTP crystal. The input beam has an intensity $I_\omega = 200$ MW/cm^2 and a diameter of 350-μm and is three times diffraction-limited ($M = 3$). KTP has a nonlinear coefficient of $C = 6.9$ GW$^{-1/2}$ and an angular sensitivity $(\beta_\theta/n_0) = 0.32$ cm^{-1} mrad^{-1}. From these values follows a beam divergence of $\theta = 11.6$ mrad and from (10.26, 27, 31) we obtain $\eta_0 = 6.1$ and $\delta = 0.74$. Figure 10.3 gives a conversion efficiency of $\eta = 0.46$ for these parameters. From Fig. 10.3 we can see that the crystal is operated at an intensity that is too high since the operating point is well beyond the optimum. For example, a shorter crystal with a length of 5 mm will result in a drive of $\eta_0 = 2.38$ and dephasing of $\delta = 0.46$. These parameters yield an efficiency of $\eta = 0.74$, that is near the optimum. The same improvement in efficiency can be obtained by adding a telescope with magnification $m = 1.6$ in front of the 8-mm-long crystal. The upcollimating telescope will reduce the intensity and dephasing.

KDP crystals have a lower nonlinear coefficient compared to KTP and for efficient conversion they require exposure to very high intensities. A typical example would be a 1.5-cm-long crystal inserted into a 1.06-μm beam having an intensity of $I_\omega = 1$ GW/cm^2. Assuming a beam of 4-cm diameter that is two times diffraction-limited, and using the nonlinear constant $C = 0.97$ GW$^{-1/2}$ and angular sensitivity $(\beta_\theta/n_0) = 1.73$ cm^{-1} mrad^{-1} for KDP, we calculate a drive of $\eta_0 = 2.1$ and a dephasing of $\delta = 0.04$. With these values a second harmonic conversion efficiency of $\eta = 0.80$ is obtained from Fig. 10.3.

Figure 10.6 shows experimental data and predicted performance for a harmonic generator comprising an 8-mm-long KTP crystal. The fundamental beam was generated by a Q-switched diode-pumped Nd:YAG laser at 1064 nm. The laser generated a pulse energy of up to 40mJ in a 12-ns pulse. At the maximum output intensity of 175 MW/cm^2 the conversion efficiency approached 80%. The beam having a diameter of 1.5 mm was weekly focused into the crystal, which resulted in a beam divergence of 5 mr. If one introduces these parameters together which the data for KTP from the previous example, one obtains the theoretical curve in Fig. 10.6. The theoretical doubling efficiency calculated from (10.30) gives quite acceptable agreement with the experimental values.

10.2.2 Phase Matching

With typical dispersion values in the visible region, the coherence length in most crystals is limited to about 10 μm. For this reason the intensity of second harmonic

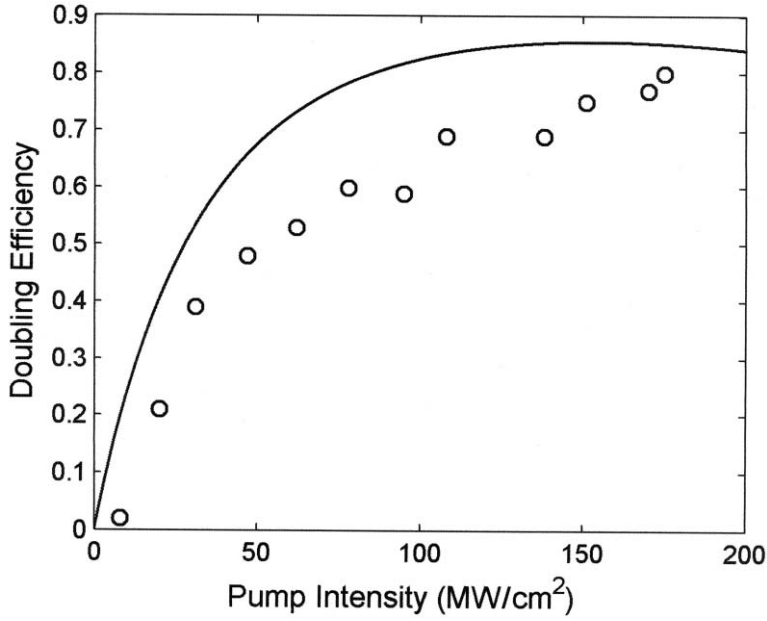

Fig. 10.6. Second harmonic conversion efficiency versus power density for a KTP crystal pumped by a Q-switched Nd:YAG laser at 1060 nm

power is small. Only if the refractive indices of the fundamental and second harmonic wave (i.e., n_ω and $n_{2\omega}$) can be made essentially equal can one expect high conversion efficiencies.

An effective method of providing equal-phase velocities for the fundamental and second harmonic waves in the nonlinear medium utilizes the fact the dispersion can be offset by using the natural birefringence of uniaxial or biaxial crystals. These crystals have two refractive indices for a given direction of propagation, corresponding to two orthogonally polarized beams; by an appropriate choice of polarization and direction of propagation it is often possible to obtain $\Delta k = 0$. This is termed phase matching or index matching.

We will illustrate the method of index matching in uniaxial crystals because of its relative simplicity. The reader interested in a review of phase matching in biaxial crystals is referred to reference [10.11]. For a general introduction to crystal optics the following references are recommended [10.12–14].

Uniaxial crystals, which include KDP and its isomorphs, BBO, and $LiNbO_3$ have an indicatrix which is an ellipsoid of revolution, with the optic axis being the axis of rotation, as shown in Fig. 10.7. The two directions of polarization and the indices for these directions are found by drawing a line through the center of the ellipsoid in the direction of beam propagation (line $0P$ in Fig. 10.7), the intersection of a plane perpendicular to $0P$ with the ellipsoid is an ellipse. The two axes of this ellipse are parallel to the two directions of polarization, and the length of each semi-axis is equal to the refractive index in that direction.

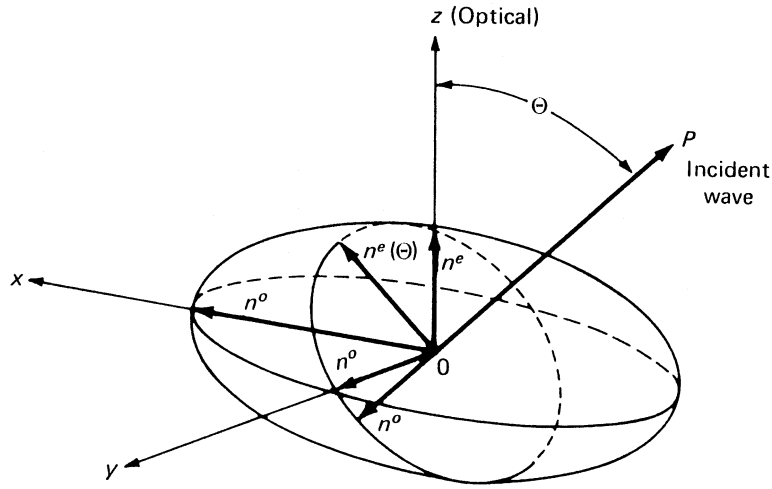

Fig. 10.7. Indicatrix ellipsoid of a uniaxial crystal. Also shown is a cross section perpendicular to the light propagation direction P

We now examine how the indices of refraction vary when the direction of propagation is changed. We notice that for the direction of polarization perpendicular to the optic axis, known as the ordinary direction, the refractive index is independent of the direction of propagation. For the other direction of polarization, called the extraordinary direction, the index changes between the value of the ordinary index n^{o} when $0P$ is parallel to z and the extraordinary index n^{e} when $0P$ is perpendicular to z. The dependence of n^{e} on the angle between the propagation direction and the optic axis is given by the index ellipsoid equation

$$[n^{\mathrm{e}}(\theta)]^{-2} = (n^{\mathrm{o}})^{-2}\cos^2\theta + (n^{\mathrm{e}})^{-2}\sin^2\theta, \tag{10.32}$$

where the superscripts "o" and "e" refer to the ordinary and the extraordinary rays.

Changing the point of view, we look now at the shape of the wavefronts for these two rays instead of their direction and polarization. Assuming that the input is a monochromatic point source at O, the expanding wavefront for the o-ray is spherical, whereas the spreading wavefront for the e-ray is an ellipsoid. This property of crystals is described by the index surface, which has the property that the distance of the surface from the origin along the direction of the wave vector is the refractive index. For a uniaxial crystal this surface has two sheets—a sphere for ordinary waves polarized perpendicular to the optic axis with index n^{o}, and an ellipsoid for extraordinary waves with index $n^{\mathrm{e}}(\theta)$. By definition the optic axis is that direction at which the o- and e-rays propagate with the same velocity. If the value of $n^{\mathrm{e}} - n^{\mathrm{o}}$ is larger than zero, the birefringence is said to be positive, and for $n^{\mathrm{e}} - n^{\mathrm{o}}$ smaller than zero the birefringence is negative; the corresponding crystals are called positive or negative uniaxial. Figure 10.7 shows a cross section of the index surface of a negative uniaxial crystal (for the moment we consider only the solid lines n^{o}_{ω} and n^{e}_{ω}). The complete surfaces are

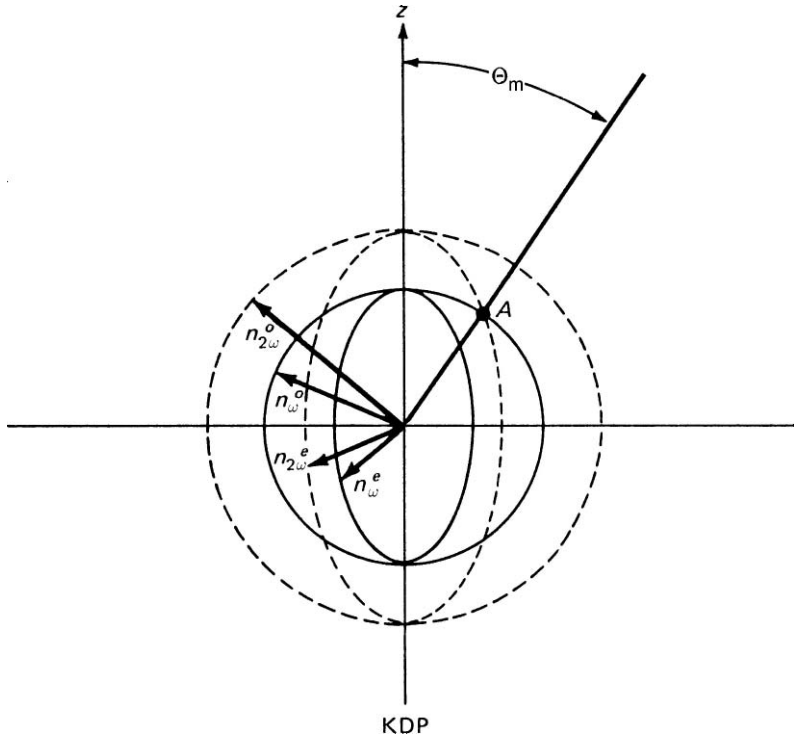

Fig. 10.8. Cross section of the index surface of a negative uniaxial crystal for two different wavelengths

generated by rotating the given sections about the z-axis. The wavefront velocity v and the refractive index n_0 are related by $v = c/n_0$, where c is the velocity of light in vaccum.

Both refractive indices n^{o} and n^{e} are a function of wavelength. Figures 10.8 and 10.9 illustrate how the dependence of the refractive index on beam direction, wavelength, and polarization can be utilized to achieve angle-tuned phase matching. The dashed lines in these figures show the cross section of the index surfaces $n_{2\omega}$ at the harmonic frequency. As can be seen, the negative uniaxial crystal has sufficient birefringence to offset dispersion, and the matching condition can be satisfied for a beam deviating from the z-axis by the angle θ_{m}.

The directions for phase-matched second harmonic generation are obtained by considering the intersection of the index surfaces at the fundamental and harmonic frequencies. As was mentioned earlier, frequency doubling may be considered as a special case, where two incident waves with electric fields E_m and E_n are identical wave forms. In a negative uniaxial crystal there are two loci where the index surfaces intersect and $\Delta k(\theta) = 0$ depending on the two possible orientations for the linear polarization vectors of the incident beams. In the type I process the two input waves have the same polarization and in the type II process the waves are orthogonally polarized.

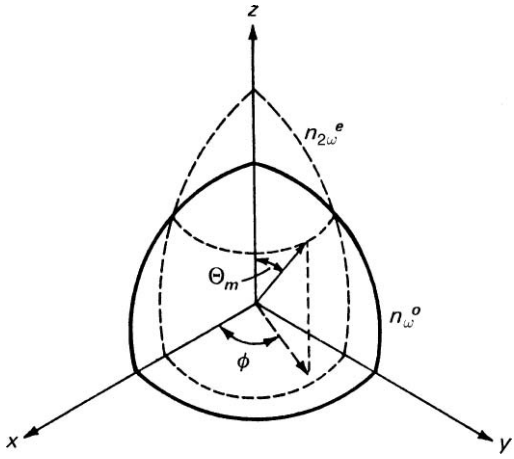

Fig. 10.9. Direction for phase-matched second harmonic generation (type I) in a uniaxial crystal, where θ_{m} is the phase matching angle measured from z, and ϕ is the azimuth angle measured from x.

Type I Phase Matching

Phase matching can occur in a symmetrical cone at θ_m about the optic axis, where two o-rays at ω are matched to an e-ray at 2ω.

$$n_{2\omega}^{\mathrm{e}}(\theta_m) = n_{\omega}^{\mathrm{o}} \tag{10.33}$$

The phase-matching angle θ_m is obtained by combining (10.32) and (10.33)

$$\sin^2\theta_m = \frac{(n_{\omega}^{\mathrm{o}})^{-2} - (n_{2\omega}^{\mathrm{o}})^{-2}}{(n_{2\omega}^{\mathrm{e}})^{-2} - (n_{2\omega}^{\mathrm{o}})^{-2}}. \tag{10.34}$$

Owing to its application in large Nd:Glass lasers, the nonlinear crystal KDP has been analyzed in great detail. We will use KDP as an example to illustrate phase matching.

For frequency doubling of 1.05-μm radiation, the beam propagation vector is at $\theta_m = 41^\circ$ with respect to the optical axis of the KDP crystal, and the azimuth angle is at $\phi = 45^\circ$ in type I phase matching. The fundamental beam is polarized perpendicular to the optical axis (ordinary direction) and the frequency doubled beam is polarized parallel to the optical axis of the crystal (extraordinary direction). The orientation of the beam propagation vector, polarization, and crystal axes is illustrated in Fig. 10.10a for the case of KDP.

The harmonic power is not independent of the azimuth angle of the phase-matched direction (Fig. 10.9). In general, d_{eff} is a combination of one or several coefficients of $\chi^{(2)}$, and the angles θ and ϕ, which define the direction of the wave propagation vector. For example, for KDP and its isomorphs and type I index matching, one obtains [10.16]

$$d_{\mathrm{eff}} = d_{36}\sin 2\phi \sin\theta_m \tag{10.35}$$

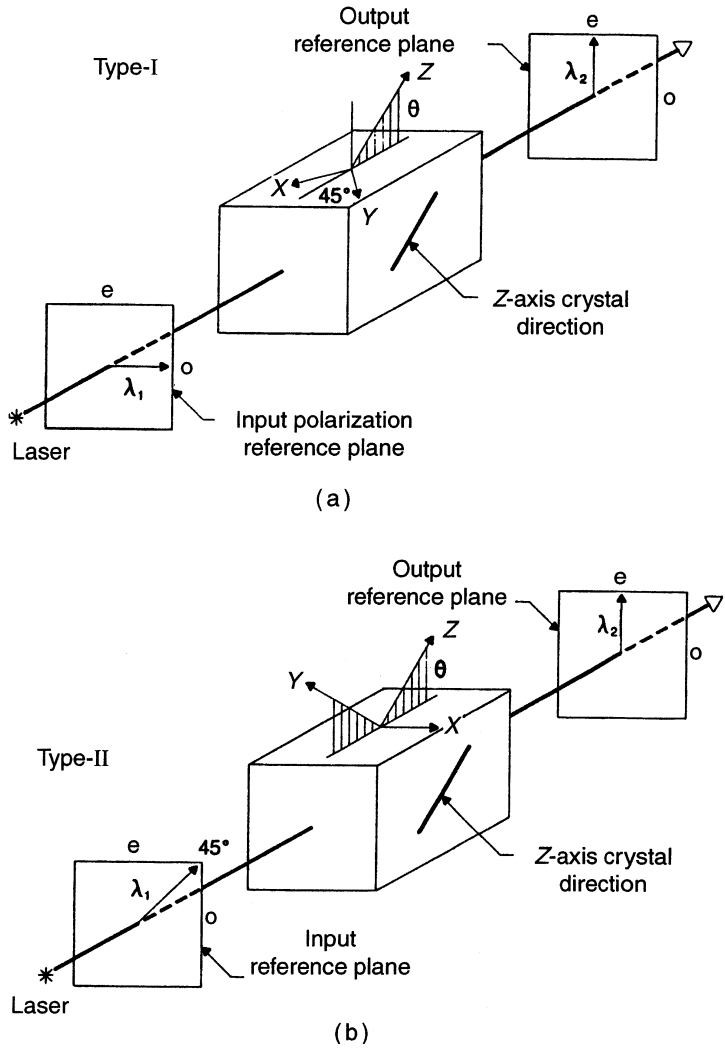

Fig. 10.10. Crystal and electric vector orientation for harmonic generation in KDP and its isomorphs for (a) type I and (b) type II phase matching [10.15]

Type II Phase Matching

In this case phase matching occurs in a cone at θ_{m} about the optic axis where an o-ray and an e-ray at ω are matched to an e-ray at 2ω. For negative uniaxial crystals

$$n^{\mathrm{e}}_{2\omega}(\theta_m) = (1/2)[n^{\mathrm{e}}_{\omega}(\theta_m) + n^{\mathrm{o}}_{\omega}]. \tag{10.36}$$

Solution of (10.36) may be obtained numerically. For KDP, the angle between the beam direction and the crystal axis is $\theta_{\mathrm{m}} = 59^\circ$ and $\phi = 90^\circ$ with respect to the x-axis.

A single linearly polarized fundamental beam incident on the crystal may be equally divided into o- and e-rays by orienting the polarization vector at 45° with respect to the x-axis. The polarization vector of the harmonic beam is rotated 45° from the fundamental beam with the polarization parallel to the optical axis (see Fig. 10.10b). For type II phase matching in KDP one obtains [10.16]

$$d_{\text{eff}} = (1/2)(d_{36} + d_{14}) \cos 2\phi \sin 2\theta_m \tag{10.37}$$

Comparing type I and type II phase matching, we find that type I is more favorable when θ_{m} is near 90°, whereas type II leads to a higher d_{eff} when θ_{m} lies near 45°.

Parameters Affecting the Phase Matching Condition

Owing to the dependence of the refractive indices on angle, temperature, and wavelength, any change of these parameters will cause a deviation from the exact phase matching condition. The sensitivity of second harmonic conversion to these parameters is obtained by treating Δk in (10.18) as a function of angle, temperature, and wavelength, i.e., $\Delta k = \Delta k(\theta, T, \lambda)$. Values of the angular, thermal, and spectral sensitivity of important nonlinear crystals are summarized in Subsect. 10.2.3.

With the exception of tunable lasers and Nd:Glass lasers, the line width of most solid-state lasers is sufficiently narrow for efficient harmonic conversion. It should be noted, however, that the sensitivity of the phase matching angle to laser line width increases dramatically at shorter wavelengths and can become an issue in frequency quadrupling of infrared lasers. In Nd:Glass lasers, the spectral line width is narrowed by employing Nd:YLF oscillators to drive the Nd:Glass amplifier chains.

Thermal loading of the nonlinear crystal caused by absorption of the fundamental or harmonic beam or by multiphoton absorption processes can result in a phase mismatch. Absorption in the crystal will lead to thermal gradients as well as thermally induced stresses. Heating of the nonlinear crystal caused by residual absorption is particularly a problem in doubling of high-power cw beams. Temperature changes of the doubling crystal may also be the result of ambient temperature variations. An example of the temperature tuning range of $Ba_2NaNb_5O_{15}$ is shown in Fig. 10.1. Because of its importance, angular sensitivity will be discussed in greater detail below.

Angular Sensitivity. Dephasing depends on the deviation of the beam direction from the phase matching angle that is caused by the divergence of the input beam or by an imperfect crystal orientation.

For type I phase matching we can derive an analytical expression for the angular sensitivity. Introducing (10.33) into (10.18) gives the following expression for the phase mismatch

$$\Delta k = \frac{4\pi}{\lambda_0}[n^{\text{o}}_{\omega} - n^{\text{e}}_{2\omega}(\theta)]. \tag{10.38}$$

For a direction close to the perfect phase matching direction θ_{m} we can express the difference of the refractive indices as follows

$$n_{\omega}^{\mathrm{o}} - n_{2\omega}^{\mathrm{e}}(\theta) = \frac{\partial[n_{\omega}^{\mathrm{o}} - n_{2\omega}^{\mathrm{e}}(\theta)]}{\partial\theta}(\theta - \theta_m) \tag{10.39}$$

The dependence of $n_{2\omega}^{\mathrm{e}}$ on the angular direction in the crystal is given in (10.32). To simplify the calculation, Eq. (10.32) can be approximated as follows:

$$n_{2\omega}^{\mathrm{e}}(\theta) = n_{2\omega}^{\mathrm{o}} - (n_{2\omega}^{\mathrm{o}} - n_{2\omega}^{\mathrm{e}})\sin^2\theta. \tag{10.40}$$

Introducing (10.40) into (10.39) yields

$$n_{\omega}^{\mathrm{o}} - n_{2\omega}^{\mathrm{e}}(\theta) = \partial\theta(n_{2\omega}^{\mathrm{o}} - n_{2\omega}^{\mathrm{e}})\sin 2\theta_m, \tag{10.41}$$

where we note that $\partial n_{\omega}^{\mathrm{o}}/\partial\theta = 0$ and $\partial n_{2\omega}^{\mathrm{o}} = \partial\theta = 0$.

With the result of (10.41) we can express the wave vector mismatch defined in (10.38) as follows:

$$\Delta k = \beta_\theta \delta\theta, \tag{10.42}$$

where

$$\beta_\theta = \frac{4\pi}{\lambda_0}(n_{2\omega}^{\mathrm{o}} - n_{2\omega}^{\mathrm{e}})\sin 2\theta_m. \tag{10.43}$$

In the above expression β_θ is the angular sensitivity of the nonlinear crystal and $\delta\theta$ is the deviation of a ray from the phase matching direction inside the crystal. We will equate this angle with the expansion half angle of a multimode beam inside the crystal

$$\theta/2 = (\lambda_0/\pi n_0 w_0)M. \tag{10.44}$$

This is the same equation as presented in Chap. 5, except for the inclusion of n_0 since beam divergence is measured inside the crystal. If we define the beam divergence outside the crystal, as is customary, the refractive index n_0 in (10.44) is removed and included in the angular sensitivity (β_θ/n_0) as was done in (10.31).

The angular sensitivity is inversely proportional to the so-called angular acceptance angle of the crystal. The angle $\Delta\theta$ describes the angular bandwidth at full width and half maximum (FWHM). In other words, it is the full acceptance angle over which the crystal can be tilted before the second harmonic power decreases to less than half. If the angular tuning range is stated for an internal angle, the value has to be multiplied by the refractive index of the crystal to convert it to an external angle.

Figure 10.11 illustrates the angular tuning range for a barium borate crystal. The curve is obtained from the expression (10.19a) for low conversion efficiency $I_{2w} \sim \mathrm{sinc}^2(\Delta kL/2)$, and $\Delta k = (\beta_\theta/n_0)\delta\theta$ given in (10.42), where $\delta\theta$ is measured external to the crystal. The values of BBO are $\beta_\theta/n_0 = 6.6$ (mrad cm)$^{-1}$ and $L = 0.7$ cm. Experimental data can be found in [10.18].

From (10.19a) it follows that the conversion efficiency will be reduced to one-half of its peak value for

$$\Delta kL/2 = 1.39. \tag{10.45}$$

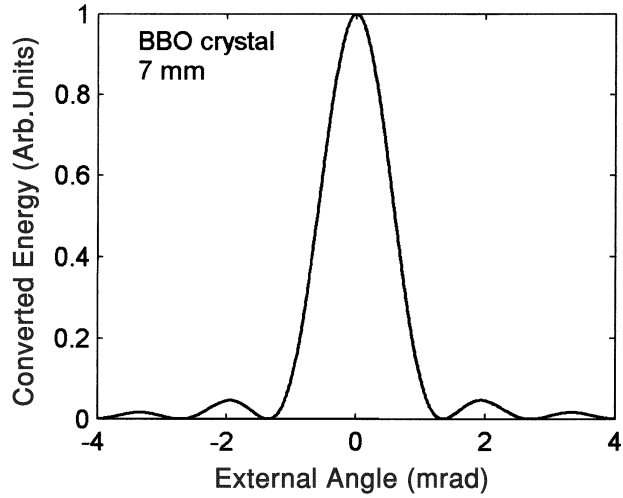

Fig. 10.11. Angular dependence of hamonic power generation in BBO at low conversion efficiency for a 7-mm-long crystal

If we eliminate Δk in (10.42) with the aid of (10.45) we obtain an expression for the acceptance angle of the crystal

$$\Delta\theta = \frac{5.56}{(\beta_\theta/n_0)L}. \tag{10.46}$$

In the literature, values for β_θ or β_θ/n_0 are published depending whether the angular deviation from the phase matching condition is measured inside or outside the crystal.

Critical and Noncritical Phase Matching

If phase matching can be accomplished at an angle of 90° with respect to the optical axis ($\theta_m = 90°$) we can make the approximation $\sin 2(90° + \delta\theta) \approx 2\delta\theta$ in (10.43). Instead of Δk being linear with $\delta\theta$, the dependence of Δk on beam divergence or angular misalignment is now a much smaller quadratic term

$$\Delta k = \beta'_\theta(\delta\theta)^2, \tag{10.47}$$

where

$$\beta'_\theta = (8\pi/\lambda_0)(n^{\mathrm{o}}_{2\omega} - n^{\mathrm{e}}_{2\omega}).$$

Another important advantage of phase matching at $\theta_m = 90°$ is the absence of walk-off caused by double refraction. If phase matching is accomplished at an angle other than 90° with respect to the optic axis, the direction of power flow (Poynting vector) of the fundamental and second harmonics will not be completely collinear but occur at a small angle. For a negative uniaxial crystal and type I phase matching,

this angle is given by [10.17]

$$\tan \rho = \frac{(n_\omega^{\mathrm{o}})^2}{2}\left[\frac{1}{(n_{2\omega}^{\mathrm{e}})^2} - \frac{1}{(n_{2\omega}^{\mathrm{o}})^2}\right]\sin 2\theta. \tag{10.48}$$

The angle ρ has the effect of limiting the effective crystal length over which harmonic generation can take place. The distance at which the fundamental and harmonic beam just separate is called the aperture length l_{a}. For Gaussian beams the aperture length is

$$l_{\mathrm{a}} = \sqrt{\pi}\, w_0/\rho \tag{10.49}$$

where w_0 is the fundamental beam radius.

Because of this beam walk-off and the much smaller angular tolerance, phase matching at angles other than one of the principal axes of the crystal is called critical phase matching. The difference between critical and noncritical phase matching can be illustrated by comparing two uniaxial crystals. Phase matching in KDP type I for second harmonic generation at 1.064-μm requires an angle of $\theta_m = 41^\circ$ between the beam direction and optic axis. Provided that n_ω^{o} and $n_{2\omega}^{\mathrm{e}}$ are nearly equal and $d(n_\omega^{\mathrm{o}} - n_{2\omega}^{\mathrm{e}})/dT \neq 0$, noncritical phase matching can be achieved by temperature-tuning the crystal for type I phase matching in uniaxial crystals. One example is $LiNbO_3$. Second harmonic generation in $LiNbO_3$ occurs at $\theta_m = 90^\circ$ for 1.064-μm radiation, provided the crystal is at a temperature of 107°C (for a crystal doped with 5% MgO). As a result of the noncritical phase matching, $LiNbO_3$ has a much larger angular tolerance, and the beam divergence introduces a phase shift Δk that is over an order of magnitude smaller in $LiNbO_3$ as compared to KDP (see next section).

10.2.3 Properties of Nonlinear Crystals

Table 10.1 lists phase matching parameters and properties of several important nonlinear materials for 1064 to 532 nm conversion [10.16, 19–25]. Frequency doubling of neodymium lasers is one of the major applications of harmonic generation.

From purely theoretical considerations it would seem that the crystal with the highest nonlinear coefficient would be the most desirable material to use in a doubling experiment. However, for a nonlinear crystal to be of practical use, damage threshold, optical quality chemical stability, and hardness are of equal importance. For example, despite the lower nonlinear coefficient of KDP compared to the other materials discussed in this section, conversion efficiencies as high as 80% have been obtained from these crystals. Since a high conversion efficiency is actually the result of material properties as well as pump source characteristics, the high peak power, narrow spectral bandwidth, small beam divergence, and clean spatial and temporal beam profiles obtained from Nd:Glass lasers employed in fusion research make possible such high harmonic conversions even in crystals with modest nonlinearity. Another example is Barium sodium niobate ($Ba_2NaNb_5O_{15}$) featured in Fig. 10.1, which has a nonlinear coefficient 38 times larger than KDP. The material showed great

Table 10.1. Phase matching parameters for 1064 to 532 nm conversion

	Crystal				
	KDP	KTP[a]	BBO	LBO[a]	$LiNbO_3$[b]
Phase matching parameters					
Type	I	II	I	I	I
Angle[°]	41.2	24.3	22.8	11	90
Temperature [°C]	25	25	25	25	107
Efficiency parameters					
Eff. nonlinear coefficient d_{eff}[pm/V]	0.37	3.18	1.94	1.16	4.7
External angular sensitivity β_θ / n_0[(mrad cm)$^{-1}$]	1.73	0.35	6.6	0.65	0.12
Walk-off angle[°]	1.60	0.26	3.19	0.35	0
Bandwidth (FWHM)					
Angular $L\Delta\theta$ [mr cm]	3.2	15.9	0.84	8.5	46.3
Thermal $L\Delta T$[°C cm]	6.7	25	55	8.4	0.7
Spectral $L\Delta\lambda$[nm cm]	0.66	0.56	0.66	0.75	0.23
Material parameters					
Refractive index n^{o}	1.49	1.74, 1.75	1.65	1.56, 1.56	2.23
n^{e}	1.46	1.84	1.54	1.61	2.15
Absorption [%/cm]	0.5	0.5	0.5	0.5	0.2
Damage threshold [GM/cm^2]	8	1	1.5	2.5	0.2

[a] Biaxial crystal.
[b] Doped with 5% MgO.

promise initially but index variations introduced during the growth process could not be eliminated and production was dropped.

At the present time, the leading candidate material for nonlinear experiments with solid-state lasers is KTP since the crystal has a large nonlinear coefficient, high damage threshold, and a large angular and temperature acceptance range. Its major drawbacks are the limited size (about 1–2 cm^3) and the high cost associated with the difficult growth process. KDP is superior to any other nonlinear crystal with regard to availability in large sizes combined with an excellent optical quality. Crystals with cross sections of 30 cm^2 have been produced. Crystals grown from the melt such as $LiNbO_3$ or KTP are generally hard, chemically stable, and can easily be polished and coated. Solution-grown crystals such as KDP and its isomorphs are soft and hygroscopic. These crystals need to be protected from the atmosphere.

From Table 10.1 it follows that KDP has the lowest nonlinear coefficient of the crystals listed but the highest damage threshold; the reverse is true for $LiNbO_3$. The other crystals KDP, LBQ, and BBO are in between these two extremes. Damage threshold is the parameter where the published values show large variations because the result of a measurement depends on pulse duration, beam quality, spot size, and whether surface or bulk damage is considered. For Q-switch pulses in the 10- to 20-ns range, typical damage threshold are about 400–500 MW/cm^2 for the crystals listed, except $LiNbO_3$ which has a much lower threshold. The values in the GW/cm^2 range listed in Table 10.1 are for subnanosecond pulses.

An idea of a crystal's sensitivity to a departure in angle, temperature, and wavelength from the ideal phase matching condition can be gleaned from the respective bandwidth data. However, it should be pointed out that the bandwidth is defined at the low conversion limit (10.19a). As we have seen from the results displayed in Fig. 10.3, second harmonic generation becomes increasingly more sensitive to changes in Δk as the intensity increases, i.e., the bandwidth decreases at high efficiencies. For example, at a nonlinear drive of $\eta_0 = 3$, the efficiency drops one half from 0.9 to 0.45 for a change in dephasing of $\delta = 1.0$. The change of δ required to reduce efficiency by one half in the low conversion limit is, according to (10.45), a factor $\delta = 1.39$.

A more useful parameter for efficiency calculations is therefore the angular sensitivity also listed in Table 10.1. As was explained earlier, in a 90° phase matching condition the effect of beam divergence on the interaction length is minimized. This explains the large acceptance angle of $LiNbO_3$.

If birefringence is a slow function of temperature, then the crystal has a wide central peak, making it easier to maintain peak output in the presence of small temperature fluctuations. In this regard, KTP and BBO outperform other crystals. Crystals which have a birefringence that is not strongly dependent on wavelength allow efficient doubling of laser beams that have a broad spectral bandwidth.

KDP and Its Isomorphs. The crystals of this family have proven to be an important group of useful second harmonic generators. The most prominent member of this group of nonlinear crystals is potassium dihydrogen phosphate, KH_2PO_4 (symbol KDP). Because of the availability of large aperture harmonic crystal assemblies, KDP is the material of choice for the large Nd:Glass lasers employed in fusion research. Other related crystals are potassium dideuterium phosphate, KD_2PO_4 (symbol KD*P); cesium dihydrogen arsenate (CDA) and cesium dideuterium arsenate, CsD_2AsO_4 (symbol CD*A); and ammonium dihydrogen phosphate, $NH_4H_2PO_4$ (symbol ADP). The crystals which are all negative uniaxial are grown at room temperature from a water solution which makes large, distortion-free, single crystals available. Transparency exists from about 0.22 to 1.6 μm.

Deuteration increases the infrared limit to about 1.9 μm. The greatest attributes of this family of crystals are their resistance to laser damage and their high optical quality. Opposing these advantages are several disadvantages. The materials have fairly low refractive indices, typically 1.50–1.55, and therefore they have small nonlinear coefficients. All of the KDP isomorphs are water-soluble and have a maximum safe operating temperature of about 100°C. The crystals are sensitive to thermal shock, and should be heated slowly at a rate of less than about 5°C/min.

ADP and KDP were the first crystals used for the demonstration of phase-matched second harmonic generation. Some of the other isomorphs have been used because the temperature dependence of their refractive index allows noncritical phase matching for particular interactions. For example, CDA and CD*A 90° phase-match the important 1.06-μm transition of Nd:YAG and Nd:Glass. With the exception of KDP, the isomorphs have been replaced by the other crystals mentioned in Table 10.1. Calculations of various basic properties of KDP related to the generation of the second, third, and fourth harmonics of 1-μm laser radiation for five different conversion processes

can be found in [10.19]. Figure 10.10 shows the crystal and electric vector orientation for harmonic generation in KDP and its isomorphs.

Potassium Titanyl Phosphate (KTP)

The crystal $KTiOPO_4$ (KTP) is a unique nonlinear optical material that is being widely used for second harmonic generation of Nd lasers emitting around 1 μm. KTP is also very attractive for various sum and difference frequency and optical parametric applications over its entire transparency range from 0.35 to 4.0 μm. Although a few specific characteristics of other materials are better, KTP has a combination of properties that make it unique for second-order nonlinear optical applications, and second harmonic generation of Nd lasers. In particular, the crystal has large nonlinear coefficients; and the adequate birefringence in the y–z and the x–z planes allows phase matching of the more efficient type II process over a large wavelength range. It has wide acceptance angles, an unusually large temperature bandwidth, relatively good thermal properties, and a high damage threshold. KTP is the best nonlinear material for Nd:lasers to emerge in recent years. The major drawback is the difficult growth process required to produce these crystals, which leads to high cost and small-size crystals.

KTP decomposes on melting (≈1150°C) and hence normal melt processes cannot be used to grow this material. However, single crystals of KTP can be grown by both hydrothermal and flux techniques. Currently crystals up to 20 mm in length are commercially available. KTP crystallizes in the orthorhombic point group mm2. The crystal structure, refractive indices, and phase matching parameters have been reported in [10.16, 22].

Figure 10.12 shows the transmission curve for KTP. The material is transparent from 0.35 μm to about 4.0 μm. The optical spectrum is structure-free except for traces of OH^- absorption bands observed at 2.8 and 3.5 μm.

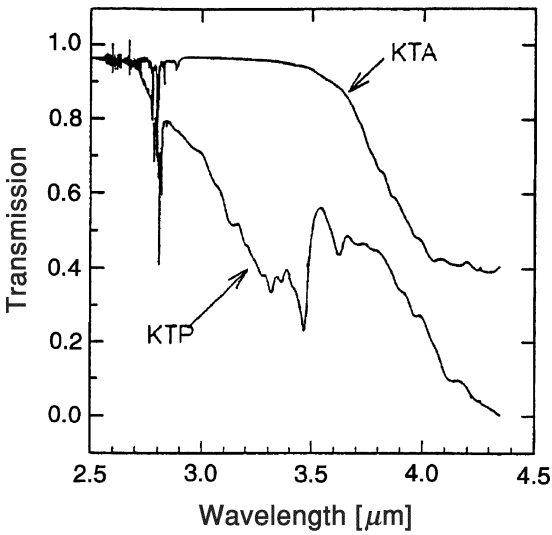

Fig. 10.12. Optical transmission of KTP and KTA [10.20]

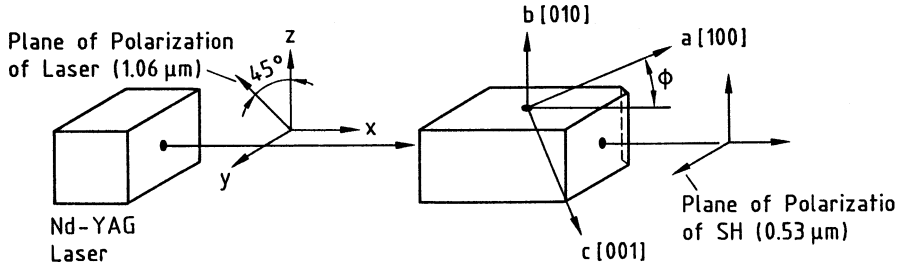

Fig. 10.13. Orientation of KTP for type-II interaction at 1.06 μm. $\phi = 26°$ for hydrothermally and $\phi = 21°$ for flux-grown material [10.21]

Figure 10.13 shows the crystal orientation for the phase match condition of the type II interaction at 1.06 μm. It should be noted that the phase match angle ϕ measured from the x-axis in the xy plane is different for flux and hydrothermally grown crystals. The phase match direction in KTP for second harmonic generation of 1.06-μm radiation results in a walk-off angle of 4.5 mrad between the fundamental and second harmonic beam.

Frequency-doubling efficiencies in excess of 65% are now routinely obtained from KTP pumped by high-quality laser beams. However, KTP suffers from gradual photochemical degradation (gray tracking) which is cumulative with exposure to a combination of second harmonic and fundamental radiation. This degradation leads to increased absorption in the crystal, which can eventually cause crystal failure. The photochemical effect is reversed by operating the KTP at an elevated temperature. Crystals operating at flux levels of 150MW/cm^2 and temperatures of 80°C have shown lifetimes in excess of 20 million pulses with >60% conversion efficiency. However, there have been failures owing to bulk damage in crystals operated at 65°C and lower. (see also Sect. 11.3.4).

Potassium Titanyl Arsenate (KTA)

KTA is isomorphic with KTP, but has lower absorption losses in the 3–6 μm region (see Fig. 10.12). It has about the same nonlinear coefficients and high damage threshold of KTP. Since KTA does not phase-match a 1.06-μm laser for second harmonic generation, the main attraction of this material is for applications in optical parametric oscillators. Properties of this material can be found in [10.23].

Lithium Triborate (LBO)

LiB_3O_5 (LBO) is a nonlinear optical crystal characterized by good UV transparency, a high optical-damage threshold, and a moderate nonlinear optical coefficient [10.24–26]. These properties, along with its mechanical hardness, chemical stability, and nonhygroscopicity, make LBO an attractive alternative to KTP. A number of laser systems have been reported that employ LBO for frequency doubling of pulsed as

well as cw-pumped introcavity-doubled Nd lasers. For example, up to 105 W in the green has been reported with a pulsed laser (see Sect. 10.2.6).

At a temperature of 148°C, LBO can be noncritically phase-matched at 1064 nm for second harmonic generation. In this case the acceptance angular bandwidth is 52 mr cm ($\theta = 90^\circ$, $\Phi = 0$). This large acceptance angle combined with the high damage threshold permits tight focusing of the fundamental beam in introcavity frequency-doubled systems.

For second harmonic generation of low- and medium-power Nd lasers KTP is generally preferred owing to its larger nonlinear coefficient. For second harmonic conversion at high peak powers or high average powers LBO has the advantage of a higher damage threshold.

Beta-Barium Borate. The material β-BaB_2O_4 (BBO) is a nonlinear optical crystal which possesses excellent properties for nonlinear frequency conversion in a. spectral range that extends from the ultraviolet to the mid-infrared. This material has a moderately large nonlinear coefficient, a large temperature tolerance, low absorption, and a very high damage threshold. The principal shortcoming with BBO is the low angular tolerance of 0.8 mr cm, which requires a diffraction-limited beam for efficient frequency doubling.

BBO is of particular interest for frequency doubling into the blue region. The transmission band for BBO extends to 200 nm in the UV so that single or multiphoton absorption is not a problem with this material. BBO has been used to double the output of a Ti:Sapphire laser with efficiencies up to 60%. Relevant data can be found in [10.16, 24, 27].

Lithium Niobate ($LiNbO_3$). This material is nonhygroscopic and hard, taking a good polish readily. The uniaxial crystal, belonging to the trigonal point group 3m, has a large nonlinear coefficient relative to KDP. The crystals of lithium niobate are transparent in the region of 0.42–4.2 μm. Temperature sensitivity of birefringence is such that, by varying the temperature, phase matching can be achieved at 90° to the optical axis.

Unfortunately, $LiNbO_3$ is particularly susceptible to photorefractive damage from visible or UV radiation. This optical-index damage is reversible if the ambient temperature of the crystal is increased to about 170°C, which is above the annealing temperature for the photorefractive damage. Doping of $LiNbO_3$ with 5% of MgO reduces photorefractive damage and permits noncritical phase matching at a somewhat lower temperature, namely 107°C [10.28].

Despite the high nonlinear coefficient, and the ease of handling and polishing, the need for operation at elevated temperatures combined with a relatively low damage threshold have severely limited practical applications for this material.

The emergence of periodically poled $LiNbO_3$ (PPLN), which will be discussed in Sect. 10.3, has attracted renewed interest in this material. In PPLN, the largest nonlinear index of $LiNbO_3$ can be utilized. This allows efficient nonlinear conversion at modest power levels which are well below the damage threshold.

Cesium Borate (CBO)

Besides BBO and LBO there are two other members of the borates that are important for harmonic generation with solid-state lasers, namely CsB_3O_5 (CBO) and $CsLiB_6O_{10}$ (CLBO). The latter two crystals are mainly of interest for UV and deep UV production. Acceptance of these crystals was hampered in the past by the availability of high-quality crystals. It has been reported that a new modified crystal growth process improved the quality of borate crystals [10.29]. Both CBO and CLBO are hygroscopic and are usually operated at elevated temperatures between 100 and 140°C.

In [10.30], third harmonic generation at 355 nm by use of a type II CBO crystal is described. The output at the third harmonic was 3 W obtained at a repetition rate of 31 KHz. Conversion efficiency from the fundamental to the third harmonic reached 30%. The same reference contains also the nonlinear characteristics of a number of borate crystals for the generation of 355-nm radiation. At a phase matching angle of 40.2° for type II conversion, CBO yields a nonlinear coefficient of $d_{\text{eff}} = 1.15$ pm/V. The acceptance angular bandwidth of type II is larger compared to the other borates.

Cesium Lithium Borate (CLBO)

Generation of short-wavelength UV radiation with solid-state lasers is of interest for photolithography and for writing gratings into fibers. Borate crystals have a UV cutoff wavelength between 160 and 190 nm. The shortest wavelength and the most powerful output in the UV regime has been obtained with the nonlinear crystal $CsLiB_6O_{10}$ (CLBO). It is the primary candidate for the generation of deep UV radiation.

By mixing the third harmonic of an Nd:YLF laser with the output from a Ti:Sapphire laser using two CLBO crystals an output of 1.5 W at 196 nm was obtained. [10.31]. Phase matching properties for the generation of 241 nm and 196 nm radiation with CLBO are also listed in this reference. With CLBO as the nonlinear crystal over 20 W at 266 nm was generated by frequency-doubling a green laser Q-switched at 10 KHz [10.32]. The 15-mm-long CLBO crystal was cut for type I conversion and heated to 140°C to prevent hygroscopic deterioration. Fourth and fifth harmonic generation in CLBO with 28% and 7% conversion efficiency, respectively, have been obtained from a repetitively Q-switched Nd:YAG laser [10.33]. The average power was 2.5 W at 266 nm and 0.6 W at 213 nm. The fifth harmonic was generated by sum frequency mixing of the fourth harmonic with the fundamental wavelength. Experiments carried out with CLBO and BBO revealed that the conversion efficiency was limited in both cases by thermal effects caused by UV absorption. However, CLBO had almost a factor 3 lower absorption.

In another system CLBO was used to produce radiation at 236 nm which is the fourth harmonic of a 946 nm Nd:YAG laser [10.34]. The crystal was operated at noncritical phase matching, which occurs at–15°C for these wavelengths. In this case, the crystal was mounted in a vacuum-tight housing to prevent deterioration. For

fourth harmonic generation of a 1064-nm Nd:YAG laser, BBO has a slightly larger nonlinear coefficient; however, at shorter wavelength than 266 nm CLBO has a larger nonlinearity.

10.2.4 Intracavity Frequency Doubling

In the previous section we discussed frequency doubling by placing a nonlinear crystal in the output beam of the laser system. Frequency-doubling a cw-pumped laser system in this manner results in an unacceptably low harmonic power because large conversion efficiencies require power densities which are not available from a cw-pumped laser. One obvious solution to this problem is to place the nonlinear crystal inside the laser resonator, where the intracavity power is approximately a factor $(1 + R)/(1 - R)$ larger than the output power. The power is coupled out of the resonator at the second harmonic wavelength by replacing the output mirror with transmission T by one which is 100% reflective at the fundamental and totally transmitting at the second harmonic. Functionally, the second harmonic crystal acts as an output coupler in a manner analogous to the transmitting mirror of a normal laser. Normally the transmitting mirror couples out power at the laser frequency, whereas the nonlinear crystal inside the laser couples out power at twice the laser frequency. Because advantage is taken of the high power density inside the laser cavity, it is only necessary to achieve a conversion efficiency equal to the optimum mirror transmission to convert completely the available output at the fundamental to the harmonic. For example, for a cw-pumped Nd:YAG laser with an optimum output coupling of $T = 0.1$, an intracavity conversion efficiency of 10% will produce an external conversion of 100%, in the sense that the total 0.53-μm power generated in both directions by the nonlinear crystal is equal to the maximum 1.06-μm power, which could be extracted from the cavity without the nonlinear crystal.

There are several disadvantages associated with intracavity doubling. A nonlinear crystal of poor optical quality will drastically degrade the performance of the laser. Amplitude fluctuations are strongly magnified by the combination of the nonlinear process and the gain of the active material. The harmonic power is generated in two directions, which requires an additional dichroic mirror for combining the two beams. The other alternative to intracavity doubling of a cw laser is external doubling with a strongly focused beam. However, crystal acceptance angles are frequently too narrow to permit tight focusing of the beam onto the crystal. For pulsed-pumped operation, on the other hand, the fraction of intracavity power that is coupled out is so high that there is little advantage in placing the crystal inside the laser.

The choice of nonlinear materials for intracavity frequency doubling of the Nd:YAG, Nd:YLF, and Nd : YVO_4 lasers are KTP, BBO, LBO, and PPLN. Compared to pulsed-pumped systems, in internally frequency-doubled cw lasers the average power is usually high and the peak power low. Therefore, a high nonlinear coefficient, small absorption losses, and good optical quality are the determining factors for the selection of a particular crystal. In order to increase the conversion efficiency of cw-pumped systems, the power density can be increased by employing an acousto-optic Q-switch or mode locker in the resonator.

Simplification of the basic introcavity doubling design is achieved by using a gain medium that also functions as the nonlinear material. Combining both gain and nonlinearity into a single crystal is appealing from a device point of view. The most attractive nonlinear gain medium is Nd:YAB, which is a dilute form of the stoichiometric neodymium compound neodymium aluminum borate (NAB). Diode-pumped Nd:YAB lasers with output powers over 1 W in the green as well as tunable output in the green/yellow spectrum have been demonstrated [10.35]. The tunable laser employed a birefringent filter for wavelength selection. Since the thermally sensitive phase matching process takes place in the presence of pump-related thermal gradients, accurate temperature control is required.

Cavity Configuration

There are several factors which affect the choice of a laser cavity configuration. In order to achieve efficient harmonic generation it is important to obtain a high power density inside the nonlinear crystal. Concurrently, the intracavity beam must be large enough inside the laser medium to utilize the maximum volume which can contribute to TEM_{00} mode oscillation. This generally requires that the beam cross-sectional area must be larger inside the laser medium than inside the nonlinear crystal.

Intracavity harmonic generation produces a beam of harmonic power in both directions. Only the harmonic wave emitted toward the output mirror is emitted; the harmonic beam traveling in the opposite direction is mostly absorbed by the laser medium. In order to capture both beams a dichroic mirror that reflects the second harmonic and transmits the fundamental can be inserted between the doubling crystal and the laser rod. If the dichroic coating is applied directly to the surface of the doubling crystal facing the laser crystal the need for an additional mirror is eliminated.

The more common approach for combining the frequency-doubled beams and for providing a large mode volume in the laser medium and tight focusing in the nonlinear crystal is accomplished with L-, V-, or Z-shaped resonators. One example of an L-shaped resonator configuration is illustrated in Fig. 10.14. The 45° dichroic mirror is

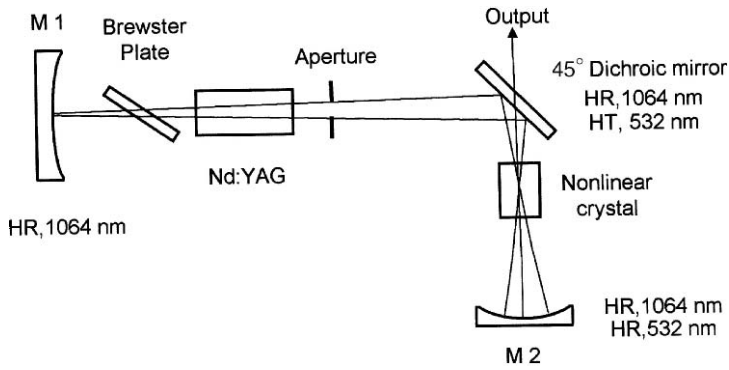

Fig. 10.14. Three-mirror L-shaped resonator configuration

designed to reflect the 1064-nm beam and transmit the orthogonally polarized 532-nm beam. Mirror M_2 is highly reflective for both wavelengths. The resonator is typically designed to obtain an adequate TEM_{00} mode volume in the laser medium and a small waist at the nonlinear crystal. This is achieved by a short-radius mirror M_2 close to the nonlinear crystal and a large-radius mirror M_1 behind the laser medium. Designs have been published with a beam diameter of 1.8 mm inside the laser rod and spot size of 25 μm inside the nonlinear crystal. More typical is a ratio of about 10 between the two diameters. If the angle between the two legs of the resonator is less than 90° a V-shaped configuration is obtained.

In long resonators the phase shifts due to dispersion between the 1.06- and 0.53-μm beams in the air path between the doubling crystal and the dielectric coating of mirror M_2 must be adjusted so that they are in phase as they reenter the doubling crystal after reflection from M_2. This is accomplished by providing a translation adjustment for the mirror M_2 to move it toward or away from the doubling crystal, such that the net phase shift between the two waves is a multiple of 2π. The computed phase shift, based on the measured 1.06- to 0.53-μm dispersion of air of 3.6×10^{-6} μm^{-1}, is approximately 29.0°/cm. For doubling of the 1.06-μm line of Nd:YAG, this requires a mirror movement of no more than 3.28 cm [10.36], and the accuracy required to correct for the phase shift is of the order of millimeters.

As the pump power in a laser is changed, the focal length of the thermal lens formed by the laser crystal varies. This changes the spot size of the beam throughout the resonator. In particular the spot size in the nonlinear crystal can decrease to a point which causes damage. A resonator that minimizes changes of the beam size inside the nonlinear crystal despite large changes of thermal lensing is the Z-shaped resonator illustrated in Fig. 10.15. The resonator consists of four mirrors, whereby the two concave mirrors represent a telescope which relays the image of the hard aperture at one end of the laser rod into the nonlinear crystal. This is the same type of optical relay described in Chap. 4 that is commonly used in large Nd:Glass amplifiers.

Depending on the magnification the relay optics also transforms the larger spot size in the laser crystal to the smaller beam inside the laser crystal. Typical magnifications determined by the ratio of the mirror radius range between 2 and 2.5. The resonator shown in Fig. 10.15 contains also a Q-switch for power enhancement. With resonators of the type illustrated in Fig. 10.15 and including an acoustic-optic Q-switch, harmonic power in excess of 100 W have been generated [10.37, 38].

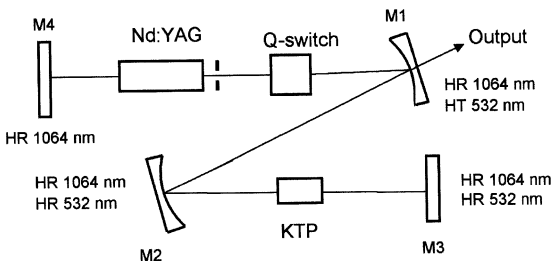

Fig. 10.15. Resonator Z-configuration for high power generation

An analysis of optical second harmonic generation internal to the laser cavity has been presented in [10.39, 40]. The steady-state condition for intracavity doubling can be determined if we equate the round-trip saturated gain of the laser to the sum of the linear and nonlinear losses

$$\frac{2g_0 l}{1 + I/I_s} = \delta + \kappa I, \tag{10.50}$$

where g_0 is the unsaturated gain coefficient, l is the length of the laser medium, I is the power density in the laser rod, and I_s is the saturation power density of the active material. All linear losses occurring at the fundamental frequency are lumped together into the parameter δ; the quantity κI is the nonlinear loss. If we express the saturated gain coefficient g by the small signal gain coefficient $g_0/(1 + I/I_s)$ in (3.7), we see that κI in (10.50) is equivalent to the transmission T of a normal laser.

The nonlinear coupling factor κ, defined by

$$I(2\omega) = \kappa I^2(\omega), \tag{10.51a}$$

is related to the nonlinear factor C defined in (10.19b)

$$\kappa = (I_{\mathrm{NC}}/I_{\mathrm{L}}) l^2 C^2, \tag{10.51b}$$

where $I_{\mathrm{NC}}/I_{\mathrm{L}}$ accounts for the different power densities in the laser medium (I_{L}) and nonlinear crystal (I_{NC}), and l is the crystal length.

The maximum second harmonic power as a function of κ is obtained from (10.50) by differentiating and $dI/d\kappa = 0$.

$$\kappa_{\max} = \delta/I_{\mathrm{s}}. \tag{10.52}$$

The magnitude of the nonlinearity required for optimum second harmonic production is proportional to the loss, inversely proportional to the saturation density, and independent of the gain. Thus, for a given loss, optimum coupling is achieved for all values of gain and, hence, all power levels. As we recall from Chap. 3, in a laser operating at the fundamental wavelength the optimum output coupling of the front mirror is gain-dependent. The usefulness of (10.52) stems from the fact that by introducing the material parameters for a particular crystal into (10.52) and combining with (10.19b), the optimum length of the nonlinear crystal is obtained.

For example, $Ba_2NaNb_5O_{15}$ has a nonlinear factor of $C = 38\ \mathrm{GW}^{-1/2}$. With $I_{\mathrm{s}} = 2.9\ \mathrm{KW/cm}^2$ for Nd:YAG, and assuming a round-trip loss of $\delta = 0.02$ and a power-density enhancement of $I_{\mathrm{NC}}/I_{\mathrm{C}} = 50$, we obtain an optimum crystal length of $l = 0.5$ cm from (10.52, 53).

From the theory presented in [10.40], it follows that if the insertion loss of the second harmonic crystal is small compared to the total internal loss, the value of κ is the same for fundamental and second harmonic output coupling. Also, the maximum second harmonic power equals the fundamental power obtainable from the same laser.

In most systems, the second harmonic power is considerably below the output power which can be achieved at the fundamental wavelength. Insertion losses of the

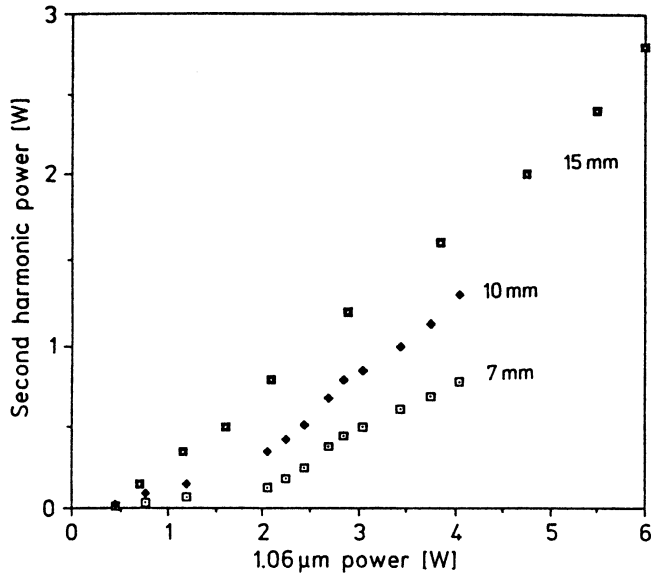

Fig. 10.16. Comparison of fundamental and second harmonic output from a cw-pumped intracavity frequency-doubled Nd:YAG laser for different KTP crystal lengths

nonlinear crystal, or any other additional intracavity element, are often the reason for the poor performance, or in the case of Nd:YAG, thermally induced depolarization losses can have a major effect. In low-gain lasers employed for intracavity harmonic generation, even small insertion losses are very detrimental to the system performance. The effect of intracavity losses on the laser performance has been analyzed in detail in [10.39]. For example, in a laser with a round-trip gain coefficient of $2g_0l = 0.2$, the output drops 20% if the internal loss is increased from 2 to 3%. Furthermore, availability of crystals and damage considerations lead often to nonoptimum conditions as far as crystal length and pump-power density are concerned.

As an example, the performance of a typical intracavity-doubled Nd:YAG laser is illustrated in Fig. 10.16. The output at the harmonic wavelength is compared to the TEM_{00} output available at 1.064 μm from the same laser. The Nd:YAG laser employed in these experiments was cw-pumped by diode arrays and intracavity-doubled with KTP. After measuring the output at 1.064 μm, a KTP crystal was inserted in the folded resonator and the output coupler was replaced with a mirror of high reflectivity at 1.064 and 0.53 μm. For the short crystals, the nonlinear coupling factor κ is too small and far from optimum. A higher output at 532 nm would require tighter focusing of the beam. However, this makes alignment very critical and sacrifices mechnical and thermal stability of the laser. A longer nonlinear crystal is therefore a better solution. However, a 15-mm-long crystal is about the longest crystal available for KTP.

It is commonly observed that the output from a continuously pumped, intracavity-doubled laser is much less stable than the output obtained from the same laser without

the nonlinear crystal in the resonator. Typically, one observes large amplitude fluctuations of the harmonic power consisting of a series of random spikes superimposed upon the cw background. The nature of these severe power instabilities, termed the green problem, is caused by the nonlinear interaction of the longitudinal modes in the harmonic generator and has been analyzed in [10.41]. A typical laser resonator contains a large number of longitudinal modes, each with a well-defined polarization and a gain and loss that is time-dependent since it is a function of the instantaneous mode intensity.

In a multimode laser two nonlinear processes occur simultaneously in the harmonic generator, namely frequency doubling and sum frequency generation. Frequency doubling converts an individual mode to the harmonic, whereas in sum frequency generation two separate modes interact to produce a harmonic. The dynamics of intracavity doubled lasers can be modeled by a set of rate equations, one for each longitudinal mode. Solutions of these nonlinear equations show instability and chaotic behavior. Hole burning has been considered in [10.42] as an additional contributor to instabilities because it forces the laser to jump to different modes.

From the analysis in [10.41] it follows that the amplitude fluctuations should disappear if the laser is restricted to operate in a single longitudinal mode. This is consistent with the observation that a laser containing etalons or a birefringent filter for mode selection does not exhibit chaotic behavior.

The birefringent filter is typically formed by a combination of the birefringent nonlinear crystal such as KTP and a polarizer or by a combination of the nonlinear crystal and a laser crystal such as Nd:YVO_4 which has a polarized output. For example, in [10.43] a single longitudinal mode laser is described that consists of an end-pumped Nd:YAG crystal, a Brewster plate, and a KTP crystal with its axis at 45° to the axis of the Brewster plate. In KTP the linearly polarized fundamental beam is split into an ordinary and extraordinary component because phase matching does not occur at 90° with respect to the optical axis. The radiation leaves the crystal elliptically polarized. After one round trip there is a certain phase difference between the ordinary and extraordinary ray. When this phase difference is an integral of π the wave still has p-plane polarization and the loss passing through the Brewster plate will be zero. Mode selection is provided because the phase shift depends on the wavelength, which is different for different modes.

If one uses an Nd:YVO_4 crystal instead of Nd:YAG, the Brewster plate can be eliminated because of the polarized output from the laser crystal. In this case the combination of the Nd:YVO_4 laser crystal and the KTP nonlinear crystal acts as a birefringent filter. Such a laser end-pumped with fiber-coupled laser diodes produced stable output of 3.2 W [10.44]. The problem with birefringent filters is the fact that they need to be temperature-controlled. For example, the above-mentioned system required temperature control of the two crystals to within 0.1°C to obtain stable single-mode output.

The coupling of orthogonal linearly polarized modes through the sum frequency generation process can be eliminated by modifying the polarization of the laser modes in the doubling crystal. The instabilities caused by coupling of modes with different polarizations are effectively suppressed by inserting a quarter wave plate in the

resonator for the fundamental wavelength [10.45]. The modes will be linearly polarized parallel to the axis of the quarter waveplate which reduces the likelihood of chaotic fluctuations.

Actually, the thermally induced birefringence in an Nd:YAG crystal was found sufficient to eliminate chaotic amplitude fluctuation of the laser by proper rotation of the Nd:YAG and KTP crystal [10.46]. Again as in the system mentioned above, modes which are linearly polarized in a specific direction have lower losses as compared to orthogonally polarized modes.

In the so-called twisted mode approach hole burning and mode hopping are avoided by placing the Nd:YAG crystal between two quarter waveplates. With the beam polarized by a Brewster plate, the laser polarization vector within the crystal rotates with a period equal to the laser wavelength. Unlike the traditional standing wave cavity where the gain exhibits nodes and antinodes, in this case the gain is constant along the beam axis.

A steady-state solution derived in [10.46] predicts that the stability of an intracavity frequency-doubled laser increases with round-trip time and the number of oscillating modes. It was indeed demonstrated experimentally [10.47] that output fluctuations and random behavior in cw frequency-doubled systems can be greatly reduced by a long resonator. The measurements were performed with a lamp-pumped Nd:YLF laser, introcavity frequency-doubled with LBO, which provided as much as 13.5 W in a 1.9 m long resonator. The instabilities arising from orthogonally polarized modes were eliminated in this laser by temperature tuning the crystal at 142°C. This provides type I noncritical phase matching and therefore the fundamental beam remains linearly polarized as it propagates through the crystal.

Most of the approaches mentioned above require the insertion of additional elements in the resonator or very accurate temperature stabilization. For this reason, a number of commercial lasers employ a long resonator as a means to achieve stable second harmonic output.

The highest average harmonic output is obtained if intracavity frequency doubling is combined with repetitive Q-switching. In a typical system the resonator contains an acoustic-optic Q-switch in addition to the harmonic generator as indicated in Fig. 10.15. The pulse repetition rate is in the KHz range. Owing to the higher gain and larger spot sizes compared to cw systems the resonator is less sensitive to adjustments and perturbations. Repetitively Q-switched and internally doubled lasers with high harmonic outputs are described in [10.37, 38, 48, 49].

The harmonic power extracted from the laser can be related to the pumping rate above threshold and to the coupling coefficient if one considers the effects of pump depletion and pulse stretching [10.50]. In a regular Q-switched laser the transmission of the output mirror is higher compared to cw operation because of the high gain. Similarly the coupling factor κ is higher in case of a repetitively Q-switched and internally doubled laser.

Intracavity harmonic generation can also be combined with mode locking [10.51, 52]. Since the harmonic conversion efficiency is highest at the peak of the mode-locked pulses, the harmonic conversion process tends to flatten and broaden the pulses, opposing the modulator's efforts to sharpen the pulses.

10.2.5 Third Harmonic Generation

Efficient conversion of the output of a laser to the third harmonic is an example of sum frequency generation via the process of three-wave mixing. The interaction of two input waves at frequencies ω and 2ω in a nonlinear medium produces a third wave at the sum frequency 3ω as a result of second-order nonlinear polarization.

The sum frequency generation is governed by three factors: (a) the nonlinear drive, i.e., the intensity of the input beams, (b) the phase mismatch between the three interacting waves, and (c) the ratio of the intensities of the two input beams.

A third harmonic converter consists of two crystals—the first crystal is a second harmonic generator (doubler) and produces at its output radiation at ω and 2ω. In the sum frequency mixing process of the second crystal (tripler) unconverted fundamental radiation of the first stage is mixed with the second harmonic to produce the third harmonic. In this arrangement, the total output of the frequency doubler becomes the input to the sum frequency stage.

Besides the nonlinear drive and dephasing, the two parameters that also determine the efficiency of frequency doubling, third harmonic generation places an additional constraint on the laser system since for efficient tripling the ratio of ω and 2ω photons incident on the sum frequency mixing crystal is very important.

The mix of ω and 2ω photons will be expressed as the ratio of second harmonic intensity to total intensity at the entrance to the sum frequency stage.

$$M = \frac{I_{2\omega}}{I_{\omega} + I_{2\omega}}. \tag{10.53}$$

The optimum situation is achieved if, for three photons at the fundamental frequency ω entering the first crystal, two photons are converted to create a photon at 2ω, and the third photon at ω is combined in the second crystal with the 2ω photon to produce one 3ω photon. This situation is depicted in Fig. 10.17 for type I/type II and type II/type II cascaded third harmonic generation.

In a nonabsorbing doubling crystal, the parameter M is also equivalent to the conversion efficiency of the doubler. Therefore, the mix of equal ω and 2ω photons at the exit of the doubling crystal requires $M = 2/3$. Given this photon ratio, in a nonabsorbing and perfectly matched crystal, a complete conversion of the fundamental beam to the third harmonic is theoretically possible.

Complete conversion as indicated in Fig. 10.17 occurs only for the experimentally unrealizable condition of perfect phase matching and photon mix over the whole cross section and pulse duration of the beam. In actual systems one can only hope to approach these conditions as close as possible. If conversion is incomplete then the output of the sum frequency stage contains, besides the third harmonic, residual outputs at the fundamental and second harmonic as indicated by $I_{\omega}{}'$ and $I_{2\omega}{}'$ in Fig. 10.18.

Third harmonic generation can be analyzed starting with the general equations (10.14) governing frequency mixing for plane waves in a nonabsorbing medium.

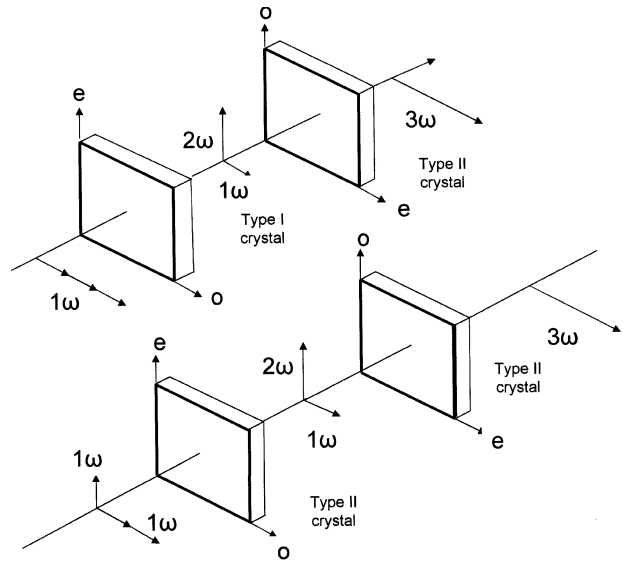

Fig. 10.17. Cascaded third harmonic generation with (a) type I/type II and (b) type II/type II phase matching

With $\omega_1 = \omega$, $\omega_2 = 2\omega$, $\omega_3 = 3\omega$, and $E_1 = E_\omega$, $E_2 = E_{2\omega}$, $E_3 = E_{3\omega}$, we can rewrite (10.14).

$$\frac{dE_\omega}{dz} = -i\omega\sqrt{\mu_0/\varepsilon_\omega}\, d_{ijk} E_{3\omega} E^*_{2\omega} \exp(-i\Delta k z) \tag{10.54a}$$

$$\frac{dE_{2\omega}}{dz} = -2i\omega\sqrt{\mu_0/\varepsilon_{2\omega}}\, d_{kij} E^*_{\omega} E_{3\omega} \exp(-i\Delta k z) \tag{10.54b}$$

$$\frac{dE_{3\omega}}{dz} = -3i\omega\sqrt{\mu_0/\varepsilon_{3\omega}}\, d_{jik} E_{\omega} E_{2\omega} \exp(i\Delta k z) \tag{10.54c}$$

Since we have omitted terms that relate to absorption losses in the nonlinear crystal, equations (10.54) can be solved analytically [10.8, 10], and the overall efficiency of

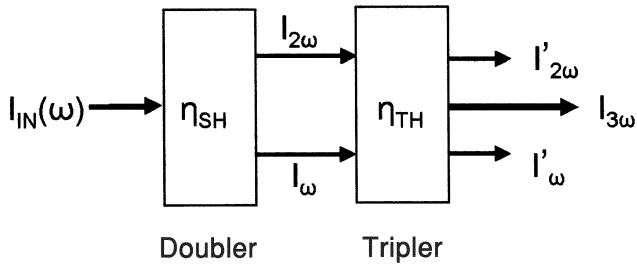

Fig. 10.18. Cascaded third harmonic generation with a second harmonic generator followed by a sum frequency stage

third harmonic generation can be calculated.

$$\eta_{\mathrm{TH}} = \frac{I_{3\omega}}{I_\omega + I_{2\omega}}. \tag{10.55}$$

In (10.55) $I_{3\omega}$ is the output at the third harmonic and $I_\omega + I_{2\omega}$ is the input to the tripler, that is, the same as the total input $I_{\mathrm{in}}(\omega)$ from the laser driving the two stages since we are assuming a lossless conversion process (see Fig. 10.18).

Integration of the coupled differential equations (10.54) for the case of perfect phase matching ($\Delta k = 0$) leads to the following expression for the efficiency of third harmonic conversion [10.10].

$$\begin{aligned}
&\eta_{\mathrm{TH}} = \eta_m sn^2[(\eta_0/\eta_m)^{1/2}, m], \\
\text{where}\quad &\eta_0 = 9M^2(1-M)C^2L^2I_{\mathrm{in}}(\omega) \\
\text{and}\quad &\eta_m = (3/2)M, \quad m = M/2(1-M) \qquad \text{for } M \le 0.67 \\
&\eta_m = 3(1-M), \quad m = 2(1-M)/M \quad \text{for } M \ge 0.67.
\end{aligned} \tag{10.56}$$

Not surprising, the expression for η_{TH} has the same form as obtained for frequency doubling since both frequency doubling and tripling are based on sum frequency mixing. Equation (10.56) contains the Jacobi elliptic function with argument $\sqrt{\eta_0/\eta_m}$ and modulus m. The nonlinear drive η_0, modulus m, and the maximum efficiency η_{m} are all functions of the mixing ratio M between ω and 2ω photons. The other parameters of (10.56) are the crystal length L, the nonlinear factor C defined in (10.21), and $I_{\mathrm{in}}(\omega) = I_\omega + I_{2\omega}$, which is the total combined beam intensity at the entrance of the tripling stage.

Figure 10.19 illustrates the overall efficiency of third harmonic generation for two different intensity ratios of the two beams entering the sum frequency stage. Illustrated is third harmonic generation of a 1064-nm fundamental beam mixed with the second harmonic entering a KDP crystal that is used in the sum frequency stage. The nonlinear crystal is characterized by $C = 0.97\ \mathrm{GW}^{-1/2}$ and $L = 1$ cm. The maximum conversion efficiency is achieved for $M = 0.67$ which represents the ideal 1:1 mix of ω and 2ω photons. For $M = 0.40$ the conversion efficiency in the doubler is too low, leading to an excess of ω photon at the entrance of the sum frequency stage. Fig. 10.19 can be applied to different crystals by scaling the input intensity according to $C^2L^2I_{in}(\omega)$.

For the ideal 1:1 mix of ω and 2ω photons we obtain with $M = 0.67$, a modulus of $m = 1$ and a maximum efficiency $\eta_m = 1$ from (10.56). This reduces the expression of (10.56) to

$$\eta_{\mathrm{TH}} = \tanh^2 \sqrt{2C^2L^2I_{\mathrm{in}}(\omega)}. \tag{10.57}$$

In this case the photons of both beams are depleted at the same rate and the result is similar to the perfect phase matching condition of second harmonic generation. The efficiency saturates at 100% as the input intensity increases. For other mixing ratios, after the waves have propagated a distance in the crystal, the number of photons in one of the waves depletes to zero, and the energy transfer reverses. The energy is then cycled between the waves, and in a nonabsorbing crystal, the conversion efficiency

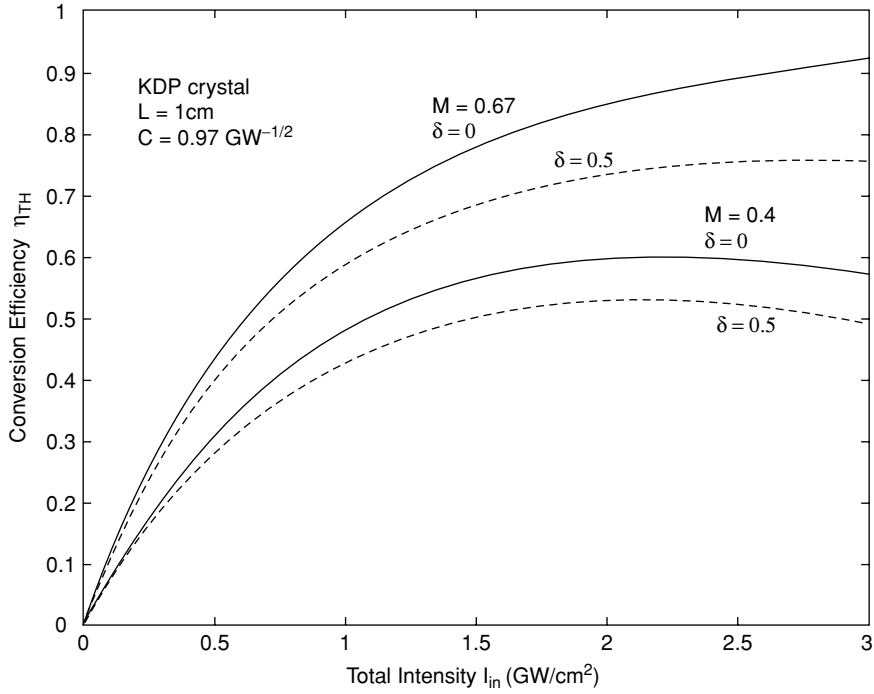

Fig. 10.19. Efficiency of third harmonic generation of a 1064 nm beam in a 10-mm-long KDP crystal. M is the ratio of the intensity of the green beam to total beam intensity entering the tripler. In a nonabsorbing crystal, M is the conversion efficiency of the doubler

oscillates as a function of the input intensity with a period determined by the modulus of the Jacobi function.

If one includes nonperfect phase matching in (10.56) the modulus m and maximum efficiency η_{m} include expressions for the dephasing δ. For the case $M \leq 0.67$ we obtain (if $\delta > 0$ minus sign, if $\delta = 0$ plus sign)

$$m = [2 - \sigma + \varepsilon \mp \sqrt{(\sigma - \varepsilon)^2 + 4\varepsilon}]^2/4(1 - \sigma) \tag{10.58a}$$

and

$$\eta_m = (3/4)M[2 - \sigma + \varepsilon \mp \sqrt{(\sigma - \varepsilon)^2 + 4\varepsilon}], \tag{10.58b}$$

where $\sigma = (3M - 2)/M, \quad \varepsilon = 3\delta^2(1 - M)/\eta_0.$

The nonlinear drive η_0 has been defined in (10.56) and dephasing δ in (10.27).

In (10.58) the conversion efficiency of the sum frequency process is described by only three parameters: the nonlinear drive η_0, phase mismatch δ, and the ratio of intensities M of the two waves being mixed.

The detrimental effect of dephasing on the overall efficiency of third harmonic generation is illustrated by the dashed curves in Fig. 10.19. A dephasing of $\delta = 0.5$ was assumed in calculating third harmonic generation for the two cases previously described. The reduction of the conversion efficiency caused by a phase mismatch between the interacting waves can be clearly seen.

Third harmonic generation is very important for frequency up-conversion of high-energy Nd:Glass lasers employed in fusion research. In these lasers the frequency converters are constructed from two potassium dihydrogen phosphate (KDP) crystals arranged in tandem. Since the diffraction-limited, high-intensity beams typically generate a second harmonic output with an efficiency around 80%, a number of schemes have been devised to detune the first stage in order to achieve the optimum 67% conversion. The desired intensity mix at the output of the doubler can be achieved by controlling the length of the doubling crystal by adjusting the propagation direction of the fundamental beam relative to the phase matching direction (angular tilt) or by a polarization mismatch [10.53, 54]. For example, in the latter approach the polarization vector of the fundamental beam is at 35° with respect to the "o" direction of the KDP crystal instead of the usual 45° as depicted in Fig. 10.10b.

10.2.6 Examples of Harmonic Generation

Examples of several different types of laser systems which incorporate harmonic generators will illustrate the technology. Figure l0.20 depicts a typical three-mirror internally frequency-doubled laser configuration. Employing a KTP crystal, harmonic generation with an output power of 3.9 W at 532 nm by intracavity frequency doubling in an Nd:YAG laser oscillator acousto-optically Q-switched at 10 KHz has been demonstrated [10.55]. The laser head contained a 25 mm by 3 mm Nd:YAG crystal side-pumped by six 1-cm-long diode arrays which were arranged symmetrically around the rod in two sets of three arrays each. The optical pump power at 807 nm was 60 W. At the fundamental output, the laser oscillator produced 12 W multimode and 5.5 W TEM_{00} Q-switched average power. The optimal fundamental power was obtained with a 96% reflecting mirror.

A hemispherical laser cavity was employed to obtain TEM_{00} operation with reasonable extraction efficiency while at the same time giving a tight beam waist for intracavity doubling. Using a type II doubling crystal, the intracavity flux incident upon the crystal was maximized by placing it at the waist of the cavity mode. The length of the KTP crystal was 15 mm. To improve the doubling efficiency, and to obtain a unidirectional output, the cavity was folded with a dichroic mirror, and the 1.06-μm output coupler used to obtain optimum fundamental output was replaced with a high reflector at 1,06 and 0.532 μm.

Figure 10.20a illustrates the optical schematic of the folded resonator-configuration. The performance of the acousto-optically Q-switched laser is depicted in Fig 10.20b, which exhibits the average power produced at 1.06 μm (for optimum coupling) and at 0.532 μm when the output coupler is replaced by a total reflector at 1.06 and 0.532 μm.

Figure 10.21 shows the schematic of an end-pumped intracavity frequency doubled and Q-switched Nd:YAG laser [10.56]. The system uses the same type of three-mirror L-shaped resonator, as shown in the previous figure. Also, the average output in the green is about the same as in the previous example. However, because of the more efficient pump arrangement, only 30 W of optical pump power is required, compared to 60 W for the side-pumped laser. In the design depicted in Fig. 10.20, the Nd:YAG

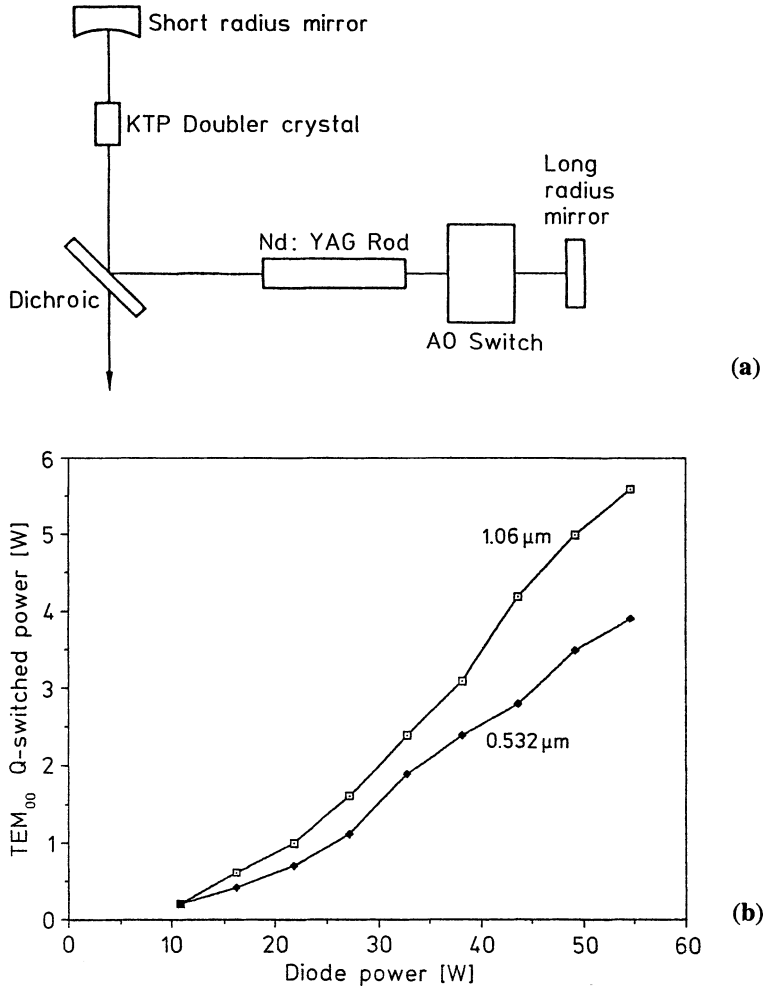

Fig. 10.20. Optical schematic (a) and fundamental and second harmonic average output power from a repetitively Q-switched cw-pumped Nd:YAG laser (b)

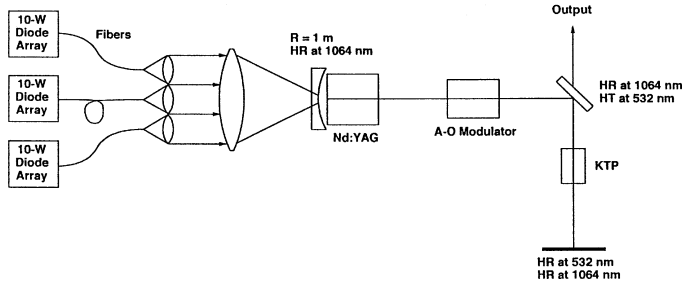

Fig. 10.21. Schematic of an end-pumped Q-switched and internally frequency-doubled cw-pumped Nd:YAG laser [10.56]

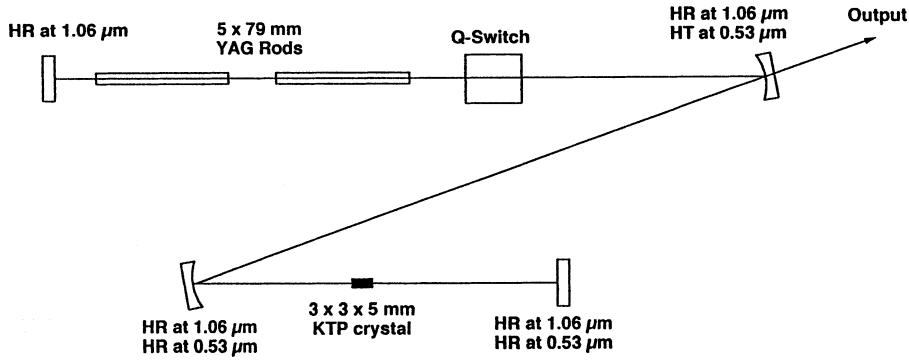

Fig. 10.22. High-power second harmonic generation in an internally frequency-doubled Nd:YAG laser featuring a "Z" resonator with relay optics [10.38]

crystal is pumped with the combined output of three fiber-coupled diode laser arrays. The fiber output of each pump was first collimated and then focused with a single lens onto one end of the Nd:YAG rod. The laser produced 3.5 W average power in the green at a repetition rate of 50 kHz in a nearly diffraction-limited beam.

At the high end of intracavity second harmonic generation, one finds krypton arc lamp and diode-pumped Nd:YAG lasers, AO Q-switched and intracavity doubled with KTP or LBO, which have generated in excess of 100 W at the harmonic [10.37, 38, 48, 49].

An illustration of such a high-average-power second harmonic generation system is given in Fig. 10.22 [10.38]. This design features a Z-shaped resonator, containing two laser heads, a Q-switch, and a KTP crystal. The laser was repetitively Q-switched with an acousto-optic device at repetition rates ranging from 4 to 25 kHz. The laser operated in high-order multitransverse mode. An interesting feature of the design is an optical relay system formed by the two curved mirrors between the Nd:YAG rod and the KTP crystal. One plane of this optical relay is at the end face of the YAG rod closest to the KTP crystal and the other plane is in the center of the KTP crystal. As explained in Sect. 10.2.4, the purpose of the relay optics is to keep the spot size in the KTP crystal as constant as possible, despite large changes of thermal lensing in the rods. The optical relay images the hard aperture of the laser rod into the KTP crystal, and therefore the multimode spot size in the KTP is fairly constant over a large range of pump power. The hard aperture at the rod was 4.9 mm, the relay optics was adjusted for a magnification of 2.5, and therefore a multimode spot size in the KTP crystal of about 2 mm was created. Particularly at these high power levels, a well-controlled and fairly large spot size in the nonlinear crystal is very important in order to avoid material damage.

The system produced 106 W of average power at 0.532 μm when Q-switched at 17 kHz. The laser was also operated at 1.32 μm with a different set of optics. In this case, 23 W at 0.659 μm has been generated. The nonlinear crystal for doubling both

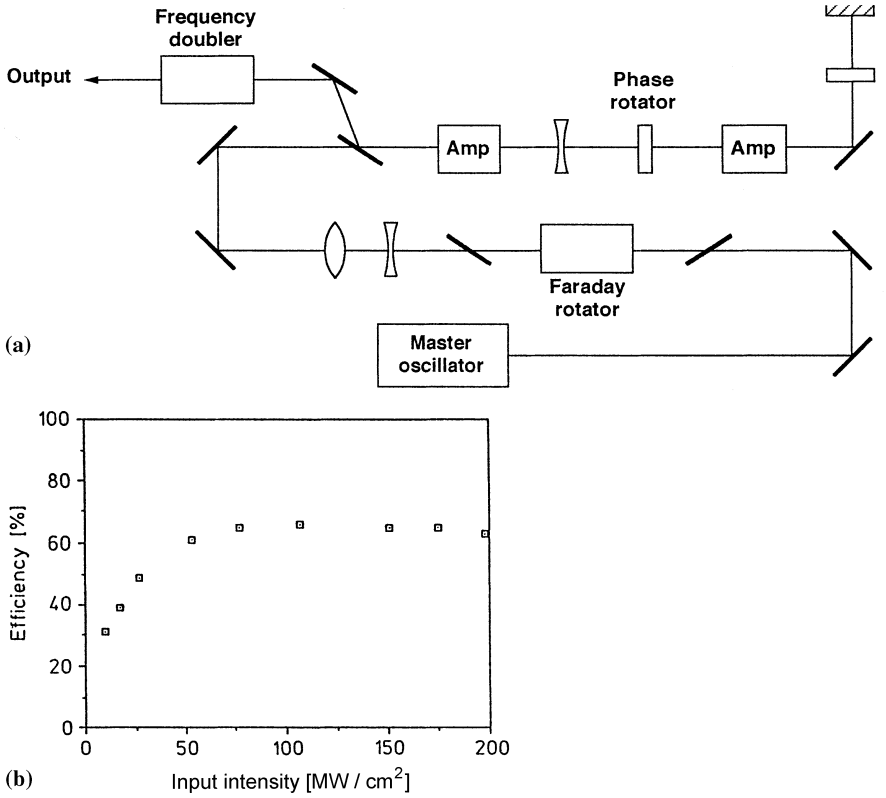

Fig. 10.23. High average power Q-switched and externally frequency doubled, MOPA system. Optical schematic (a) and conversion efficiency vs. pump intensity at the KTP crystal (b)

wavelengths was KTP. For 0.532 μm generation, the crystal was cut such that critical phase matching was obtained at the usual x–y plane, at $\theta = 90^\circ$ and $\phi = 23.5^\circ$. The cut used for 0.694 μm generation was such that phase matching in the x–z plane was achieved at $\phi = 0^\circ$ and $\theta = 60^\circ$.

Output of up to 40 W average power from an externally frequency-doubled, diode-pumped Nd:YAG oscillator amplifier system has been obtained. The system architecture is shown schematically in Fig. 10.23a [10.57]. The oscillator was Q-switched at a repetition rate of 100 Hz. The output from the amplifiers was 0.7 J per pulse at 1.064 μm in a 2×; diffraction-limited beam. At 0.532 μm, the energy per pulse was 400 mJ in a 17-ns pulse. Each laser head contains an Nd:YAG rod side-pumped with 5-bar laser diode arrays operated at 60 W/bar. In the oscillator, 80 bars pump a 5-mm-diameter rod, whereas in the amplifiers 160 bars are used each to pump the 9-mm rods.

Thermal lensing and birefringence of the amplifier is compensated with a lens and a 90° phase rotator. The output is doubled to the green with a 1-cm-long KTP

Table 10.2. Frequency conversion efficiencies achieved on the Argus laser

Wavelength [nm]	Conversion efficiency[%]	Maximum energy generated [J]	Output power [GW]
532	83	346	495
355	55	41	68
266	51	50	83

crystal heated to 100°C. As shown in Fig. 10.23b, near 60% conversion efficiency was achieved.

The requirement for generation of short wavelengths from inertial-confinement-fusion lasers has prompted the development of large-aperture harmonic converters for doubling, tripling, and quadrupling of the Nd:Glass laser output. As an example, we will consider conversion experiments originally carried out on the now dismantled Argus laser at the Lawrence Livermore National Laboratory [10.58]. Argus was an image-relayed, spatially filtered laser system capable of delivering up to 1 kJ output energy in a 600-ps pulse. Frequency conversion experiments were performed with a beam of 10-cm diameter and beam divergence of about 100 μrad. Table 10.2 summarizes the results for second, third, and fourth harmonic generation. Doubling efficiency as a function of input intensity for type I phase matching in a 2.29-cm-long KDP crystal is illustrated in Fig. 10.24. At intensities above 2.8 GW/cm^2 the crystal is overdriven and reconversion of 532 nm radiation to 1064 nm photons takes place as discussed earlier in this chapter. The plot shows, also the sensitivity of the conversion process on crystal alignment.

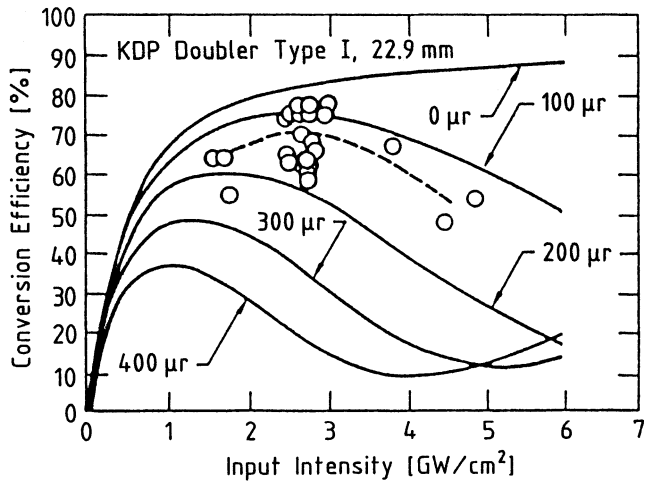

Fig. 10.24. Frequency-doubling efficiency as a function of input power [10.58]

10.3 Optical Parametric Oscillators

As was mentioned at the beginning of this chapter, two beams with different frequencies incident on a nonlinear crystal will generate a traveling polarization wave at the difference frequency. Provided the polarization wave travels at the same velocity as a freely propagating electromagnetic wave, cumulative growth will result. For reasons that will soon become clear, the two incident beams are termed "pump" and "signal" waves having a frequency of ν_p and ν_s, and the resulting third wave is termed an "idler" wave with frequency ν_i. Under proper conditions, the idler wave can mix with the pump beam to produce a traveling polarization wave at the signal frequency, phased such that growth of the signal wave results. The process continues with the signal and idler waves both growing, and the pump wave decaying as a function of distance in the crystal.

Since each pump photon with energy $h\nu_p$ is generating a photon at the signal ($h\nu_s$) and idler frequency ($h\nu_i$), energy conservation requires that

$$\frac{1}{\lambda_p} = \frac{1}{\lambda_s} + \frac{1}{\lambda_i}. \tag{10.59}$$

In order to achieve significant parametric amplification, it is required that at each of the three frequencies the generated polarization waves travel at the same velocity as a freely propagating electromagnetic wave. This will be the case if the refractive indices of the material are such that the k vectors satisfy the momentum-matching condition $k_p = k_s + k_i$. For collinearly propagating waves this may be written as

$$\frac{n_p}{\lambda_p} - \frac{n_s}{\lambda_s} - \frac{n_i}{\lambda_i} = 0, \tag{10.60}$$

where n_s, n_i, and n_p are the refractive indices at the signal, idler, and pump frequency, respectively.

Since the three indices of refraction depend on the wavelength, the direction of propagation in the crystal, and on the polarization of the waves, it is generally possible, by using birefringence and dispersion, to find conditions under which (10.60) is satisfied.

Tunability is a fundamental characteristic of all parametric devices. With the pump providing input at the fixed wavelength λ_p, small changes of the refractive index around the phase matching condition will change the signal and idler wavelengths such that a new phase matching condition is achieved. Tuning is possible by making use of the angular dependence of the birefringence of anisotropic crystals.

Figure 10.25 illustrates different configurations that make use of the parametric interaction process of three waves. The simplest device is a nonresonant configuration, namely an optical parametric amplifier (OPA), exhibited in Fig. 10.25(a). In this case, a pump beam and a signal beam are present at the input. If the output of a Q-switched laser is focused into the crystal and if the intensity of the pump is sufficiently high, and phase matching conditions are met, gain is obtained for the signal wave and at the

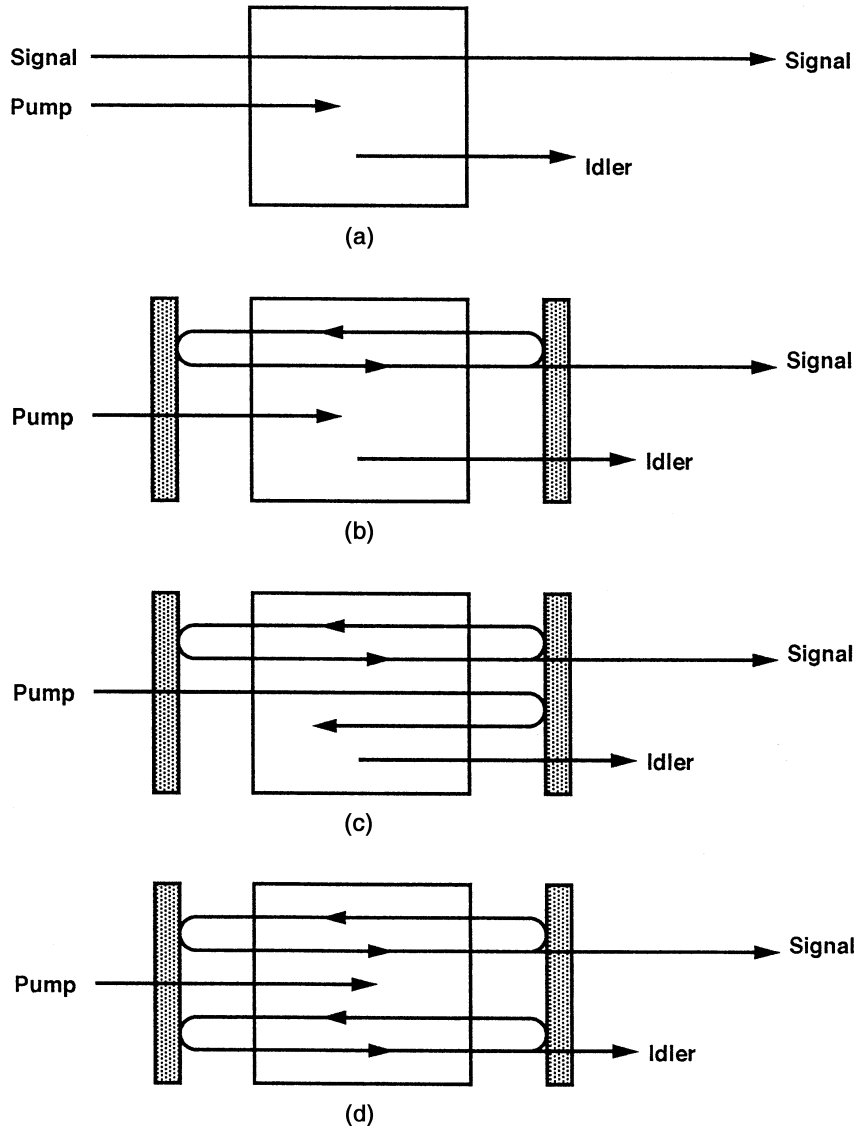

Fig. 10.25. Configurations for parametric interactions: (a) optical parametric amplifier (OPA); (b) singly resonant optical parametric oscillator (SRO); (c) singly resonant oscillator with pump beam reflected; (d) doubly resonant OPO (DRO)

same time an idler wave is generated. Typically, an OPA is used if the signal obtained from an optical parametric oscillator (OPO) is too weak and further amplification is desired.

The most common optical parametric device is the singly resonant oscillator depicted in Figs. 10.25b and c. In this device, the crystal is located inside a resonator that

provides feedback at either the signal or idler frequency. In the example illustrated, the pump beam enters through a mirror that is highly transmitting at the pump wavelength and highly reflective for the signal wavelength. In Fig. 10.25b the opposite mirror, which is the output coupler, has typically 80–95% reflectivity for the signal wavelength, and high transmission for the idler and pump beam. Only the signal wavelength is resonant in the cavity, and a small fraction is coupled out through the front mirror. In the configuration in Fig. 10.25c the pump beam is reflected at the output mirror and makes one return pass through the crystal. Since the input mirror through which the pump enters is highly transmissive for this wavelength, no resonance condition is set up for the pump wavelength. However, threshold is lowered, because on the return path the pump beam provides gain for the resonant signal wave.

Figure 10.25d depicts a doubly resonant oscillator (DRO), which provides feedback at both the signal and idler wavelengths. The double-resonance condition, in which both the signal and the idler waves are simultaneously resonant within the optical cavity, lowers the threshold significantly. However, this advantage of a DRO is offset by a reduction in stability and tunability. Maintaining the doubly resonant condition in a common resonator requires that the pump be single frequency and stable, and that the OPO cavity length be actively controlled to maintain the resonance condition.

Since the gain of a parametric device depends on power density, the design of a cw OPO presents a particular challenge. In the past, the design of cw OPOs was based on the use of doubly resonant oscillator configurations because of the lower pump power requirements. The need for active stabilization and single frequency pump lasers has placed major limitations on the utility of doubly resonant OPOs for practical devices outside the laboratory.

In recent years the increased availability of new nonlinear materials and high-power laser pump sources of high spatial and spectral beam quality have led to great advances in the development of singly resonant cw OPOs. Today, essentially all cw OPOs are singly resonant devices.

The first successful operation of an optical parametric oscillator was achieved by Giordmaine and Miller [10.59] in 1965. Their oscillator employed lithium niobate as the nonlinear material and used a 530-nm pump signal derived by frequency-doubling the 1.06-μm output of an Nd:$CaWO_4$ laser.

Since then considerable effort has been expended in understanding and improving the device performance, and numerous nonlinear materials were evaluated for possible use in practical devices. While the process of optical parametric conversion is conceptually simple and elegant, many difficulties have been encountered in realizing practical systems. Among the most serious has been optical damage to the nonlinear crystal, caused by the high electric fields necessary for nonlinear conversion. Typical damage thresholds for nonlinear materials are in the same range as the intensities required for efficient conversion. Another limitation for achieving high parametric conversion has been the poor beam quality of the pump sources themselves.

In recent times, however, these two problems have been overcome. First, new nonlinear crystals with high damage thresholds became available (for example, KTP, BBO, LBO) and a new class of nonlinear materials has been developed, namely

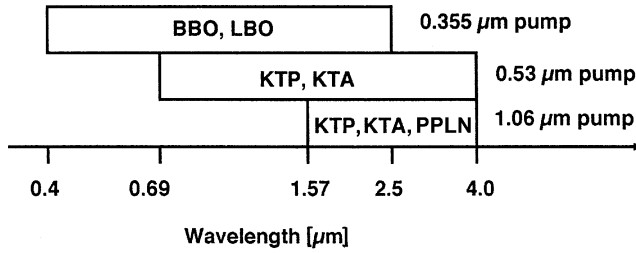

Fig. 10.26. Wavelength coverage of Nd:YAG or Nd:YLF pumped OPOs

periodically poled crystals such as $LiNbO_3$, that allow quasi phase matching, which has a number of advantages over birefringence phase matching, as will be explained in Sect. 10.3.3.

Second, diode pumping has provided a new generation of efficient high-power solid-state lasers with single-transverse-mode outputs and a high degree of pulse-to-pulse stability. The introduction of these new nonlinear materials in conjunction with diode-pumped solid-state lasers have resulted in a fairly mature technology, and pulsed or cw-pumped singly resonant OPOs are now common devices used to extend the spectral range of solid-state lasers.

As an example, Fig. 10.26 depicts the wavelength coverage of Nd:YAG or Nd:YLF laser pumped OPOs employing the above-mentioned nonlinear crystals. The optical parametric oscillator has been the subject of many papers and review articles; detailed discussions of the theory and summaries of earlier work on OPOs can be found in [10.60–62].

10.3.1 Performance Modeling

Of greatest interest for the design of parametric devices are simple models which describe gain, threshold, phase matching, and conversion efficiency as a function of device and input parameters.

For the amplifier depicted in Fig. 10.25a, a parametric gain coefficient for the amplification of the signal wave can be defined [10.62]

$$g = \sqrt{\kappa I_\mathrm{p}}, \tag{10.61}$$

where I_p is the pump flux and κ is a coupling constant

$$\kappa = \frac{8\pi^2 d_\mathrm{eff}^2}{\lambda_\mathrm{s}\lambda_\mathrm{i} n_\mathrm{s} n_\mathrm{i} n_\mathrm{p} \varepsilon_0 c}. \tag{10.62}$$

The effective nonlinear coefficient d_eff connects the pump, signal, and idler fields. The parameters n_p, n_s, n_i and λ_s and λ_i are the refractive indices of the three waves, and the wavelengths of the signal and idler wave, respectively.

The single-pass power gain of the parametric amplifier in the high-gain limit can be approximated by

$$G = \frac{1}{4}\exp(2gl), \tag{10.63}$$

where l is the length of the crystal.

A phase mismatch between the waves can be expressed by

$$\Delta k = k_{\mathrm{p}} - k_{\mathrm{s}} - k_{\mathrm{i}}, \tag{10.64}$$

where $k_j = 2\pi n_j/\lambda_j$, with $j = \mathrm{p}, \mathrm{s}, \mathrm{i}$, are the propagation constants of the three waves.

In the presence of phase mismatch, the gain coefficient is reduced according to

$$g_{\mathrm{eff}} = \left[g^2 - \left(\frac{1}{2}\Delta k\right)^2\right]^{1/2}. \tag{10.65}$$

The reduction of gain resulting from momentum or phase mismatch is clearly evident. Maximum gain is achieved for $\Delta kl = 0$. Typical values for the coupling constant are on the order of $\kappa = 10^{-8}$/W, as will be discussed later. Therefore, a power density of at least 100 MW/cm^2 is required to obtain a gain coefficient of $g = 1$ cm^{-1} and a modest power gain of $G = 1.8$ in a 1-cm-long crystal. At a 1-μm wavelength, the propagation constant is $k \approx 10^5$/cm in a material with a $n = 1.7$ refractive index. In order to minimize the effect of phase mismatch, we require from (10.65) that $\Delta k/2 \ll g$. This means that the propagation constants have to be phase-matched to better than 10^{-5}/cm.

From these very basic considerations, one can already draw several conclusions which govern the design of parametric devices. The optimum configuration of a parametric converter depends critically on the pump intensity in the nonlinear crystal. There is a strong incentive to operate at the highest attainable levels for a given pump source. However, the practical and acceptable pump intensity depends strongly on the optical damage threshold of the crystal and its coatings. The importance of a high nonlinear coefficient d_{eff} is also clearly evident from these equations, as is the detrimental effect of phase mismatch.

Singly-Resonant OPO. The singly-resonant OPO is the most common configuration owing to the ease of mirror and resonator design, good conversion efficiency, frequency, and power output stability. These advantages more than offset the disadvantage of increased threshold relative to the DRO. The pump wave makes a single pass through the nonlinear crystal. The generated signal and idle waves increase during the single pass in the pump-wave direction. Following reflection and backward trip in the resonator, the signal wave travels again with the pump wave and is amplified.

Threshold condition for steady-state operation for a singly-resonant OPO is given by

$$g^2 l^2 = 2\sqrt{1 - R_{\mathrm{s}}}(1 - \delta), \tag{10.66}$$

where R_s, the reflectivity of the output coupler for the signal wave, and δ are combined reflection and absorption losses.

Threshold Condition. Singly-resonant OPOs are usually pumped with the output from a Q-switched Nd:YAG laser at either the fundamental or a harmonic of 1.06 μm, depending on the desired output wavelength and nonlinear material. The signal wave is amplified from an initial noise power, as it makes m cavity transits. A model which calculates the threshold pump intensity of a pulsed singly-resonant oscillator has been described by Brosnan and Byer [10.61]. The model assumes that only the signal wave is resonated, whereas the idler wave is free to accept the profile of its driving polarization. The pump flux required to reach threshold is given by

$$I_{\text{th}} = \frac{1.12}{\kappa g_s l_{\text{eff}}^2}\left(\frac{L}{t_p c}\ln\frac{P_s}{P_n} + 2\alpha l + \ln\frac{1}{\sqrt{R}} + \ln 2\right)^2 . \tag{10.67}$$

The pump flux I_{th} on the left-hand side of this equation relates to gain [see (10.61)], and the right-hand side represents loss terms.

The coupling constant κ has been previously defined, and g_s is the signal spatial mode coupling coefficient defined as

$$g_s = \frac{1}{1 + (w_s/w_p)^2}. \tag{10.68}$$

The signal spot size w_s for a Gaussian beam is always smaller than the pump beam w_p because of the nonlinear conversion process. The effective parametric gain length l_{eff} is determined by the walk-off length

$$l_{\text{eff}} = \frac{\sqrt{\pi}\, w_p}{2\rho}, \tag{10.69}$$

where ρ is the double refraction walk-off angle. The walk-off length is closely related to the aperture length introduced in (10.49). In short crystals, or under noncritically phase-matched conditions, the effective length can equal the crystal length l, i.e., $l_{\text{eff}} = l$. From (10.69) follows that walk-off has a greater influence on a small beam. The pump spot size dependence of parametric gain for critically phase-matched interactions is well known [10.63]. Actually for maximum efficiency, the beam diameter must be increased until the effective walk-off length is equal to the crystal length.

The first term in the bracket of (10.67) represents the loss of the pump beam due to the buildup time required to increase signal power from the noise level P_n to a signal level P_s defined as threshold. It was found that best agreement between the model and experimental data was obtained if threshold signal power P_s was defined as an increase of 10^{14} over the noise floor, or $\ln(P_s/P_n) = 33$. The logarithmic term is divided by the number of round trips it takes to reach P_s. The quantity L is the cavity length, t_p is the $(1/e^2)$ intensity full width of the pump pulse and c is the velocity of light. If more round trips $(t_p c/L)$ are allowed for the noise to build up to the signal level, then the pump-power density to reach threshold is lowered. In practice, this means a long pump pulse and a short OPO cavity lower the threshold.

The second term in (10.67) describes the absorption losses in the crystal where α is the absorption coefficient and l is the crystal length. The next term is the cavity output coupling loss, determined by the reflectivity R of the output mirror. The final term is due to SRO operation.

Inspection of (10.67) reveals that a high d_{eff} and long l_{eff} are the key to a low threshold for a parametric oscillator. The threshold input power is inversely proportional to the square of these terms. A long pump pulse and short cavity also tend to decrease the threshold somewhat as was already mentioned.

The model assumes a collimated Gaussian beam with a uniform wavefront. A transverse phase variation in the pump beam, caused by the laser or by intervening optics, acts as an effective phase mismatch in the presence of beam walk-off. If the beam has a transverse phase variation, and propagates at the walk-off angle with respect to the resonator axis, the generated signal wave sees a pump beam with a changing phase. As a result, threshold can be noticeably increased.

Singly-Resonant OPO with Return Pump Beam. The threshold in a singly-resonant OPO can be reduced by reflecting the pump radiation for a second pass through the crystal. This creates signal gain on both the forward and backward passes through the crystal. The changes in the OPO design are minimal; it only requires that the coating of the output mirror has to reflect both the resonated signal wave and the pump wave. If we let γ be the ratio of backward to forward pump intensity inside the crystal, then the threshold condition is as follows:

$$I_{\text{th}} = \frac{1.12}{\kappa g_s l_{\text{eff}}^2 (1+\gamma)^2} \left(\frac{L}{t_{\text{p}} c} \ln \frac{P_s}{P_{\text{n}}} + 2\alpha l + \ln \frac{1}{\sqrt{R}} + \ln 4 \right)^2 . \tag{10.70}$$

The reduction in threshold can be clearly seen from this equation. It should also be noted that in this scheme the fluence of the forward and backward pump beams are superimposed in the crystal, which leads to higher power densities compared to the previous case, and therefore damage considerations are important.

We found the model describing singly-resonant OPOs to be of adequate accuracy for design purposes, particularly in view of the fact that different qualities of nonlinear crystals can easily change threshold by a factor of 2.

We use (10.70) to calculate the threshold of an OPO build in our laboratory. The OPO contains a 15-mm-long KTP crystal as the nonlinear material which is pumped by a Q-switched Nd:YAG laser at 1.064 μm. The maximum output energy of the pump laser was 10 mJ, produced in a 50 ns pulse. This OPO is not used for generating a tunable output, but for providing an eye-safe wavelength at 1.6 μm [10.64–66]. The crystal was positioned to achieve type II noncritical phase matching for a pump wavelength of 1.06 μm (Nd:YAG) and a signal wavelength near 1.6 μm; the idler wavelength was therefore near 3.2 μm. Noncritical phase matching maximizes the effective nonlinear coefficient and essentially eliminates walk-off. The crystal was positioned inside an optical cavity formed by a pair of plane-parallel mirrors, as shown in Fig. 10.27. The input mirror, through which the pump enters, was antireflection-coated at the pump wavelength (1.06 μm) and highly reflecting at

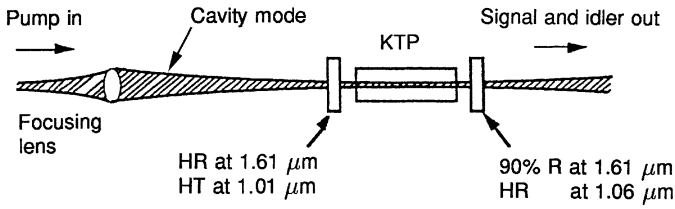

Fig. 10.27. Plane-parallel resonator for optical parametric oscillator, showing mode matching of focused pump beam to OPO cavity mode

the signal wavelength (1.6 μm) while the output mirror was highly reflecting at the pump wavelength and 10% transmitting at the signal wavelength. The laser output was focused by a 100-cm focal length lens, carefully positioned so as to mode-match the waist of the pump to the cavity mode of the OPO resonator.

In this noncritically phase-matched configuration, the wavelengths are $\lambda_s = 1.61\,\mu m$, $\lambda_i; = 3.2\,\mu m$, $\lambda_p = 1.06\,\mu m$ and the respective indices of refraction are $n_s = 1.7348$, $n_i = 1.7793$, and $n_p = 1.7474$. One can approximate the effective nonlinear coefficient for both type II doubling and this OPO by use of [10.16]

$$d_{\text{eff}} \approx (d_{24} - d_{15}) \sin 2\phi \sin 2\theta - (d_{15} \sin^2 \phi + d_{24} \cos^2 \phi \sin \theta), \tag{10.71}$$

which reduces to $|d_{\text{eff}}| = 0.15 d_{15} + 0.84 d_{24}$ for $\theta = 90^\circ$ and $\phi = 23^\circ$. With the values of $d_{24} = 3.64$ pm/V and $d_{15} = 1.91$ pm/V [10.67], one obtains $d_{\text{eff}} \approx 3.3$pm/V. Using these parameters, we calculate from (10.62) $\kappa = 1.2 \times 10^{-8} \text{W}^{-1}$.

In order to calculate the threshold of an SRO with pump reflection according to (10.70), we need the following system parameters: because of the noncritical phase matching condition, l_{eff} is as long as the physical length of the crystal, i.e., $l_{\text{eff}} = 1.5$ cm, the round-trip loss is about $2\alpha l = 0.01$, the optical length of the OPO resonator is $L = 5$ cm, output reflectivity is $R = 0.9$, pump length is $t_p = 50$ ns. At threshold, we can make the following approximation: the ratio of backward to forward pump intensity is $\gamma \approx 1$, and the mode sizes are about equal at this low-power level with $w_s \approx w_p$, one obtains for the mode-coupling coefficient $g_s = 1/2$. Introducing these parameters into (10.70) yields a value for the threshold power density of $I_{\text{th}} = 52\ \text{MW/cm}^2$.

The performance of this OPO is illustrated in Figs. 10.28 and 29. In the experiment, a confocal configuration was also evaluated and its performance is displayed. In the confocal design, the plane mirrors were replaced with a pair of 5-cm concave mirrors with identical coatings to those used in the plane-parallel cavity. The use of this cavity allows the pump to be more tightly focused while still maintaining good matching of the pump, to reduce the pump energy threshold for the device. This matching proved critical to successful operation of the OPO. Any mismatch between the pump mode and the TEM_{00} mode of the OPO cavity will cause a reduction in gain for optical parametric oscillation and a subsequent increase in threshold. For this reason, a single-transverse-mode pump is essential for obtaining high OPO efficiency. The OPO employing a plane-parallel resonator reached threshold at a pump energy of 1.5 mJ, with a maximum output energy of 2.5 mJ obtained at 10 mJ pump energy.

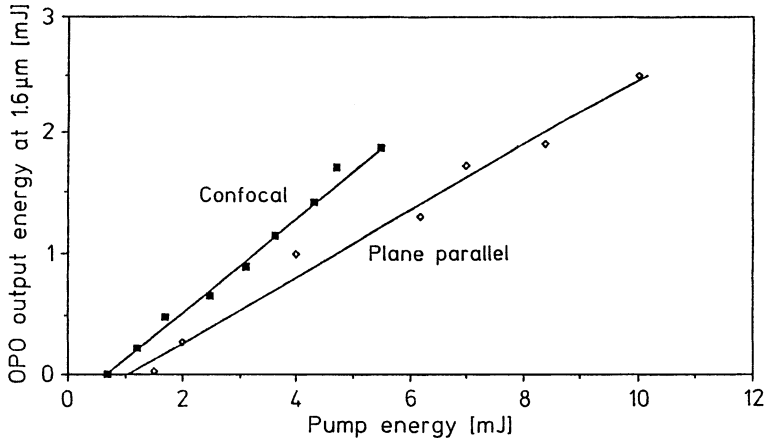

Fig. 10.28. Signal (1.6 μm) energy vs. pump energy for confocal and plane-parallel OPO resonator configurations

This corresponds to an energy conversion efficiency of 25%. Since the 25-ns duration signal pulse is only half as long as the pump pulse, the power conversion efficiency of the OPO is 50%.

Higher conversion efficiencies were observed with the confocal resonator than with the plane-parallel resonator, because of the lower threshold energy required in

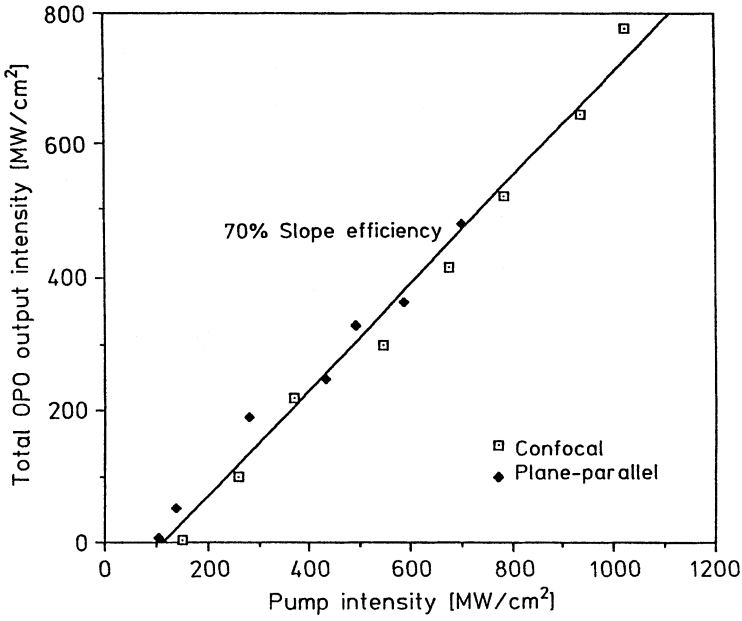

Fig. 10.29. Total OPO output intensity vs. pump intensity

the former configuration. Threshold energy is reduced because the pump is focused more tightly into the KTP crystal to obtain optimum matching for the confocal resonator. The threshold pump energy of this device was only 0.8 mJ, considerably lower than that of the plane-parallel configuration. A maximum output energy at 1.6 μm of 1.8 mJ was obtained for 5.5 mJ input pump energy. This corresponds to an energy-conversion efficiency of 33%. In the confocal configuration, the power conversion efficiency of 1.06 μm pump to 1.61 μm signal exceeds 50%, and the overall power conversion efficiency of the OPO, to both signal and idler outputs, exceeds 70%.

Optical parametric oscillation is intensity-dependent, so the pump intensity is a more meaningful parameter for gauging OPO performance than is pump energy. In Fig. 10.29, total output intensity is plotted vs. pump intensity. From the data presented in this figure follows that both resonator configurations produce similar results. Compared to the measured threshold, the theoretical value is a factor 2 lower. Crystal quality and its influence on the actual interaction length and resonator losses are probably the major reason for the discrepancy.

Saturation and Pump Beam Depletion

When the Q-switched pump pulse is incident on the nonlinear crystal, the signal and idler waves are amplified from the initial noise level. The number of round trips in the optical cavity necessary to amplify the signal and idler waves, multiplied by the cavity round-trip time, determines the delay in achieving threshold. This buildup time, required to achieve parametric oscillation, causes a temporal compression of the OPO output with respect to the pump pulse. Above threshold, after a short transition period during which a steady-state condition is established, the pump power is limited at the threshold value. Any pump input power above threshold is divided into power at the signal and idler beams. Since $\nu_3 = \nu_1 + \nu_2$, it follows that for each input pump photon above threshold, one photon at the signal and idler wavelengths is generated.

In other words energy of the pump beam is depleted, and in a lossless system, the depleted energy goes into the signal and idler beams.

The oscilloscope trace in Fig. 10.30, taken from the OPO described earlier, shows the dynamics of signal generation very nicely. The dashed curve is the input pump pulse. The two solid curves display the signal pulse and the depleted pump pulse at the output of the OPO. During the early part of the pump pulse, there is a transient period during which the oscillation builds up from noise. After the transient period, the pump beam is clamped at its threshold value until the pump power falls below threshold.

The onset of depletion to full limiting occurs quite rapidly. The fast-falling part of the pump beam has a time constant characteristic of the rise time of the signal wave. The buildup time required to achieve parametric oscillation causes a temporal compression of the OPO output with respect to the pump pulse. It is also clear from these considerations that the pump power must remain on long enough to allow the fields to build up to the threshold value. This leads to the consideration of a minimum pump fluence as well as flux.

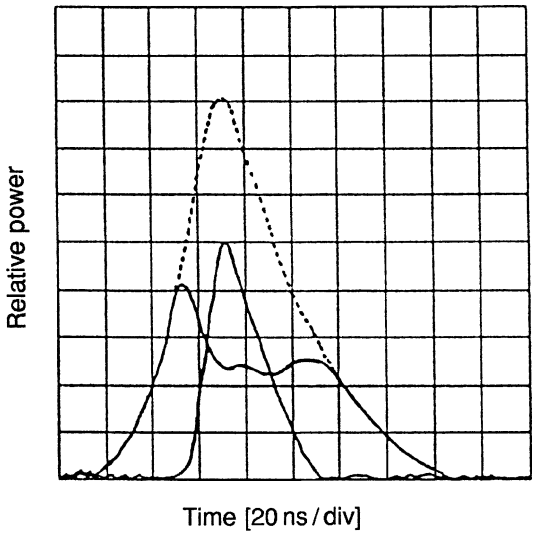

Fig. 10.30. Oscilloscope trace showing the depleted pump and the generated OPO output at 1.61 μm (solid curves) and the input pump (dashed curve)

Conversion Efficiency: In the plane-wave approximation, the conversion efficiency of an SRO for the ideal case of perfect phase matching and zero losses is given by [10.68]

$$\eta_{\text{par}} = \sin^2 gl, \tag{10.72}$$

where g and l have been defined in (10.61, 63).

Using this expression, total conversion of the pump can be achieved in theory. As the point of total conversion is exceeded, power starts to couple back into the pump field at the expense of the signal and idler fields, and the conversion efficiency decreases.

In practice, Gaussian beams are employed rather than plane waves. In this case, as in the case of frequency doubling, the maximum theoretical conversion efficiency is reduced. Although the center of the beam may be achieving total conversion, the intensity in the wings is considerably lower than the optimum. As one increases the pump power to convert the wings, the center exceeds the optimum and some back conversion occurs, resulting in an overall decrease in the conversion efficiency.

Theoretical conversion efficiencies for a plane wave and a Gaussian pump beam are plotted in Fig. 10.31 as a function of pump intensity above threshold. For a phase-matched uniform plane wave, the conversion can be 100% and occurs for $I/I_{\text{th}} = (\pi/2)^2$, where I and I_{th} are the input and threshold pump intensities, respectively. For a phase mismatch of $\Delta kl = \pi/2$, efficiency is around 75% for the plane-wave pump beam. Using a Gaussian pump beam, maximum efficiency is about 71% and occurs for $I/I_{\text{th}} \approx 6.5$.

The dependence of the conversion efficiency on pump power is illustrated in Fig. 10.32. Plotted is experimental data from several OPO experiments carried out with KTP as the nonlinear crystal and an Nd:YAG laser pump at 1.064 μm. The solid curve

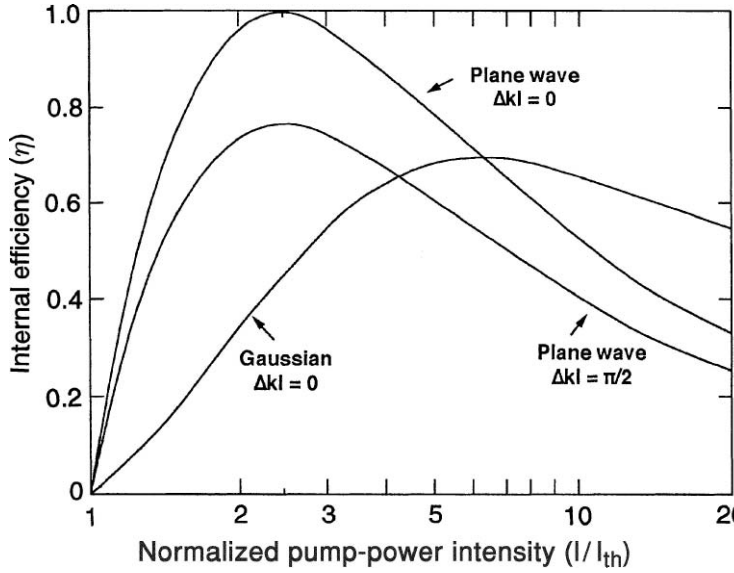

Fig. 10.31. Theoretical conversion efficiencies for a phase-matched plane wave and Gaussian pump beam and a plane-wave beam with a phase mismatch of $\pi/2$

was obtained by integrating the equations for plane wave OPOs over the spatial profile of the Gaussian beam, as described in [10.68].

One can derive a generic relationship between the factor by which pump power exceeds threshold power, and the OPO conversion efficiency. While there is some spread in the data, the general agreement is surprisingly good. The general "rule of

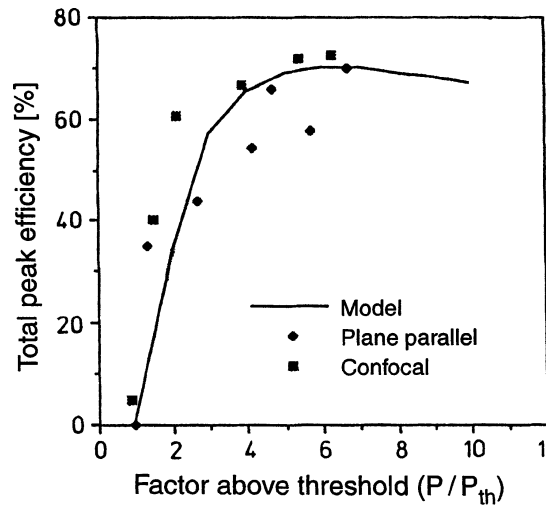

Fig. 10.32. Efficiency of an OPO vs. factor above threshold

thumb" for design of an efficient OPO is to pump at least four times above threshold for maximum efficiency. Thus one can calculate the threshold for a given OPO, then multiply this value by a factor 4 to determine the required pump intensity.

The conversion efficiency in (10.72) is defined as the ratio of the sum of signal and idler power to pump power. The energy or power between the signal and idler beams is divided according to the ratio of the photon energies, that is,

$$\frac{h\nu_{\mathrm{s}}}{h\nu_{\mathrm{i}}} = \frac{\lambda_{\mathrm{i}}}{\lambda_{\mathrm{s}}}. \tag{10.73}$$

From this follows the ratio of the energy of the signal compared to the total energy converted by the OPO

$$\frac{h\nu_{\mathrm{s}}}{h\nu_{\mathrm{s}} + h\nu_{\mathrm{i}}} = \frac{1}{1 + \lambda_{\mathrm{s}}/\lambda_{\mathrm{i}}}. \tag{10.74}$$

Phase Matching

In order to achieve significant gain in the parametric device, the pump, signal, and idler waves have to be phase-matched according to (10.60). In a medium without dispersion, all waves propagate with the same velocity, hence $\Delta k = 0$. In reality, Δk is not zero for different wavelengths, and just as in harmonic generation, dispersion is compensated for by birefringence. The index of refraction at a given wavelength is a function of the direction of propagation in the crystal as well as orientation of polarization.

When the signal and idler waves are both ordinary rays, one has type I phase matching. When either one is an ordinary ray, it is referred to as type II phase matching.

In a uniaxial crystal, if the signal and idler are ordinary rays (type I) with indices of refraction n_{s} and n_{i}, then the index of refraction for the pump wave necessary to achieve phase matching is

$$n_{\mathrm{p}} = (\lambda_{\mathrm{p}}/\lambda_{\mathrm{s}})n_{\mathrm{s}} = (\lambda_{\mathrm{p}}/\lambda_{\mathrm{i}})n_{\mathrm{i}}. \tag{10.75}$$

In uniaxial crystals, the index of refraction n_{o} for an extraordinary wave propagating at an angle θ to the optic axis is given by

$$\frac{1}{n_0(\theta)^2} = \frac{\cos^2\theta}{(n^{\mathrm{o}})^2} + \frac{\sin^2\theta}{(n^{\mathrm{e}})^2}, \tag{10.76}$$

where n^{o} and n^{e} are the ordinary and extraordinary indices of refraction, respectively. The index n_0 is thus limited by n^{o} and n^{e}. If n_{p} falls between n^{o} and n^{e}, then an angle θ_m exists for which $n_0 = n_{\mathrm{p}}$. Propagation with $\Delta k = 0$ results, and all three waves travel at the phase matching angle θ_m with respect to the optical axis.

Phase matching with a propagation direction normal to the optic axis (90° phase matching) is preferred if possible. In that direction, the double refraction angle is zero and the nonlinear interaction is not limited by the effective gain length but by the crystal's physical length. Non-90° phase matching does, however, allow angle tuning.

Line Width Control and Wavelength Tuning. The gain line width of an OPO is set by crystal dispersion; therefore the device has a rather broad line width, limited only by the phase-matching bandwidth of the crystal. Small dispersion and birefringence leads to relatively large bandwidths and tuning ranges, vice versa. In [10.62], a simple relationship is given for the bandwidth $\delta\nu$(in wave numbers) and birefringence Δn,

$$\delta\nu[\mathrm{cm}^{-1}] \approx \frac{1}{\Delta n l[cm]}, \tag{10.77}$$

where l is the crystal length. Crystals with small birefringence have larger bandwidth than crystals with large birefringence.

The line widths of OPOs are generally too broad for spectroscopic applications. Line width control can be achieved by using highly dispersive resonators which contain etalons, diffraction gratings, or resonant reflectors [10.61]. A more recent development is line width control by means of injection seeding of the OPO [10.69]. Similar to the technique described for line width control of a laser oscillator, a cw beam is injected into the pulsed SRO cavity. The length of the oscillator cavity is adjusted so that it is resonant at the injected frequency. When the pump is then applied, the desired mode starts from the level of the injected signal, whereas the competing modes begin from spontaneous emission. Provided the injected power level is sufficiently high, the injected signal will be the first to build up to a high power level and will deplete the pump.

Tuning curves for parametric oscillators can be determined by solving the phase matching equations (10.59,60) for signal and idler frequencies at a given pump frequency as a function of the tuning variable. The most common tuning methods are varying the direction of propagation with respect to the crystal axes or by changing the crystal temperature. To carry out the calculations, the indices of refraction must be known over the entire tuning range. For most nonlinear crystals of interest, the indices can be obtained from the Sellmeier equations.

We will consider KTP pumped by an Nd:YAG laser at 1.06 μm, as an illustration of the type of calculation which has to be performed to determine the tuning range and appropriate phase matching angle for an optical parametric oscillator [10.70]

Potassium titanyl phosphate (KTP) belongs to the orthorombic crystal system, and therefore is optically biaxial (having two optical axes). The mutually orthogonal principal axes of the index ellipsoid are defined such that $n_x < n_y < n_z$, and the optical axes lie in the x–z plane (at 18° to the z-axis in KTP [10.71] (Fig. 10.33)).

The indices of refraction for any propagation direction are given by the index ellipsoid defined by

$$k_x^2/(n_{\omega j}^{-2} - n_{x,\omega j}^{-2}) + k_y^2/(n_{\omega j}^{-2} - n_{y,\omega j}^{-2}) + k_z^2/(n_{\omega j}^{-2} - n_{z,\omega j}^{-2}) = 0, \quad j = \mathrm{p, s, i}, \tag{10.78}$$

where $k_x = \sin\theta\cos\phi$, $k_y = \sin\theta\sin\phi$, $k_z = \cos\theta$; θ is the angle to the z-axis and ϕ is the angle to the x-axis in the x–y plane. The subscript "j" refers to either the pump, signal, or idler frequency. Equation (10.78) must be solved to determine the

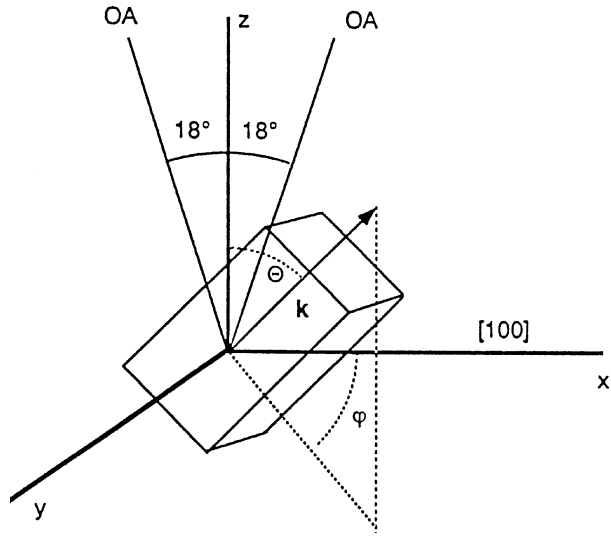

Fig. 10.33. KTP phase-matching angles

refractive indices ($n_{\omega j1}, n_{\omega j2}$) for the two eigen-polarizations perpendicular to the propagation direction for each wavelength. The equations can be solved numerically using the technique described in [10.71, 72]. In our work, this has been done using a spreadsheet (Excel) program.

The indices of refraction are obtained from the appropriate Sellmeier equation [10.67, 73]

$$\begin{aligned} n_x^2 &= 3.0065 + \frac{0.03901}{\lambda^2 - 0.04251} - 0.01327\lambda^2, \\ n_y^2 &= 3.0333 + \frac{0.04154}{\lambda^2 - 0.04547} - 0.01408\lambda^2, \\ n_z^2 &= 3.3134 + \frac{0.05694}{\lambda^2 - 0.05658} - 0.01682\lambda^2, \end{aligned} \tag{10.79}$$

where λ is in micrometers.

The phase matching condition for optical parametric conversion in KTP is given by [10.71, 72]

$$\omega_{\mathrm{p}} n_{\omega_{\mathrm{p}1}} = \omega_{\mathrm{s}} n_{\omega s2} + w_{\mathrm{i}} n_{\omega i2} \quad \text{(type I)} \tag{10.80}$$

or

$$\omega_{\mathrm{p}} n_{\omega_{\mathrm{p}1}} = \omega_{\mathrm{s}} n_{\omega s1} + w_{\mathrm{i}} n_{\omega i2} \quad \text{(type IIa)} \tag{10.81}$$

or

$$\omega_{\mathrm{p}} n_{\omega_{\mathrm{p}1}} = \omega_{\mathrm{s}} n_{\omega s2} + w_{\mathrm{i}} n_{\omega i1} \quad \text{(type IIb).} \tag{10.82}$$

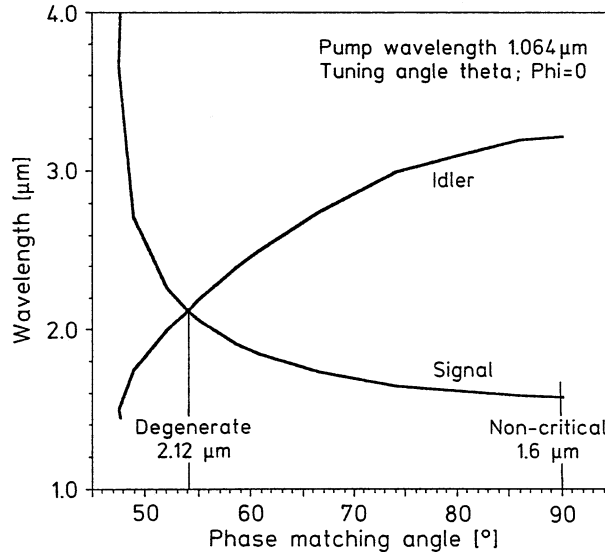

Fig. 10.34. Tuning range of an OPO pumped by a 1.06 μm Nd laser and employing a type II KTP crystal

In KTP, type I interactions have very low nonlinear coefficients, and therefore are not useful. For propagation in the x–z plane ($\phi = 0$) in KTP, type II interactions correspond to type II phase matching in a positive uniaxial crystal (e.g., $\omega_p n_p^o = \omega_s n_s^o + w_i n_i^e$). where "o" and "e" represent the ordinary and extraordinary rays, respectively.

Figure 10.34 exhibits the calculated phase matching angles for a KTP optical parametric converter pumped at 1.064 μm. The two curves correspond to the signal and idler wavelengths for type II phase matching with $\phi = 0$. The polarization of the pump wave is along the y-axis (o-wave) of the crystal as is that of the signal wave. The idler wave is polarized in the x–z plane (e-wave). The degenerate point at 2.12 μm corresponds to a phase matching angle of $\theta = 54°$.

10.3.2 Crystals

The nonlinear crystals used for parametric oscillators must be transparent and have low loss at the pump as well as the signal and idler wavelengths. Very important for reliable OPO operation is a high damage threshold, and a large ratio of optical damage threshold to pump threshold. Table 10.3 lists a number of nonlinear materials for use in OPOs. The critical parameters for OPO crystals are slightly different to those for doubling where one requires broad angular acceptance, low-temperature sensitivity, and broad-frequency acceptance. In OPOs, absence of these qualities merely leads to broad linewidth output from the OPO owing to the inherent tunability of the OPO. For example, exceeding the acceptance angle prevents phase matching at one pair of signal and idler wavelengths; however, the OPO will tune these wavelengths until phase matching is recovered, producing an output of broader line width.

Table 10.3. Common crystals employed in OPOs

	LBO	BBO	KTP	KTA	$AgGaS_2$	$LiNbO_3$	PPLN
d_{eff}[pm/V]	1.16	1.94	3.64	4.47	13.5	5.1	17.2
Transparency [μm]	0.16–2.6	0.19–2.5	0.4–3.5	0.4–4.0	0.5–12	0.5–5	0.5–5
Damage threshold [GW/cm^2]	2.5	1.5	0.5	0.5	0.03	0.2	0.2
Typical length [cm]	0.5–1	0.5–1	1–2	1–2	2–4	2–5	2–6

Listed in Table 10.3 is also the maximum crystal size currently available from commercial sources. A minimum crystal length of at least 1 cm is usually required for the achievement of a high conversion efficiency, and a sufficient crystal cross section is important to keep the pump intensity substantially below the damage threshold. For example, when pumping at the joule level, one typically needs to expand the pump beam to lower the pump intensity. In this case, operation at 100 MW/cm^2, with a typical pulse length of 20 ns, requires a beam diameter of 0.8 cm. Thus, one requires a crystal size on the order of 1 cm^3. The use of a larger pump-beam diameter also reduces the effect of walk-off; for example, the walk-off angle in a mid-IR KTP OPO is 2.6°, which reduces the effective interaction length to 4 mm for a 200-μm pump beam diameter. However, if the pump-beam diameter is increased to 8 mm, the interaction length is dramatically increased to 160 mm, so that walk-off is negligible over the typical 15-mm-long crystals employed in practice.

Most of the materials listed in Table 10.3 have already been described in Sect. 10.2.3. For OPOs operating in the UV, visible, or near-infrared, BBO and LBO are the preferred materials because of the transparency range which extends to very short wavelengths. As an example. Fig. 10.35 displays tuning curves for OPOs using BBO

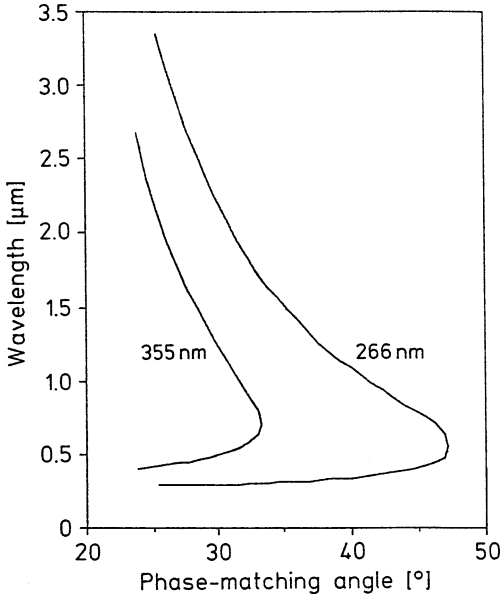

Fig. 10.35. Tuning curves for BBO in a type I configuration pumped at the wavelength of 266 and 355 nm [10.75]

in a type I configuration pumped at the tripled or quadrupled output from an Nd laser [10.74,75]

KTP is the material of choice for the design of OPOs pumped with Nd lasers at 1.064 μm [10.64–66, 76–78]. This material has already been described in the previous sections. It has been observed that the damage threshold of KTP when used in an OPO can be considerably lower compared to second harmonic generation [10.79]

Potassium titanyl arsenate (KTA) is a new nonlinear material which is isomorphic with KTP. Substitution of arsenic for phosphorous extends the transparency range further into the infrared. However, the major difference between the two materials is the considerably lower absorption losses in the 3–5 μm region of KTA, as illustrated in Fig. 10.12. Usually, the wavelength beyond 3 μm is the idler wavelength when a KTA or a KTP OPO is pumped by an Nd:YAG or an Nd:YLF laser. For example, a pump wavelength of 1.06 μm and signal wavelength of 1.54 μm produce an idler wavelength at 3.44μm. Since KTA does not have any appreciable absorption at the idler wavelength, this material has fewer problems associated with thermal lensing and heating of the crystal in high-average-power OPOs. In terms of damage threshold and nonlinear coefficient, the materials are quite similar although d_{eff} is somewhat higher in KTA. With a 1.064-μm pump beam from an Nd:YAG laser, noncritical phase matching produces a signal at 1.538 μm in KTA, whereas in KTP the signal output is at 1.574 μm. OPOs featuring KTA crystals are described in [10.79–81].

Although silver gallium selenide ($AgGaSe_2$) has a low damage threshold, it is of interest for the design of low-power OPOs because its transparency reaches far into the infrared. Optical parametric oscillators using $AgGaSe_2$ have been pumped by Nd:YAG lasers to produce output from 6 to 14 μm. This tuning range was achieved in a two-stage OPO system, with an Nd:YAG laser pumping a noncritically phase-matched KTP OPO at fixed wavelength of 1.57 μm, which was used to pump a $AgGaSe_2$ OPO [10.82]. Also continuously tunable output from 6.7 to 9.8 μm was achieved by directly pumping a $AgGaSe_2$ OPO with a Q-switched pulse from an Nd:YAG laser [10.83].

Another crystal that is used to produce output in the mid-infrared region is $ZnGeP_2$. The crystal has a transparency range from 2 to 8.4 μm; therefore, pump sources such as Ho:YAG or Tm:Ho:YAG lasers are required, which emit at or above 2 μm. $ZnGeP_2$ has a higher thermal conductivity and nonlinear coefficient compared to $AgGaSe_2$. Disadvantages are the increasing losses above 8 μm and the fact that none of the common Nd-based laser sources can be used to pump this material.

$LiNbO_3$ is a nonlinear crystal which has been employed widely in the past. Unfortunately, it has a much lower damage threshold compared to newer materials such as KTP and KTA which cover the same wavelength regime. However, recently a different version of this material, namely periodically poled $LiNbO_3$ (PPLN), has become available. PPLN has a very large nonlinear coefficient, and therfore it is well suited for low-peak-power OPOs in the near- and mid-infrared. Because of the unique concept underlying PPLN, it will be described in more detail below.

10.3.3 Quasi Phase Matching

In this subsection we will briefly review the concept of quasi phase matching (QPM), and summarize the properties of periodically poled $LiNbO_3$ (PPLN). Although QPM is applicable to any nonlinear process, the subject is covered here because of the importance of PPLN and its application in OPOs for the generation of mid-infrared radiation.

PPLN is the first commercially available crystal in which efficient nonlinear conversion processes, such as harmonic generation or parametric interactions, are not based on birefringence phase matching but on a periodic structure engineered into the crystal. We will briefly explain this technique, termed quasi phase matching, by referring to Sect. 10.2.1. An in-depth treatment of this subject can be found in [10.84–86].

As illustrated in Fig. 10.2 and expressed by (10.19), in a phase-matched condition $\Delta k = 0$ the harmonic power increases with the square of the interaction length ℓ. In the situation of a fixed phase mismatch Δk, energy flows back and forth sinusoidally between the fundamental and harmonic beams with a period of $\Delta k\ell/2 = \pi$ as the waves propagate through the crystal. Half of this period is the coherence length ℓ_c given by (10.24), which is the maximum distance over which the second harmonic can grow. In a non-phase-matched condition, this distance is on the order of 2–20 μm for conversion processes of interest. The objective of birefringence phase matching is to make this distance as long as possible by taking advantage of the wavelength and polarization dependence of the refractive indices in a crystal. By arranging proper balance between dispersion and birefringence the technique of phase matching increases ℓ_c by a factor of 10^3.

Even before the concept of birefringence phase matching was invented, it was proposed that a periodic structure in the crystal which corrects the phase of the propagating beams each time it reaches π would enable continued energy flow from the fundamental to the harmonic beam [10.8]. An implementation of this concept is a crystal where the sign of the nonlinear coefficient is reversed after each distance ℓ_c. In this case the relative phase between the waves is inverted after the conversion has reached its maximum. Therefore, on the average the proper phase relationship between the beams is maintained and the second harmonic power, increases with the square of crystal length similar to the birefringence phase matching case. The nonlinear coefficient d_Q for QPM is, however, reduced as compared to the phase-matched interaction according to [10.84]

$$d_Q = \frac{2}{\pi} d_{\text{eff}}. \tag{10.83}$$

A phase reversal is equivalent of slicing a crystal in thin wafers and stacking the wafers by rotating alternate wafers by 180°. The periodicity $\wedge$ of this structure is twice that of ℓ_c, i.e.,

$$\wedge = 2\ell_c. \tag{10.84}$$

Because of the micrometer-size thickness of alternating layers, the practical realization of QPM had to wait until it was possible to engineer a periodic phase reversal into a monolithic crystal. Only recently has the technique of periodically reversed polarization domains in ferroelectric crystals, combined with advances in lithography, made it possible to realize this concept. A reversal of the ferroelectric domains corresponds to a sign reversal of the nonlinear coefficient. In this process, standard lithography produces a patterned electrode with a period between 5 and 30μm on the surface of a ferroelectric crystal such as $LiNbO_3$. A high-voltage pulse is applied to the crystal which is sandwiched between the patterned electrode and a uniform electrode. The high electric field strength of the voltage pulse permanently reverses the sign of the nonlinear coefficient in a pattern determined by the electrode structure.

This electric-field-poling technique is employed to reproducibly manufacture PPLN suitable for applications in infrared parametric oscillators and second harmonic generation.

We will now derive an expression for the QPM condition in OPOs for periodically poled crystals. Parametric conversion requires energy conservation and momentum matching conditions, as given by (10.59 and 60). A momentum mismatch expressed as a phase mismatch between the pump, signal, and idler waves has been defined in (10.64). In the frequency domain, a periodic structure can be represented by a grating wave vector

$$k_g = 2\pi/\wedge_g, \tag{10.85}$$

where $\wedge_g$ is the period of the grating.

In the presence of a grating structure in the crystal, the equation for phase mismatch (10.64) includes as an additional term the grating wave vector k_g [10.85]

$$\Delta k = k_p - k_s - k_i - k_g, \tag{10.86}$$

the first three terms being the conventional phase matching condition. It is assumed that all wave vectors are collinear with the grating vector.

The objective of high parametric conversion is to eliminate the phase mismatch caused by dispersion by selecting the appropriate crystal orientation, temperature, and polarization such that $\Delta k = 0$ is achieved. The grating vector in (10.86) provides an additional adjustable parameter that is independent of inherent material properties.

Differences of the three wave vectors k_p, k_s, and k_i can be compensated by an appropriate choice of the grating vector k_g such that $\Delta k = 0$ can be achieved. Introducing (10.85) into (10.86) and with $\Delta k = 0$ the grating period under QPM conditions is given by

$$\wedge_g = \frac{2\pi}{k_p - k_s - k_i}. \tag{10.87}$$

Equation (10.87) can also be expressed by

$$\frac{1}{\wedge_g} = \frac{n_p}{\lambda_p} - \frac{n_s}{\lambda_s} - \frac{n_i}{\lambda_i}. \tag{10.88}$$

This equation is the equivalent of (10.60), which was derived for the birefringence phase matching case. If one substitutes Δk in (10.18) with k_g from (10.85), then one obtains the following condition for harmonic generation:

$$\Lambda_g = \frac{\lambda_1}{2(n_{2\omega} - n_{1\omega})}. \tag{10.89}$$

The fact that the domain thickness is a free parameter which can be customized for a particular nonlinear process offers significant advantages over birefringent phase matching. For example, QPM permits wavelength selection over the entire transmission window of the crystal, it allows utilization of the largest nonlinear coefficient, and it eliminates problems associated with walk-off since all interactions are noncritical.

For example, $LiNbO_3$ interactions with all waves polarized parallel to the crystal optic axis utilize the largest nonlinear coefficient d_{33} = 27 pm/V. PPLN permits noncritical phase matching with this coefficient. Birefringent phase matching requiring orthogonally polarized beams can only be accomplished with the smaller coefficient $d_{31} = 4.3$ pm/V, Therefore, PPLN has a parametric gain enhancement over single-domain material of $(2d_{33}/\pi d_{31})^2 \approx 16$.

The grating period of PPLN for a particular OPO can be calculated from (10.88), with the indices of refraction obtained from the Sellmeier equation. For example, if it is desired to shift the wavelength of an Nd:YAG laser with output at $\lambda_p = 1.064$ μm to the eye-safe region of $\lambda_s = 1.540$ μm, then one obtains from (10.59) an idler wavelength of $\lambda_i = 3.442$ μm. The next step is the determination of the indices of refraction at these wavelengths. The most recent coefficients of the Sellmeier equation for the extraordinary index of refraction have been published in [10.87]. At an operating temperature of 120°C we obtain $n_p = 2.160$, $n_s = 2.142$, and $n_i = 2.085$. Introducing these values into (10.88) yields $\wedge_g = 29.8$ μm.

PPLN is commercially available as 1-mm-thick crystals, with lengths ranging from 20 to 60 mm, and a width depending on the number of different gratings desired. For example, a width of 11 mm may contain up to eight separate grating periods. Translation of the crystal normal to the beam moves a different grating into the beam, which shifts the signal and idler waves to a new wavelength band. Fine tuning can be accomplished by changing the temperature.

$LiNbO_3$ has a relatively low damage threshold in comparison to, for example, KTP. Also, PPLN, like single-domain $LiNbO_3$, has to be heated to eliminate photorefractive effects. Although photorefractive damage is mainly caused at shorter wavelengths, it can be a problem also in infrared OPOs because a certain amount of visible radiation is generated in these devices by second harmonic and sum frequency processes.

Pulsed and cw optical parametric oscillators using PPLN, and pumped by Nd:YAG lasers, have been operated over the wavelength range from to 1.4 to 4 μm and with outputs from cw [10.86, 88] to Q-switched pulses in the nanosecond regime [10.89–91] up to femtosecond pulses [10.92, 93]. Tuning has been accomplished by translation of the PPLN crystal or by temperature changes or by both.

Peak powers and pulse energies are limited by the small aperture of available crystals and the relatively low damage threshold of this material. Therefore, PPLN has become the crystal of choice for OPOs pumped by cw or high-repetition-rate

Nd:YAG lasers producing up to several watts of mid-infrared radiation. These lasers have pulse energies and peak powers that are relatively low and provide a natural match for PPLN. In addition, the high-gain and noncritical phase matching permit the design of highly efficient OPOs.

Although PPLN is used mainly in OPOs for infrared interactions, the five times higher nonlinear coefficient compared to KTP allows efficient single-pass cw frequency doubling external to the resonator [10.94]. The efficiency obtained is comparable to the performance of intracavity doubling but without the complications associated with output fluctuations discussed in Sect. 10.2.4. Since dispersion is larger at shorter wavelengths, the period of the domain structure must be reduced according to (10.89). This poses a fabrication problem since the domain period for frequency doubling a Nd:YAG laser is only 6.5 μm for a PPLN crystal operated at 200°C. As mentioned earlier, suppression of photorefractive damage requires operation of a PPLN at a fairly high temperature. However, it seems that PPLN is more resistant to photorefractive damage compared to ordinary $LiNbO_3$ [10.95].

As already pointed out in Sect. 10.2.3, $LiNbO_3$ crystals doped with MgO show improved photorefractive damage resistance at visible wavelengths [10.96].

Although not available commercially, other ferroelectric crystals such as KTP, RTA rubidium titanyl arsenate), and $LiTaO_3$ (lithium tantalate) have been periodically poled, and promising results have been achieved with these materials in harmonic generators and OPOs [10.97–100]. Since these crystals have high damage thresholds they hold promise for efficient nonlinear interactions at higher pulse energies compared to PPLN.

It is anticipated that the research for new and improved periodically poled crystals remains very active in the future because QPM has a number of advantages over birefringence phase matching. Since QPM allows noncritically phase-matching beams can be tightly focused. New nonlinear materials which have a low birefringence such as $LiTaO_3$ can be used as nonlinear material. This is particularly important at shorter wavelengths where the dispersion increases more dramatically than birefringence. Also QPM allows the largest nonlinear coefficient to be used and provides the ability to phase-match over the full transparency range of crystal.

10.3.4 Design and Performance

As mentioned at the beginning of this section, the advent of new nonlinear materials such as KTP, KTA, BBO, LBO, and PPLN in combination with the high beam quality obtained from diode-pumped lasers has led to the practical realization of pulsed or cw-tunable radiation sources with output in the UV, visible, and IR region of the spectrum. The most mature OPO technology exists for the generation of radiation in the 1.5–4 μm region utilizing Nd:YAG lasers as pump sources.

Figure 10.36 illustrates the generation of mid-infrared radiation using PPLN employed in an intracavity OPO pumped by Nd:YAG laser emitting at 1.064 μm [10.101].

The fundamental pump laser was quasi-cw-pumped and repetitively Q-switched from 30 to 100 KHz. The output of the intracavity OPO consisted of a signal wave

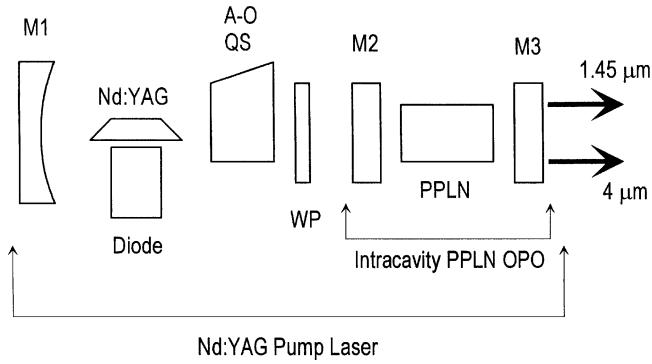

Fig. 10.36. Generation of mid-infrared radiation using PPLN employed in an intracavity OPO pumped by an Nd:YAG laser

near 1.45 μm and an idler wave near 4 μm. For applications that require high repetition rate or cw output, achieving high pump intensity often poses difficulty for the system architecture. One way to overcome this difficulty, yet still maintain the high pump intensity, is to use the intracavity configuration, which is employed frequently in second harmonic generation. Intracavity parametric conversion utilizes the high intracavity intensity available inside an optical resonator. The one way intracavity power density is enhanced by a factor $1/(1-R)$ over the output beam intensity, where R is the reflectivity of the output coupler.

The energy transfer in a Q-switched intracavity OPO consists of three steps: First, energy is stored in the upper laser level with the Q-switch turned off. When the laser cavity is Q-switched, pump radiation for the OPO builds up. When the pump intensity exceeds the OPO threshold, the signal and idler fields build up and the energy is transferred from the pump field to the signal and idler beam. A fraction of the signal and idler radiation leaves the cavity as useful output. The OPO acts as a nonlinear output coupler for the laser.

The layout of the intracavity OPO is shown in Fig. 10.36. It consists of a Nd:YAG, 1064 nm fundamental pump laser, and an intracavity PPLN OPO resonator. The Nd:YAG laser was a side-pumped slab design. An acousto-optic Q-switch was placed inside the pump laser resonator to provide repeated Q-switching. A half wave plate at 1064 nm was positioned between the Q-switch and PPLN OPO to provide the correct polarization of the pump laser for the quasi phase matching of the PPLN. The PPLN crystal had eight grating periods. The wavelength indicated in Fig. 10.36 was achieved with a period of 28.2 μm. The PPLN crystal kept at 116°C was 19-mm long and had a thickness of 0.5 mm. Mirror M_1 had a radius of curvature of 20 cm and produced a beam waist at the PPLN crystal. The intracavity OPO was formed by mirrors M_2 and M_3, where mirror M_3 served also as one resonator mirror of the pump laser resonator. Mirror M_2 had a AR coating for 1064 mm and a high reflectivity coating for 1.45 μm and 4 μm. Mirror M_3 had a high reflectivity at 1064 nm, and 10% transmission at 1.45 μm and high transmission for the idler at 4 μm. The OPO is therefore singly resonant.

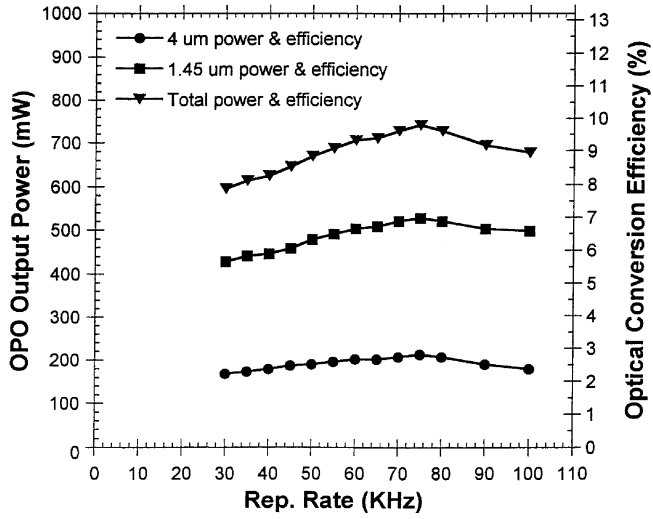

Fig. 10.37. Average power (left scale) and optical conversion efficiencies (right scale) of an intracavity-pumped PPLN OPO as function of the Q-switching repetition rate

Figure 10.37 shows the average power performance (left scale) and the optical conversion efficiency (right scale) of the intracavity PPLN OPO as function of the Q-switching repetition rate. The optical conversion efficiency of the intracavity PPLN OPO is defined as the ratio of the OPO average power to the average diode pump power.

Three sets of data are shown, representing the average output powers and optical conversion efficiencies at 1.45 μm, 4 μm, and the total, respectively. The best power performance appeared to be near 75 KHz, at which the average powers of 1.45 μm and 4 μm lasers were 528 mW and 212 mW, respectively, and the total output power was 740 mW.

Other examples of intracavity-pumped OPOs for the generation of 1.5- or 2-μm radiation can be found in [10.102, 103].

The wavelength coverage of OPOs has been extended as far as 10 μm. For example, tunable output from 3.7 to 10.2 μm was achieved with a system comprising an Nd:YAG laser and two OPOs in series. The first OPO contained a PPLN crystal and was pumped by the Nd:YAG laser that provided tunable radiation over the range 2.3–3.7 μm. This output was the pump source for an OPO containing a zinc germanium phosphide ($ZnGeP_2$) crystal [10.104]. In another system a $ZnGeP_2$ was pumped by a Ho:YAG laser at 2.09 μm to yield tunable output in the 3–5 μm region. [10.105].

Tunable output in the visible spectral region can be achieved in two ways. One approach is to use a UV pump source such as a frequency tripled or quadrupled Nd:YAG laser. An alternative approach is the frequency conversion of the signal or idler wavelength of a near-infrared OPO. An example of each approach is illustrated below.

Optical parametric oscillation in the UV, visible, and near-infrared region has been demonstrated in BBO and LBO which have been pumped with Q-switched, frequency

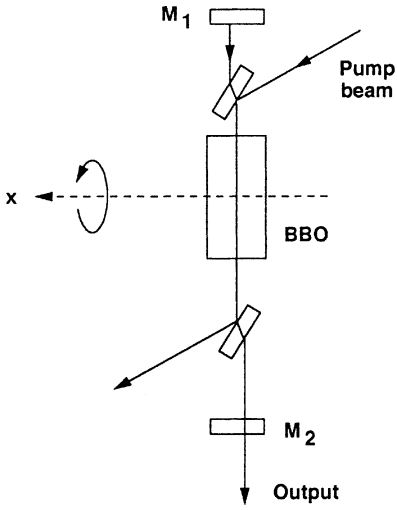

Fig. 10.38. Optical parametric oscillator featuring a BBO crystal pumped by the fourth harmonic of a Nd:YAG laser [10.110]

tripled [10.106–109] and quadrupled [10.110] Nd:YAG lasers. An example of such a device is the singly resonant OPO, shown in Fig. 10.38 [10.110]. A 20.5-mm-long BBO crystal pumped by a Q-switched and quadrupled Nd:YAG laser with output at 266 nm provided tunable output from 0.33 to 1.37 μm with different sets of mirrors. The BBO crystal was cut for type I phase matching at 39.1°. The optical cavity length was 7.5 cm, which allowed about 20 round-trip passes through the crystal during the 9-ns-long pump pulse. Threshold was obtained at 4.5 mJ or 23 MW/cm^2.

Optical damage of the mirrors is a major consideration in the design of OPOs. In a singly-resonant OPO, trichroic dielectric mirrors are required which are highly transmissive at the pump and idler wavelengths and highly reflective at the signal wavelength. In addition, the mirrors must have a high damage threshold. With a pump wavelength in the ultraviolet, demands on mirror coatings are particularly severe. An interesting feature of this OPO is the introduction of the pump beam into the OPO resonator by means of a separate set of mirrors oriented at Brewster's angle. The advantage of this design is the fact that the resonator mirrors M_1 and M_2 of the OPO do not have to transmit the intense UV pump beam.

Figure 10.39 illustrates a configuration of an intracavity-doubled OPO designed to produce output in the UV/blue wavelength region [10.111]. The device generates radiation between 760 and 1040 nm, which is internally doubled to produce tunable output from 380 to 520 nm. The OPO employs a 15-mm-long KTP crystal, antireflection-coated at 911 nm, cut for normal incidence at $\phi = 0°$ and $\theta = 69°$. The angles correspond to type II phase matching for a signal wavelength of 911 nm.

The pump source is a diode-pumped Nd:YAG laser which is frequency-doubled by a 1-cm-long KTP crystal. The waist of the pump beam is positioned at the center of the 5-cm-long OPO cavity.

The 532-nm pulse enters the OPO cavity through a flat dichroic turning mirror (M_1; highly reflecting at 800–950 nm and highly transmitting at 440–540 nm). The

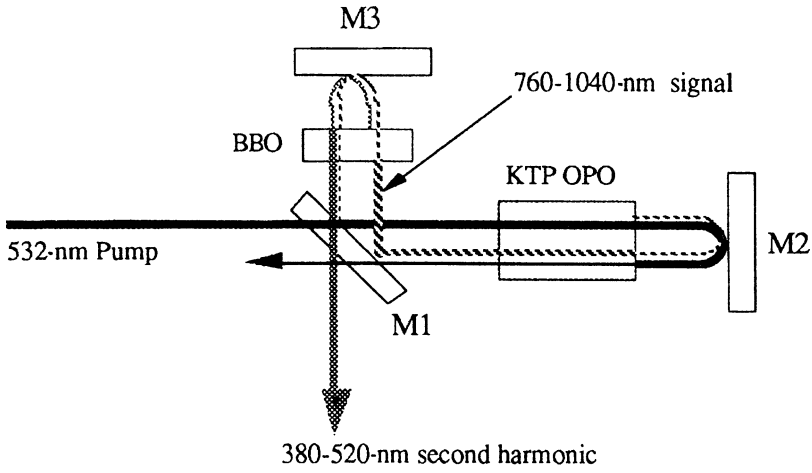

Fig. 10.39. Layout of intracavity OPO, showing the different pump wavelengths involved: the 532-nm pump, the 760–1040-nm signal, and the 380–520-nm intracavity-doubled signal [10.111]

532-nm pulse passes through the OPO crystal and is reflected off the flat rear cavity mirror (M_2; highly reflecting at 532 nm and 880–950 nm), to leave the cavity through mirror M_1 after making a second pass through the OPO crystal.

All mirrors have minimal reflectivity at the idler wavelength, making the OPO singly resonant. The intracavity 911-nm flux is reflected by the turning mirror (M_1) to pass through a 3-mm-long BBO type I doubling crystal. The final cavity mirror (M_3) is highly reflective at both 880–950 nm and 410–480 nm, which allows the doubled output to be extracted through the turning mirror (M_1) after making another pass through the doubling crystal. The use of two-pass nonlinear generation in both the doubler and the OPO significantly improves the conversion efficiency of these processes. The advantage of this configuration is that the KTP crystal is not exposed to the blue-UV flux, which could cause damage problems.

The output energies obtained at the various wavelengths are shown in Fig. 10.40, plotted as a function of the electrical input energy to the diode arrays of the Nd:YAG pump laser.

The large nonlinear coefficient of PPLN in combination with significant advances in manufacturing of PPLN now allow for the production of long crystals with excellent quality. This means that efficient operation of OPOs is no longer limited to high peak powers, thereby easing the requirements on the pump source for cw OPOs. The flexibility of grating-engineered phase matching has been particularly significant for cw OPOs and allowed a drastic reduction of the threshold of cw singly resonant OPOs. Threshold can be reduced to a few watts that make it possible that for example the devices can be directly pumped with diode lasers [10.112]. Continuous-wave OPOs have been established as practical and efficient sources of tunable radiation in the near- to mid-infrared spectral region. Devices for the ultraviolet and visible spectrum have not reached the same level of maturity.

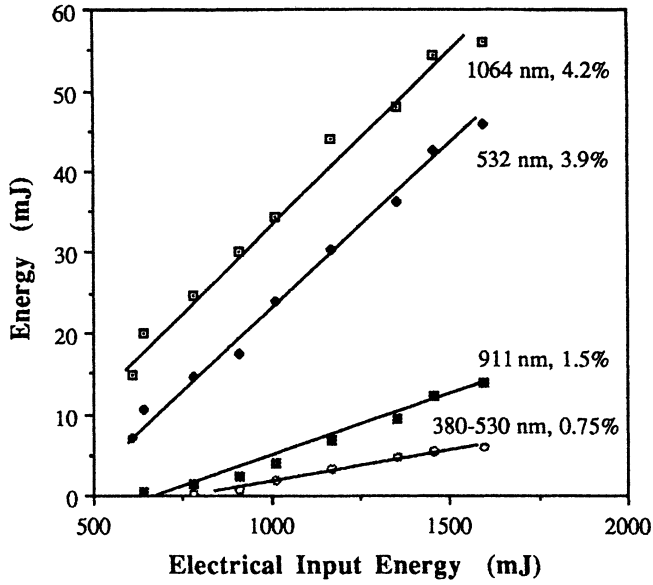

Fig. 10.40. Output at various wavelengths of the OPO depicted in Fig. 10.39 as a function of electrical input to the Nd:YAG pump laser

A common configuration for singly resonant cw OPOs is a four-mirror ring resonator with PPLN as the nonlinear crystal as depicted in Fig. 10.41 [10.112–115]. The bow-tie ring cavity is formed by two concave and two flat mirrors. Singly resonant operation is achieved with resonator mirrors that are highly reflecting for the signal beam and transmitting for the idler and pump beam. The concave mirrors which serve as input and output couplers generate a beam waist for the signal wave in the middle of the crystal. Many cw OPOs employ crystals in length up to 50 mm. The pump beam is usually mode-matched to the OPO cavity with a single lens which creates the appropriate beam waist inside the crystal.

It was found that a four-mirror resonator produces a higher output and has a narrower line width compared to a linear resonator [10.115]. Therefore ring resonators

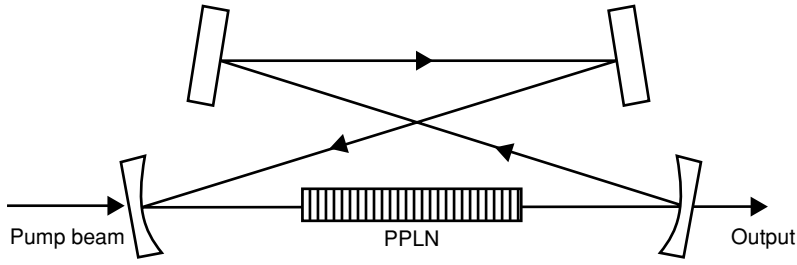

Fig. 10.41. Four-mirror ring cavity of a singly resonant cw OPO

are the most common resonator configuration for cw OPOs. The pump source is in most cases the fundamental or second harmonic of an Nd:YAG laser, but cw OPOs have also been designed with a diode laser as the pump source [10.112]. In this latter approach the singly resonant OPO was pumped by 2.25 W of 924-nm radiation from a InGaAs diode laser which generated up to 200 mW of 2.1-μm idler radiation.

The versatility of engineering and fabricating PPLN with nearly arbitrary grating periods is demonstrated in a system that integrates two separate frequency conversion steps in a single crystal [10.114]. The PPLN crystal has two grating periods in series. The first region is designed to produce a signal beam at 1540 nm and idler at 3450 nm from a 1064-nm Nd:YAG pump. The second region is designed to quasi-phase-match a sum frequency process whereby the signal and idler beams are combined to produce red light at 629 nm. The conversion of 1064 nm to 629 nm was 21% efficient and produced 2.5 W of red output.

A very efficient intracavity singly resonant cw-OPO-pumped Nd:YVO_4 laser is described in [10.116]. The high intracavity circulating power reduces the pump power requirement and an extremely low pump threshold for oscillations can be achieved. In the above system the pump source was a longitudinally pumped cw Nd:YVO_4 mini laser. At 1 W output from the laser diode, the single resonant OPO featuring a 50-mm-long PPLN crystal delivered 70 mW of output power at the idler wavelength of 3.66 μm.

Although most cw OPOs contain PPLN as the nonlinear material, other crystals such as periodically poled $LiTaO_3$ [10.117] and RbTiOAsO [10.118] have also been used.

OPOs have also been employed to provide tunable output from mode-locked lasers. The short pulse width of pico- or femtosecond pulses precludes the use of the standard OPO cavity in which the oscillating field builds up during the pump pulse. Such a cavity would have to be on the order of a few millimeters or less.

The basic approach that has been followed is synchronous pumping of OPO in which the resonator length of the OPO is matched to that of the pump laser cavity. This requires that one of the mirrors of the OPO is mounted on a piezoelectric transducer for precision adjustment of the OPO cavity length via a servo loop. Most synchronously pumped OPOs employ PPLN as the nonlinear material within a four-mirror ring resonator.

More than 12 W total output at the 1.85-μm signal and 2.5-μm idler has been obtained from a synchronously pumped OPO. The 47-mm-long and 1-mm-thick PPLN crystal was pumped by 80-ps-long pulses at 1064 nm with a repetition rate of 76 MHz [10.119]. The two concave mirrors of the four mirror resonator created a waist of the pump beam of 37 μm, and the signal and idler beams had a waist of 58 and 66 μm, respectively.

Synchronously pumped OPOs generating short pulses including femtosecond pulses have been reported in [10.99,119].

Figure 10.42 illustrates the technique of injection seeding an OPO in order to generate narrow-bandwidth output; [10.69]. A three-mirror L-shaped cavity configuration, containing a 50-mm-long $LiNbO_3$ crystal, was used to couple the pump and

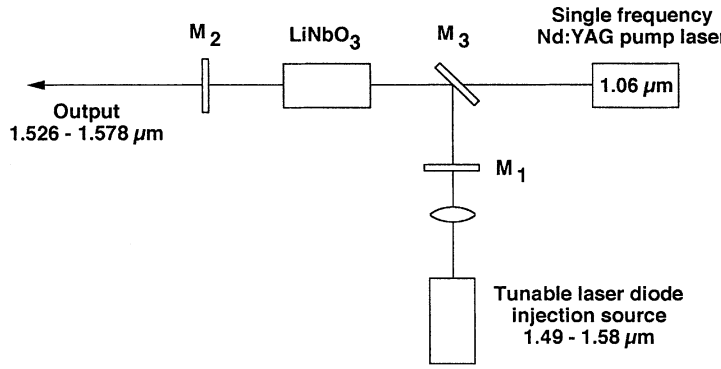

Fig. 10.42. Schematic diagram of an injection-seeded OPO

seed beam into the crystal. The OPO was pumped at 1.064 μm by an Nd:YAG laser with a pulse length of 8 ns and a pump energy of 75 mJ. The injection source was a grating tuned, external cavity InGaAsP diode laser tunable from 1.49 to 1.58 μm with a line width of 150 kHz.

The rear mirror (M_1) had a reflectivity of 90% at the signal wavelength and was mounted upon a piezoelectric stack that was used to adjust the length of the cavity. Mirrors M_2 and M_3 had signal reflectivities of 74 and 95%, respectively. All three mirrors had high transmission at 1.06 μm. A 50-cm lens was used to focus the seed radiation into the cavity.

The nonlinear medium used for the OPO was a 5-cm-long lithium niobate crystal cut at 47° to the optic axis and antireflection coated at the signal wavelength. The crystal was kept at a constant temperature of 38°C and was angle-tuned by type I phase matching. In the unseeded operation, a pump energy of 75 mJ generated an output of 22 mJ at 1.535 μm with a bandwidth of 50 GHz. With injection seeding, the output was 7.6 mJ and the bandwidth was reduced to 180 MHz. Injection seeding was achieved over a signal wavelength ranging from 1.526 to 1.578 μm, with a corresponding idler of 3.26–3.51 μm.

10.4 Raman Laser

Raman scattering occurs when a molecule or atom absorbs a photon and then emits a photon with a different energy. The difference in energy changes the energy state of the molecule or atom. The particular wavelength shift depends on the material in which Raman scattering takes place. The process can either raise or lower the energy state of a molecule or atom, but the effect is stronger if the emitted photon has a lower energy than the incident photon. If a Raman material is pumped by a high-power laser, a fraction of the beam is shifted to a longer wavelength. If the power level of the pump source is increased, additional spectral lines will appear at longer as well as shorter wavelengths with respect to the pump wavelength.

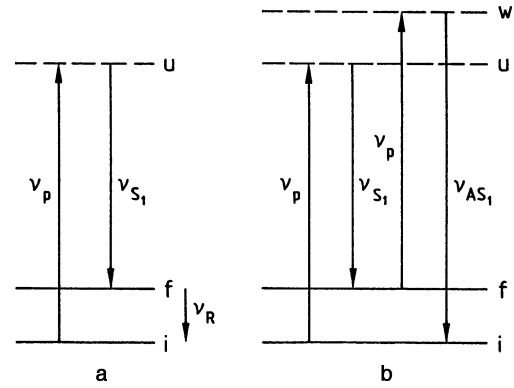

Fig. 10.43. Raman process. Generation of first Stokes light (a) and first anti-Stokes light (b)

Stimulated Raman scattering (SRS) occurs when a strong pump beam and a weak signal beam at a longer wavelength pass the Raman medium simultaneously. The molecule or atom, excited by the pump beam, releases energy to the signal wavelength thereby providing gain for the signal beam.

In its basic form, a Raman laser consists of a Raman medium such as a high-pressure gas cell or a crystal, a resonator that provides feedback for the Raman shifted wavelength, and a powerful pump beam.

10.4.1 Theory

The basic Raman effect is an inelastic light scattering process. The energy levels of interest for Raman scattering are shown in Fig. 10.43. An incident quantum $h\nu_p$ is scattered into a quantum $h\nu_s$, while the difference in energy $h(\nu_p - \nu_s) = h\nu_R$ is absorbed by the material. In Fig. 10.43 the u is upper state of the molecule, and i and f are the initial and final states. In principle, the excitation of the material may be a pure electronic excitation, or a vibrational or rotational excitation of a molecule. Solid-state-laser-pumped Raman lasers typically employ gases such as hydrogen or methane; therefore level i and f are the vibrational levels of the ground state of the molecule. The upper level u can be a real state or a "virtual" upper state. The frequency ν_s is called a Stokes frequency and is lower than the incident light frequency ν_p. The difference between ν_p and ν_s

$$\nu_p - \nu_s = \nu_R \tag{10.90}$$

is the Raman shift, which is characteristic of the material in which the Raman process is observed.

If the system is in an excited state to begin with, it may make a transition downward while the light is scattered. In that case the scattered light contains anti-Stokes frequencies which are higher than the incident frequency.

In the stimulated Raman effect, the pump laser at the frequency ν_p excites molecules to the level u, and if a population inversion exists between levels u and f, it can produce lasing action. In this case the radiation ν_s becomes amplified, while the

pump radiation ν_p loses energy. The process has typical laser characteristics, such as a pump energy threshold, exponential gain, and narrow line width. The emission in Fig. 10.43a is called the first Stokes line, usually written S_1. If a high-power laser is focused into a Raman medium, additional lines will appear at the output. Actually, a single laser frequency interacting with molecules will produce a "comb" of frequencies, each separated from its neighbor by the frequency spacing ν_R. These additional lines will be to the left and right of the wavelength scale with regard to the laser pump wavelength.

The additional lines are produced by parametric four-wave mixing of the various waves propagating in the Raman medium. As an example Fig. 10.43b illustrates the generation of one such line, having a wavelength shorter than the pump wavelength. This so-called anti-Stokes line is the result of the interaction of ν_p and ν_{s1} both propagating in the same direction. The parametric four-wave mixing process does not require a population inversion between w and i, and therefore there is no well-defined threshold. The simplest way of looking at this interaction is that the two frequencies beat together to produce polarization (induced dipole moments in the molecules) at the difference frequency. This polarization then modulates the laser-molecule interaction and produces light beams at the side frequencies.

Stokes lines have lower frequency (longer wavelength) and anti-Stokes lines have higher frequency (shorter wavelength). In each case the line is labeled first, second, etc., by counting the number of frequency shifts from the pump laser.

The gain equations given below, which are taken from [10.120], provide the basic design parameters of the Raman lasers. A rigorous mathematical treatment of stimulated Raman scattering can be found in [10.121–123]. These references also provide comprehensive introductions to all areas of coherent Raman spectroscopy.

SRS can be described as a nonlinear interaction involving the third-order nonlinear susceptibility χ^3. At a medium's Raman resonance, the third-order susceptibility reduces to the peak Raman susceptibility χ''_R, where the double prime indicates the imaginary part of the total susceptibility.

The growth of the electric field E_2 at the Stokes wavelength and depletion of the pump field E_1 is governed by the equations

$$\frac{\partial E_1}{\partial z} = -\frac{\omega_p}{2cn_p}\chi''_R|E_2|^2E_1, \tag{10.91}$$

$$\frac{\partial E_2}{\partial z} = \frac{\omega_s}{2cn_s}\chi''_R|E_1|^2E_2, \tag{10.92}$$

where $\omega_p - \omega_s = \omega_R$ are the frequencies, n_s and n_p are the indices of refraction, and c is the velocity of light. For a constant pump field, the Stokes field grows exponentially with a power gain given by

$$P_s(l) = P_s(0)\,\exp(g_s l), \tag{10.93}$$

where g_s is the gain coefficient and l the interaction length in the Raman medium.

$$g_s = \frac{\omega_s\chi''_R|E_1|^2}{n_s c} = \frac{4\pi\chi''_R I_p}{\lambda_s n_s n_p \varepsilon_0 c}. \tag{10.94}$$

Table 10.4. Stokes shift and Raman scattering cross section for several gases

Medium	$\nu_R[cm^{-1}]$	$d\sigma/d\Omega[cm^2/Ster]$
H_2	4155	8.1×10^{-31}
CH_4	2914	3.0×10^{-30}
N_2	2330	3.7×10^{-31}
HF	3962	4.8×10^{-31}

If one expresses the third-order Raman susceptibility, χ''_R in terms of spontaneous Raman scattering cross section, $d\sigma/d\Omega$, one obtains

$$g_s = \frac{\lambda_p \lambda_s^2 N(d\sigma/d\Omega) I_p}{n_s^2 hc\pi \Delta\nu_R}, \tag{10.95}$$

where λ_s is the Stokes wavelength, I_p is the pump intensity, N is the number density of molecules, h is Planck's constant, and $\Delta\nu_R$ is the full-width, half-maximum Raman line width.

From these equations follows that the gain for a single-pass Raman medium is proportional to the incident intensity, the active media cross section (which includes pressure and line width dependencies), and the length of the Raman cell.

The threshold of a Raman laser is usually defined as the gain required to achieve an output power at the Stokes wavelength that is of the same order as the pump radiation. For example, to achieve a 1 MW Stokes shifted power output, one requires a gain-length product of $g_s l = 36$ in the Raman medium in order for the radiation to build up from the initial spontaneous noise level which is $P_s = h\nu_s \Delta\nu_s \approx 10^{-9}$ W in the visible. Quantitative information such as gain coefficient and Stokes wavelength for many gases, liquids, and solids are listed in [10.124]. Table 10.4 summarizes the data for the most important Raman media.

The maximum theoretical conversion efficiency of a Raman laser is

$$\eta_{Ram} = \frac{\nu_p - \nu_R}{\nu_p}. \tag{10.96}$$

If one introduces into (10.96) the numbers given for ν_R in Table 10.4, it is obvious that the conversion efficiency can be very high. For example, a frequency-doubled Nd:YAG laser Raman-shifted with CH_4 provides an output at 630 nm. With $\nu_R = 2914$ cm^{-1} and $\nu_p = 18,797$ cm^{-1} one obtains $\eta = 84\%$.

Stimulated Raman scattering in crystals does not have as long a history as the well-established technique of frequency conversion in pressurized gases. The design of a practical device is very challenging because high power density is required to obtain efficient conversion in a Raman active material, and at the same time damage to the crystal must be avoided. Also, in contrast to harmonic generation which is a lossless process, Raman conversion deposits heat into the crystal which leads to strong thermal lensing and birefringence.

Despite these difficulties, a number of diode-pumped solid-state Raman lasers have been successfully operated at the 1 W level and above. For example, an externally

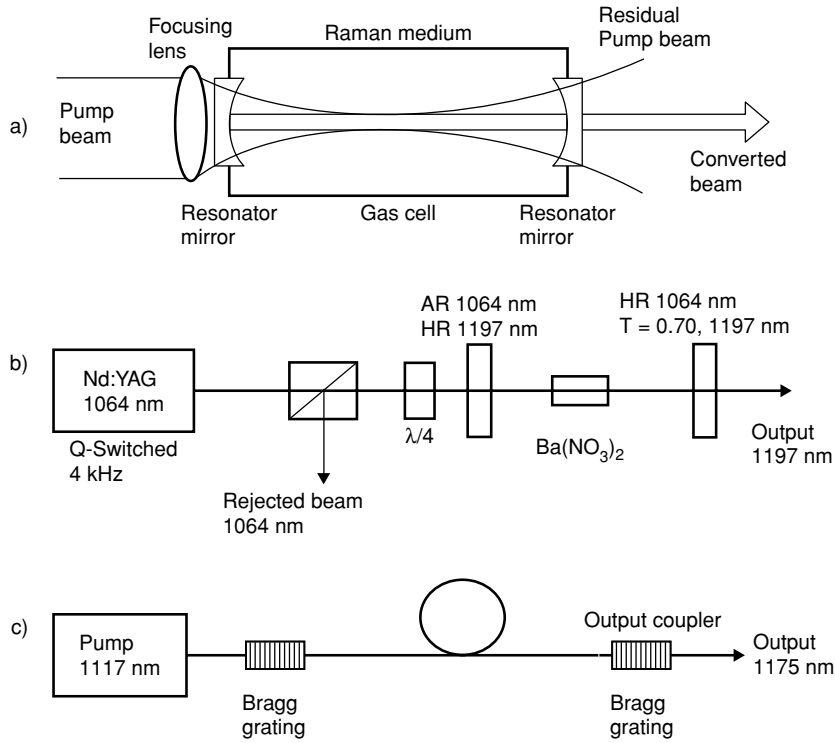

Fig. 10.44. Raman laser configurations. (a) Stimulated Raman scattering in a high-pressure gas cell; (b) solid-state Raman laser; (c) Raman fiber laser

pumped Raman laser containing a $Ba(NO_3)_2$ crystal produced up to 1.3 W at the first Stokes wavelength of 1197 nm [10.125]. The pump laser was a diode-pumped Nd:YAG slab laser and the optical design was similar to the schematic of Fig. 10.44b.

Similar to intracavity frequency doubling, a Raman laser can also be designed to share the resonator of the pump laser. Intracavity Raman lasers are described in [10.126.127]. The conversion efficiency can be very high and a nearly quantum limited conversion of 85% has been reported for 35-ps pulses at 532 nm, which were wavelength-shifted in $BaWO_4$ to 559 nm [10.127].

Table 10.5 lists properties of crystal that have been used in the design of solid-state Raman laser [10.128]. The materials include crystalline $Ba(NO_3)_2$, $LiIO_3$, and various tungstates. The first column shows the Raman shift which is larger for Ba $(NO_3)_2$. The Raman gain is expressed by g_s/I_p [see Eq. (10.95)] and the last column lists the output wavelength if the crystal is pumped by an Nd:YAG laser at 1064 nm.

10.4.2 Device Implementation

The most important parameters for a Raman laser medium are the Raman gain which is a function of the cross section for Raman scattering, the Raman frequency shift,

Table 10.5. Properties of crystals used in Raman lasers

Crystal	Raman shift [cm^{-1}]	Gain [cm/GW]	Stokes output[a] [nm]
$Ba(NO_3)_2$	1048	11	1197
$LiIO_3$	770	4.8	1156
$KGd(WO_4)_2$	901, 768	3.3, 4.4	1158,1177
$Pb\,WO_4$	901	3.1	1170

[a] Pumped at 1064 nm.

and the damage threshold of the material. The latter is important because gain for Raman scattering must occur at power densities well below the onset of self-focusing and catastrophic damage.

Stimulated Raman scattering in high-pressure gas cells has been utilized for frequency conversion of high-power Q-switched solid-state lasers for many years. A typical optical design is depicted in Fig. 10.44a. A focusing lens concentrates the pump beam inside the pressurized cell containing the Raman medium. The resonator mirrors can either be located outside the cell or serve also as windows.

Liquids such as the tetrachlorides ($GeCl_4$, $SiCl_4$, $SnCl_4$) have also been used in Raman lasers. However, chemical stability, and heating by the intense laser beam due to submicron particles suspended in the liquid, has been a problem.

More recently, crystals have been recognized as an efficient Raman medium for low-average-power systems. Owing to the inelastic nature of the nonlinear process, a fraction of the pump power is deposited as heat in the Raman medium. This limits Raman lasers to the realm of low-repetition-rate or low-average-power systems. Figure 10.44b depicts a solid-state Raman laser containing a $Ba(NO_3)_2$ crystal. The resonator mirrors are coated to provide feedback only at the first Stokes wavelength. The figure shows an externally pumped Raman laser. The combination of a quarter waveplate and a polarization beam splitting cube protects the Nd:YAG laser from feedback of the Raman resonator.

Raman lasers require high peak power Q-switched lasers as pump sources. However, in fibers where the beam is confined to the 8-μm core of a single-mode fiber, the Raman process becomes very strong and efficient even at a few watts of continuous power. In a typical Raman fiber laser, the output from a 20- to 50-W fiber-coupled diode bar is used to pump the cladding of a double-clad yttrium fiber laser. The radiation from the Yb fiber laser is then used to pump a Raman laser.

Figure 10.44c depicts a Raman fiber laser that shifts the pump source at 1117 nm to a wavelength of 1175 nm. Fiber Bragg gratings at 1175 nm are incorporated at both ends of a long single-mode fiber. In glass the pump radiation is down-shifted by the vibrational modes of the molecular bonds in the glass. Both the Raman scattering cross sections and wavelength shifts are different for silica, germanium, phosphorus, and borate glasses.

The design and performance of a hydrogen gas Raman laser which converts the frequency-doubled output of an Nd:YAG laser from 532 to 683 nm with an efficiency of up to 40% will be illustrated below [10.129].

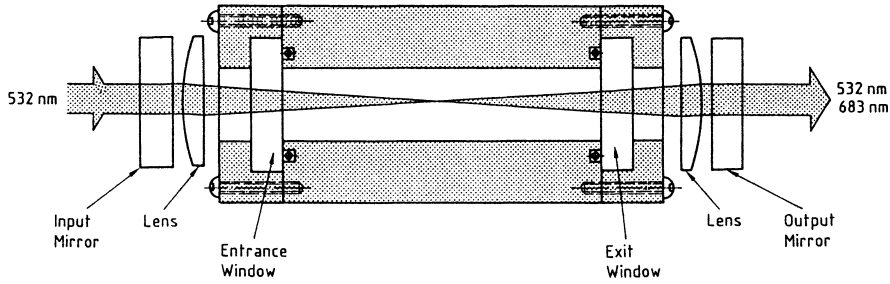

Fig. 10.45. Schematic diagram of a high-energy Raman cell

The 532-nm pump beam had an output energy up to 210 mJ, a pulse width of 24 ns, a beam diameter of 4.9 mm, and a beam divergence of 7 mrad. The repetition rate of the system was 2 Hz. The Raman laser consisted of the gas-pressure cell and the resonator optics, as shown in Fig. 10.45. The Raman cell is made from a block of aluminum bored with a 16-mm-diameter hole, fitted with O-ring grooves and windows held together by end caps. The 25-mm diameter by 12.5-mm thick fused silica windows are antireflection-coated at both the pump and the first Stokes wavelengths. The output of the Raman laser was measured as a function of input power with gas pressure, resonator configuration, and length as parameters. Figure 10.45 depicts the concentric resonator configuration comprising two flat mirrors and a pair of plano-convex lenses. The resonator length was 20 cm. The entrance mirror has high transmission at 532 nm and high reflection at 683 nm. The exit mirror has high transmission for the pump wavelength at 532 nm and 50% reflectance at the first Stokes wavelength. The reflectance for the second Stokes (954 nm) and first anti-Stokes (436 nm) wavelength was only a few percent at both mirrors.

Figure 10.46 exhibits the output vs. input for the resonator at the exact length for the concentric geometry (solid line) and for slight variations in length. As is apparent

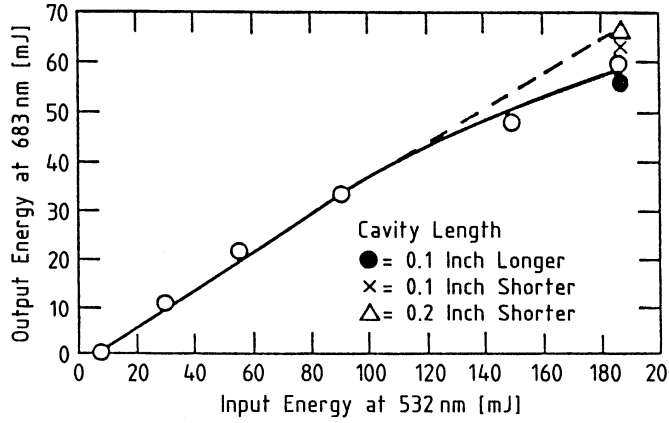

Fig. 10.46. Concentric resonator output energy for different pump input energies and cavity lengths. The solid line corresponds to the concentric position. (Hydrogen pressure: 1000 psi, output reflector 50% at 683 nm, 20 cm resonator)

from the data, the resonator length becomes more critical for the higher input energies, and a change of (1–2)% in resonator length has a noticeable effect. The output energy of 65 mJ at 683 nm for 185 mJ input at 532 nm was the highest energy achieved with the concentric resonator. Optical breakdown, probably caused by small particles and impurities in the gas, set this upper limit.

10.5 Optical Phase Conjugation

Optical phase conjugation, also referred to as wavefront reversal, has been demonstrated in solids, liquids, and gaseous media using a number of nonlinear optical interactions, such as three-wave and four-wave mixing, stimulated Brillouin scattering (SBS), stimulated Raman scattering (SRS), and photon echoes.

From the standpoint of solid-state laser engineering, phase conjugation via SBS is particularly important because it provides the simplest and most efficient interaction, and initial work in this area carried out by Zel'dovich et al. [10.130] revealed that optical aberrations produced by a laser amplifier stage could be corrected. The concept of reflecting an amplifier beam off an SBS cell and passing it back a second time through the amplifier was first used to compensate phase distortions in a ruby amplifier [10.131]. Following that initial work, SBS mirrors have been investigated in a number of solid-state lasers, using different nonlinear materials and optical arrangements [10.132–134]. Comprehensive descriptions of the principle of phase conjugation are contained in [10.135–138].

10.5.1 Basic Considerations

From a mathematical point of view, phase conjugation can be explained by considering an optical wave of frequency ω moving in the $(+z)$ direction,

$$E_1(x, y, z, t) = A(x, y) \exp\{j[kz + \varphi(x, y)] - j\omega t\}, \tag{10.97}$$

where E_1 is the electric field of the wave with wavelength $\lambda = 2\pi/k$. The transverse beam profile is given by the function $A(x, y)$ and the phase factor $\varphi(x, y)$, indicating how the wave deviates from a uniform, ideal plane wave. In particular, the phase factor carries all the information about how the wave is aberrated.

If the beam given by (10.97) is incident upon an ordinary mirror, it is reflected upon itself and the sign of z changes to $-z$, and all other terms of the equation remain unchanged. However, if the beam is incident upon a phase-conjugate mirror it will be reflected as a conjugated wave E_2 given by

$$E_2(x, y, z, t) = A(x, y) \exp\{j[-kz - \varphi(x, y)] - j\omega t\}. \tag{10.98}$$

In addition to the sign change of z, the phase term has a changed sign too. The conjugate beam corresponds to a wave moving in the $(-z)$-direction, with the phase $\varphi(x, y)$ reversed relative to the incident wave. We can think of the process as a reflection combined with phase or wavefront reversal. The phase reversal expressed by (10.98), for example, means that a diverging beam emitted from a point source,

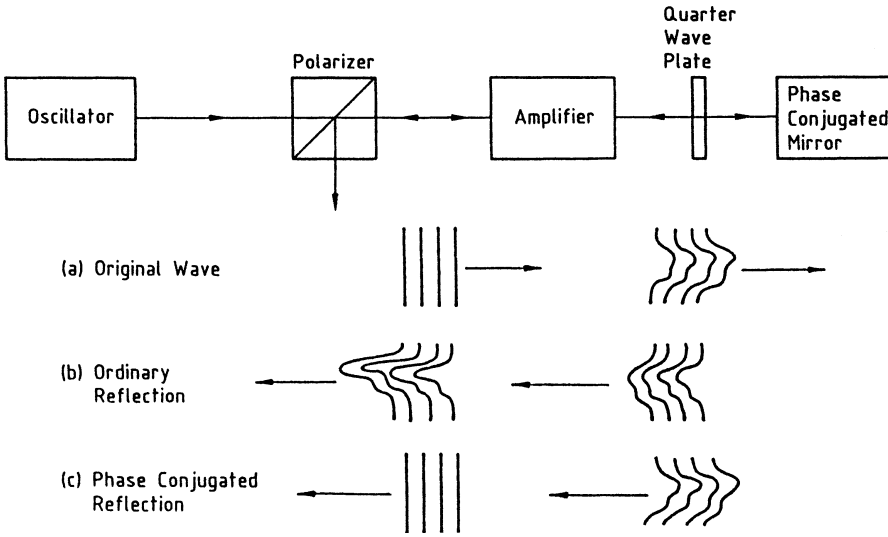

Fig. 10.47. Compensation for optical phase distortions caused by an amplifying medium using optical phase conjugation

after reflection at a phase-conjugate mirror, will be converging and be focused back to the point of origin.

A practical application of phase reversal in a laser system is depicted in Fig. 10.47. Shown is an oscillator which produces an output with a uniform flat wave front that is distorted in the amplifier medium. An ordinary mirror merely inverts the distortion as it reflects the beam, thereby keeping the distortion fixed with respect to the propagation direction. With a second pass through the amplifier, the distortion is essentially doubled. A phase-conjugate mirror, on the other hand, reverses the wavefronts relative to the wave propagation direction; hence, the same region of the amplifier that originally created the distortion compensates for it during the second pass through the amplifier.

However, it should be noted that although the wavefront is conjugated, the polarization state of the backward-going field is not conjugated. As far as the polarization vector is concerned, the SBS mirror behaves like an ordinary mirror. As we shall see, this has important implications with regard to the compensation of optical distortions caused by thermally induced birefringence in the amplifier rods.

As already mentioned, SBS of laser radiation in liquids or gases is the preferred approach for designing phase-conjugate mirrors. SBS involves the scattering of light by sound waves, i.e., acoustic phonons, or pressure/density waves. The incoming laser radiation generates an ultrasound wave by electrostriction corresponding to a spatial density modulation in the material. This modulation changes the refractive index and therefore a refractive index grating is created in the material.

The resultant Stokes scattered light is down-shifted in frequency by a relatively small amount ($\approx 10^9 - 10^{10}$ Hz). The gain of the Stokes-shifted wave is generally

the highest in a direction opposite to that of the incident beam. The efficiency of the SBS process (defined as the ratio of the Stokes-shifted, backward-going energy or power to the incident optical energy or power) can be as high as 90%. SBS has been studied extensively in liquids, solids, and gases. The steady-state gain factor of SBS is generally large, making SBS the dominant stimulated scattering process in many substances. Phase-conjugate mirrors can be employed to compensate thermal lensing in double-pass amplifiers if the beam intensity is high enough to provide sufficient reflectivity from the SBS process.

Reflectivity is an important parameter in designing an SBS mirror since it greatly influences the overall laser-system efficiency. The calculation of the reflectivity of SBS mirrors requires the solution of coupled differential equations for the incident and reflected light waves and the sound wave grating. The calculations of the scattering processes require a great numerical effort, assuming steady-state, or plane wave approximations solutions have been derived in [10.139–141].

The reflectivities of SBS mirrors depend on the excitation condition and the material properties of the nonlinear medium. Reflectivity vs. pump power or energy can be described by a threshold condition and a nonlinear power relationship. Threshold depends mainly on materials properties and cell geometry, whereas the increase of reflectivity is a function of the pump-beam power. Both threshold and the slope of reflectivity depend on the coherence properties of the beam. As will be explained later, there is a minimum requirement on the coherence or line width of the incident beam such that a coherent spatial and temporal interaction with the sound-wave grating is possible.

Design parameters which affect the performance of an SBS mirror will be examined in the following section.

10.5.2 Material Properties

Pressurized gases such as CH_4 and SF_6 or liquids such as CCl_4, acetone, and CS_2 are usually employed to provide efficient SBS for a 1.06-μm pump. SBS materials can be characterized by a gain coefficient and an acoustic decay time. The gain coefficient g_B determines threshold and slope of the reflectivity curve. Materials with a lower gain show a higher threshold and a slower increase of the reflectivity with increased pumping.

The acoustic-decay time τ_B establishes a criterion for the coherence or line width of the pump beam. For efficient interaction with the sound-wave grating, a coherent interaction on the order of the acoustic decay time is required. An inverse bandwidth of the pump pulse which is larger than the acoustic-phonon damping time describes the steady-state condition, i.e., $(\Delta\nu)^{-1} > \tau_B$. Maximum gain is achieved if this condition is satisfied. Most calculations, as well as the simple relationships for gain and threshold given below, are for this case.

Table 10.6 lists steady-state SBS gain coefficient g_B and acoustic decay time τ_B of representative gases and fluids.

Quite noticeable is the longer phonon lifetime in gases compared to liguids. Single longitudinal mode Q-switched lasers have a pulse length of 10–20 ns; therefore, the

Table 10.6. Steady-state SBS gain coefficients and acoustic decay time of representative gases and fluids, taken from [10.133, 134, 142]

Medium	g_B[cm/GW]	τ_B [ns]
CH_4 (30 atm)	8	6
CH_4 (100 atm)	65	17
SF_6 (20 bar)	14	17
SF_6 (22 atm)	35	24
CCl_4	6	0.6
Acetone	20	2.1
CS_2	130	5.2

coherence requirement for steady-state conditions, stated above, will barely be met in gases. SBS in gases will be highly transient, while in liquids, it will reach a steady state. This has the important implication that the effective gain for gases is actually considerably lower than the values in Table 10.6. The effective gain in a transient SBS process can be as much as 5–10 times less than the value given in the table. The lower SBS threshold and higher gain is the reason most current systems employ liquids as the nonlinear medium. Also, liquid cells are not as long as gas-filled cells. liquid cells are typically 10–15 cm long, whereas gas cells are between 30 and 100 cm in length.

Gases employed as nonlinear elements have the advantage that they eliminate problems which can arise in liquids owing to optical breakdown caused by bubbles or suspended particles.

The gain of an SBS process is a function of the frequency ω of the pump radiation, the phonon lifetime τ_B, the electrostrictive coefficient γ, the velocity of light and sound c and v, and the refractive index n_0 and density p_o of the material [10.141].

$$g_B = \frac{\omega^2 \gamma^2 \tau_B}{c^3 v n_0 \rho_0} \tag{10.99}$$

The threshold pump power for SBS is a parameter of practical importance. If one measures reflectivity versus pump power input, one observes that at a particular input power, reflectivity changes over many orders of magnitude for just a few percent increase in power. In this regime of rapid signal growth, a threshold is usually defined if the gain has reached exp (30).

The gain of the backward reflected Stokes wave over a length l of the nonlinear medium is $\exp(g_B I_P l)$ for a plane wave of pump intensity I_P. If the threshold P_{th} is defined as the condition when the gain reaches exp(30), then one obtains [10.133] for a high-pressure CH_4 gas as the SBS medium

$$P_{th} = \frac{30A}{g_B l} \tag{10.100}$$

where A is the area of the pump beam.

For a Gaussian pump beam, one obtains [10.143]

$$P_{\text{th}} = \frac{\lambda_{\text{p}}}{4g_{\text{B}}}\{1 + [1 + 30/\arctan(l/b)]^{1/2}\}^2, \tag{10.101}$$

where b is the confocal parameter defined in (5.7) and l is the length of the SBS cell. If the cell is long compared to the confocal parameter $l \gg b$, the lowest threshold is obtained, since $\arctan(l/b) = \pi/2$ and (10.101) reduces to

$$P_{\text{th}} = 7.5\frac{\lambda_{\text{p}}}{g_{\text{B}}}. \tag{10.102}$$

10.5.3 Focusing Geometry

An SBS mirror in its most common form consists of a lens which focuses the incident beam into the bulk nonlinear material. The first buildup of the sound-wave amplitude is concentrated in the focal region of the incident beam. However, the sound wave can have a wide distribution over large parts of the cell.

As confirmed in experiments [10.141], in a first approximation, a change in focal length should not affect threshold or reflectivity, since a shorter focal length, which leads to a shorter interaction length l in (10.100) is compensated by stronger focusing leading to a smaller area A of the pump beam. Choosing short focal lengths will lead to a very compact sound-wave distribution with the advantage of a lower demand on the coherence of the laser radiation. The main disadvantage of a very short focal length is the high intensity and therefore the occurrence of optical breakdown.

Depending on the focal length of the lens, the sound wave may be sharply concentrated in the cell or distributed over the whole cell length.

There is also a difference whether the lens is the front window of the cell, and the nonlinear medium fills the space between the lens and the beam waist, or if the lens is positioned outside the cell and only the area around the beam waist is covered by the medium. The choice of a focusing lens, for an incident laser beam of given pulse energy and duration, has to be such that at the focal region the intensity is well above threshold but below optical breakdown.

10.5.4 Pump-Beam Properties

The pump power has to be well above the threshold of the nonlinear reflectivity curve. Otherwise, the fidelity of the reflected signal becomes small, because the parts of the beam away from the central peak, with energies below this threshold value are not reflected. The useful power range of the incident radiation is limited by the SBS threshold at the lower limit and by optical breakdown at the upper end.

A typical curve for SBS reflectivity vs. input energy is shown in Fig. 10.48. These experimental data were obtained by focusing a Q-switched Nd:YAG laser into a CCl_4 cell with a 80-mm-long focal length lens [10.142]. The general shape of the increase

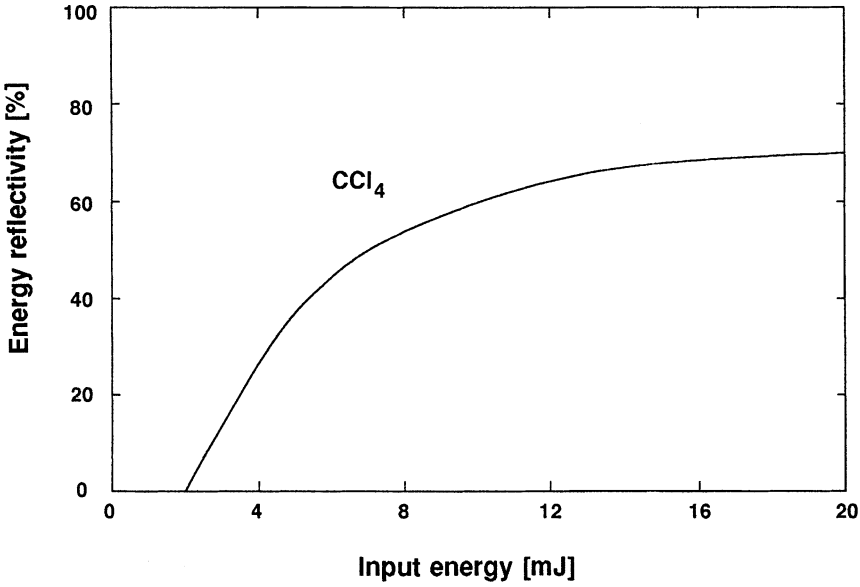

Fig. 10.48. SBS energy reflectivity of CCl_4 as a function of pump energy for a Q-switched Nd:YAG laser [10.142]. Curve represents a best fit of experimental data

in reflectivity with intensity can be approximated by a simple expression [10.139]

$$R = \frac{C(E_{\text{in}}/E_{\text{th}})}{1 + C(E_{\text{in}}/E_{\text{th}})} \quad \text{for} \quad E_{\text{in}} \gg E_{\text{th}}, \tag{10.103}$$

where E_{in}, and E_{th} are the input energy of the incident beam and threshold value, respectively, and C is a constant which depends on the beam and nonlinear material properties.

In order to obtain a low SBS threshold and high reflectivity, an efficient coherent wave interaction is necessary between the pump beam and the sound-wave grating. There is a spatial and temporal requirement on the coherence of the incident beam. First, the coherence length of the beam should exceed the longitudinal sound-wave extension. If the pump beam has a Gaussian spatial profile, the sound wave has a longitudinal extent approximately given by the confocal parameter. Second, the coherence time (i-e., the inverse of the line width, $1/\Delta\nu$) of the pump beam should exceed the response time τ_{B} of the acoustic phonons. Typically, τ_{B} is on the order of nanoseconds for liquids, and tens of nanoseconds for pressurized gases. Therefore, high-efficiency SBS requires line width narrowing or preferably single longitudinal mode operation. If the laser operates in a single longitudinal mode, this means that the pulse length should be longer than τ_{B}.

If these conditions are not met, the steady-state SBS process changes to transient SBS with a correspondingly lower gain parameter. The effect of multimode lasers on the SBS threshold and experiments which address the issue of multimode operation will be discussed next.

Carr and Hanna [10.133] investigated SBS with a Q-switched single transverse and longitudinal mode Nd-YAG laser which had a pulse duration of 30 ns and a coherence length of 6 m. The 1-m-long cell filled with CH_4 at 30 atm results in a 6-ns acoustic decay time and a gain coefficient of 8 cm/GW. The beam was focused to a waist of $w_T = 150$ μm, from which follows, with $\lambda = 1.06$μm, a confocal parameter of $b = 13$ cm [see (5.7)]. Introducing these parameters into (10.102) yields a threshold for SBS of $P_{th} = 100$ kW. Even for a ratio of pulse width to phonon decay time of a factor of $5(t_p/\tau_p = 5)$, a significant degradation from steady-state conditions can be expected. The theory predicts a threshold 2.5 times greater than for steady-state conditions or 250 kW in this particular case [10.144]. The actual observed threshold was 400 kW. Since the coherence length l_{coh} was 6 m and the confocal parameter b was 13 cm, the condition $l_{coh} \gg b$ in (10.102) is clearly satisfied.

The coherence length is reduced for multimode operation according to $l_{coh} = 2L/n$, where L is the length of the resonator and n the number of longitudinal modes. For the 1-m-long resonator, the condition $l_{coh} \gg b$ is satisfied even in the presence of several modes. The experimental results confirmed that the SBS threshold was little affected if the laser was operated in several modes. However, when the oscillator was operated on 15 modes ($l_{coh} = 15$ cm or a bandwidth of ≈2 GHz) threshold increased by 75%. Phase conjugation still occurred, but was less reliable and resulted in poor beam reconstruction.

The dependence of SBS reflectivity on coherence length and input energy is illustrated in Fig. 10.49. In this experiment, radiation from a Nd:YAG laser was

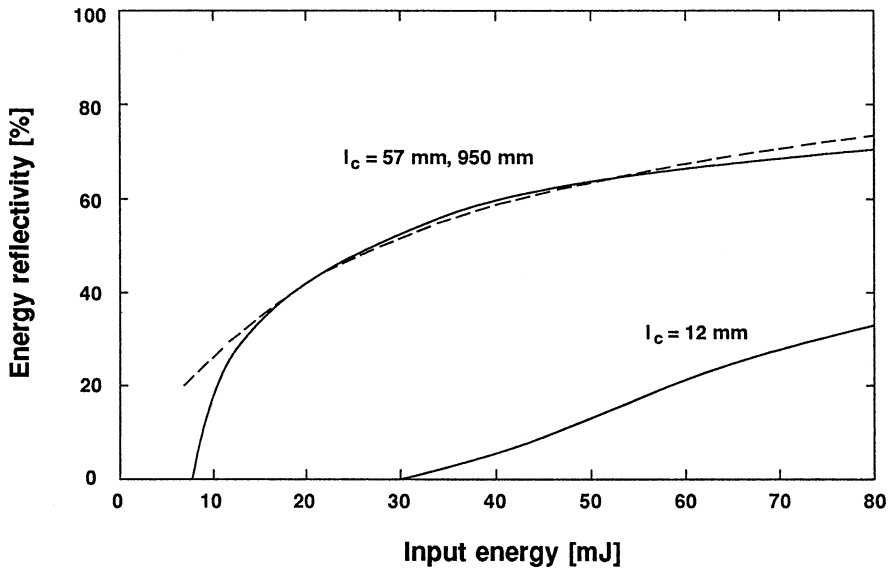

Fig. 10.49. SBS energy reflectivity in SF_6 for a Q-switched Nd:YAG laser with different coherence lengths l_c. Dashed line is an approximation according to (10.103) with $C = 0.25$

focused with a lens of 100-mm focal length into a cell containing SF_6 at a pressure of 20 bar [10.142].

The lens was positioned about 40 mm in front of the cell entrance window. In Fig. 10.49, measured energy reflectivities with different coherent laser pulses are shown. As can be seen from this figure, the energy reflectivity is different for the shortest coherence length of 12 mm compared to the two others. No difference was detectable between the pulses with 57 mm and 950 mm coherence length. In both cases, the coherence length was longer than the whole interaction length between the entrance window of the cell and the focus of the beams inside. The measured data agreed quite well with predicted values calculated from the theory described in [10.141].

10.5.5 System Design

In Fig. 7.21 we have already exhibited the most common configuration of compensating thermally induced lensing in amplifiers with an SBS mirror. The output from the oscillator passes through the amplifiers, is reflected by the SBS mirror, and propagates a second time through the amplifier chain. Output coupling is realized by a polarizer and a 90° polarization rotation carried out by a $\lambda/4$ waveplate which is passed twice. Conjugate reflectivities in this type of configuration are typically 50–80%, so that the efficiency of the amplifier stage is reduced by a fraction which depends on the ratio of energy extraction between the first and second pass in the amplifiers.

As already pointed out, phase conjugation will invert the wavefront and correct thermal lensing introduced by the amplifier chain; however, it will not correct for depolarization caused by birefringence. Depolarization causes distortion of the output beam profile, leads to polarization losses, and the wrongly polarized light is back-reflected toward the oscillator.

Several approaches have been explored to deal with this problem. One approach is to minimize the effect of birefringence as one would in any system independent of the use of an SBS mirror. This includes rotation of the birefringence axis in single- and double-stage amplifiers and the use of a naturally birefringent laser crystal. The second approach is unique to SBS and involves separating the depolarized beam into its two components of orthogonal polarization and individual conjugation of each polarization state. These approaches will be illustrated in more detail in the following section.

One approach of minimizing birefringence is utilized in the design exhibited in Fig. 7.21 in which a 90° rotator is placed between two identical amplifier stages. A ray passing through the amplifier has its electric field component along the fast birefringence axis rotated by 90° so that it lies along the slow axis in the second amplifier, and vice versa. Thus, regardless of the orientation of the fast and slow axes, the birefringence in one amplifier is canceled in the second. A commercially available Nd:YAG oscillator–amplifier system with an SBS mirror uses this architecture.

If the laser system employs only a single amplifier, a Faraday rotator with 45° rotation placed between the amplifier and mirror is equivalent to a 90° rotation between two identical amplifier stages. With the arrangement shown in Fig. 10.50 and using

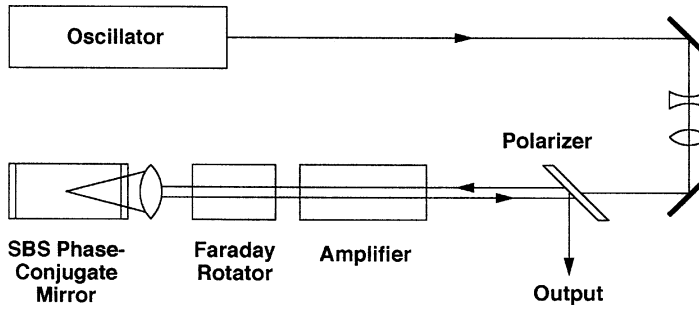

Fig. 10.50. Depolarization compensation in a single amplifier with a Faraday rotator in a double-pass configuration using an SBS mirror [10.133]

methane at 30 atm, nearly 300 mJ of diffraction-limited output was obtained in an Nd:YAG amplifier operating at 15 Hz [10.133].

Thermally induced birefringence effects can be greatly reduced if an anisotropic crystal such as Nd:YAlO or Nd:YLF is used as laser rod. These crystals have a poorer thermal conductivity compared to Nd:YAG, and therefore exhibit higher thermal lensing. But the latter can be compensated with a phase-conjugate mirror. Using this rationale, Eichler et al. [10.145] constructed an Nd:YAlO oscillator–amplifier system which produces 100-W average power in a 1.2 diffraction-limited beam. The amplifier had negligible depolarization losses but a strong thermal lens of less than 15 cm at the maximum lamp input of 8 kW. The experimental setup is depicted in Fig. 10.51. The oscillator, which was passively Q-switched with a LiF:F_2 color center crystal, contained two intracavity etalons with thicknesses of 2 and 20 mm, which resulted in a coherence length of 2.5 m. The output from the amplifier was focused with a 200-mm lens into the SBS cell, which contained CS_2 as the nonlinear material.

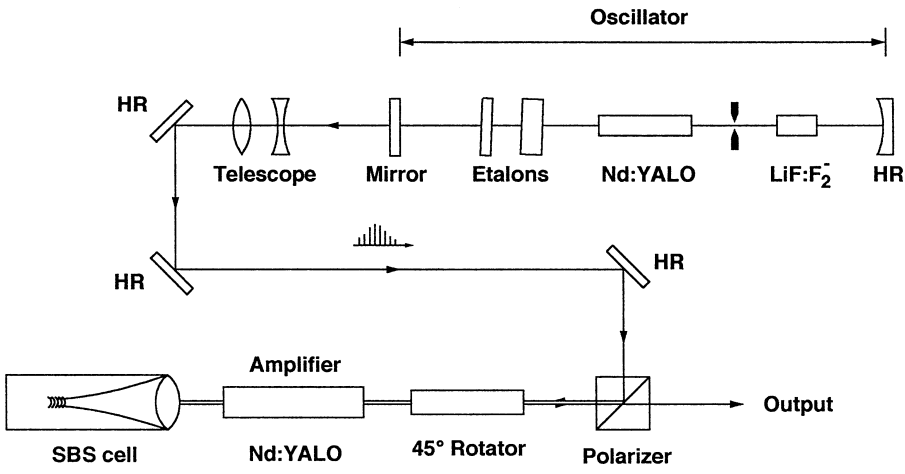

Fig. 10.51. Nd: YAlO oscillator and double pass single amplifier with SBS mirror [10.145]

An extension of this work covering phase conjugation in multi-amplifier architectures is described in [10.146].

In the approaches described so far, birefringence effects are minimized before the beam enters the SBS cell. There is a limit to the compensation capabilities of these schemes. Compensation will be acceptable if bifocusing effects are not too strong, otherwise the second-pass beam will not return exactly along the path of the first beam and the fidelity of beam restoration will suffer [10.147]. The best compensation can be achieved if the polarization is uniform and linear at the SBS cell.

An approach investigated by Basov et al. [10.148] is to split the beam into two orthogonal polarizations after passing through the amplifier. One of the beams is then rotated 90° so it has the same polarization as the other. The two beams will cooperatively reflect from the SBS phase-conjugate mirror. The back-reflected phase-conjugated beams then pass back through their respective optical paths and are recombined at the beam splitter before propagating through the amplifier for a second time. The beam emerging from the amplifier has the same beam quality and polarization as the original incident beam. A more recent implementation of this general approach was described in [10.149].

From a design point, the question that needs to be answered is whether a phase-conjugation system is necessary, or whether insertion of internal elements such as lenses, phase plates, or 90° rotators is sufficient to remove troublesome distortions associated with the amplifier stages. Other techniques which reduce beam aberrations are diode pumping and a zigzag slab design. The former reduces the heat load on the laser crystal and the latter compensates to a first-order beam distortion by virtue of its geometry. Of course, these techniques are not exclusive of each other and can be combined in one system. It should be mentioned that besides compensating for thermal lensing, a phase-conjugating mirror has some additional interesting features. Misalignment of a conventional rear mirror caused by mechanical, thermal, or vibration effects which will lead to beam wander and power loss is eliminated because the beam reflected from the phase-conjugated mirror is self-aligned. It greatly depends on the particular application and average-power requirements of the system, when it is justified to remove the troublesome aberrations associated with the amplifier stages by means of a phase-conjugate mirror. Also, a simple SBS mirror arrangement does not remove aberrations and losses due to birefringence, and the schemes for correction of stress birefringence by resolving the depolarized beam into components for separate conjugation are too complicated and require a large number of additional optical components.

Conceptually, the replacement of a conventional mirror at the end of an amplifier chain with an SBS cell and a lens appears straight-forward. However, a number of issues have to be resolved in a practical implementation of this technique. In order to achieve an acceptable overall system efficiency, the oscillator requires longitudinal mode selection, and the cell has to be operated at high beam intensities without causing optical breakdown. The latter is always a concern because impurities in the liquid could cause breakdown at the GW/cm^2 power levels, which are required to achieve a high SBS reflectivity.

Oscillators with SBS Q-Switching Mirrors. By far the most common application of SBS mirrors is in double-pass amplifier configurations. However, SBS mirrors have also been employed in oscillators. Since the amplified spontaneous emission is too small to start the SBS process, a conventional mirror is placed behind the SBS cell to start lasing action. As soon as the reflectivity of the SBS mirror is high enough, it will take over and form the main resonator. Since the losses decrease (i.e., reflectivity increases) as the flux in the resonator builds up, Q-switching occurs. Oscillators employing SBS Q-switching mirrors have been described in [10.150, 151].